

INFORMATION TO USERS

This manuscript has been reproduced from the microfilm master. UMI films the text directly from the original or copy submitted. Thus, some thesis and dissertation copies are in typewriter face, while others may be from any type of computer printer.

The quality of this reproduction is dependent upon the quality of the copy submitted. Broken or indistinct print, colored or poor quality illustrations and photographs, print bleedthrough, substandard margins, and improper alignment can adversely affect reproduction.

In the unlikely event that the author did not send UMI a complete manuscript and there are missing pages, these will be noted. Also, if unauthorized copyright material had to be removed, a note will indicate the deletion.

Oversize materials (e.g., maps, drawings, charts) are reproduced by sectioning the original, beginning at the upper left-hand corner and continuing from left to right in equal sections with small overlaps. Each original is also photographed in one exposure and is included in reduced form at the back of the book.

Photographs included in the original manuscript have been reproduced xerographically in this copy. Higher quality 6" x 9" black and white photographic prints are available for any photographs or illustrations appearing in this copy for an additional charge. Contact UMI directly to order.

UMI

**A Bell & Howell Information Company
300 North Zeeb Road, Ann Arbor MI 48106-1346 USA
313/761-4700 800/521-0600**

University of Alberta

SOL-GEL PROCESSING OF METAL SULFIDES

by

Vesna Stanić



A thesis submitted to the Faculty of Graduate Studies and Research in partial fulfillment of the requirements for the degree of Doctor of Philosophy

in

Materials Engineering

Department of Chemical and Materials Engineering

Edmonton, Alberta

Spring 1997



**National Library
of Canada**

**Acquisitions and
Bibliographic Services**

**395 Wellington Street
Ottawa ON K1A 0N4
Canada**

**Bibliothèque nationale
du Canada**

**Acquisitions et
services bibliographiques**

**395, rue Wellington
Ottawa ON K1A 0N4
Canada**

Your file Votre référence

Our file Notre référence

The author has granted a non-exclusive licence allowing the National Library of Canada to reproduce, loan, distribute or sell copies of his/her thesis by any means and in any form or format, making this thesis available to interested persons.

The author retains ownership of the copyright in his/her thesis. Neither the thesis nor substantial extracts from it may be printed or otherwise reproduced with the author's permission.

L'auteur a accordé une licence non exclusive permettant à la Bibliothèque nationale du Canada de reproduire, prêter, distribuer ou vendre des copies de sa thèse de quelque manière et sous quelque forme que ce soit pour mettre des exemplaires de cette thèse à la disposition des personnes intéressées.

L'auteur conserve la propriété du droit d'auteur qui protège sa thèse. Ni la thèse ni des extraits substantiels de celle-ci ne doivent être imprimés ou autrement reproduits sans son autorisation.

0-612-21641-1

University of Alberta

Library Release Form

Name of Author: Vesna Stanić

Title of Thesis: Sol-gel processing of metal sulfides

Degree: Doctor of Philosophy

Year this Degree Granted: 1997

Permission is hereby granted to the University of Alberta Library to reproduce single copies of this thesis and to lend or sell such copies for private, scholarly, or scientific research purposes only.

The author reserves all other publication and other rights in association with the copyright in the thesis, and except as hereinbefore provided, neither the thesis nor any substantial portion thereof may be printed or otherwise reproduced in any form whatever without the author's prior written permission.

V. Stanić

#301, 10528-29Ave

Edmonton, AB, T6J 4J2

Canada

Date: March 6, 1997

University of Alberta

Faculty of Graduate Studies and Research

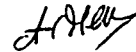
The undersigned certify that they have read, and recommend to the Faculty of Graduate Studies and Research for acceptance, a thesis entitled:

SOL-GEL PROCESSING OF METAL SULFIDES

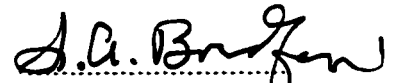
submitted by **VESNA STANIĆ** in partial fulfillment of the requirements for the degree of
Doctor of Philosophy in **Materials Engineering**.



Dr. T.H. Etsell
supervisor



Dr. A.C. Pierre
supervisor



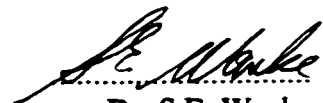
Dr. S.A. Bradford



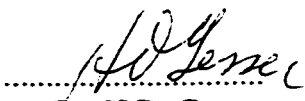
Dr. R.L. Eddie



Prof. L.R. Plitt



Dr. S.E. Wanke



Dr. H.D. Gesser

Date February 10, 1997

To my family for love and support.

ABSTRACT

Metal sulfides were synthesised via a sol-gel process using various metal alkoxides and hydrogen sulfide in toluene. Colloidal gels were prepared from germanium ethoxide, germanium isopropoxide, zinc tert-butoxide and tungsten (VI) ethoxide, whereas colloidal powder was produced from tungsten (V) dichloride ethoxide. Special precautions were necessary to protect the reaction mixture from water contamination which produced metal oxides. Results indicated that the main source of water is the hydrogen sulfide gas. In addition, synthesis of metal sulfides from a mixture of metal oxide and sulfide was demonstrated by the example of monoclinic germanium disulfide. It was produced by reaction of the sol-gel product with sulfur. Heat treatment of the sol-gel product and sulfur yielded single phase GeS₂. The sol-gel prepared materials and their heat treated products were characterized by various methods.

A chemical kinetics study of the functional groups -OR, -SH and S²⁻ was carried out for the sol-gel processing of GeS₂ from of hydrogen sulfide and two different alkoxides, germanium ethoxide and germanium isopropoxide. The study was performed for different concentrations of precursors at different molar ratios and temperatures. The results indicate that the proposed reaction mechanism was simplified under appropriate reaction conditions. Experimentally determined rate constants of thiolysis and condensations demonstrate that thiolysis is slow and that condensations are fast steps, regardless of the studied reaction conditions. A study of the temperature effect on the reaction rate constant shows that it increases with temperature in accord with both Arrhenius law and transition-state theory. Activation energies, E_a, and activation parameters ΔS[‡], ΔH[‡] and

ΔG^\ddagger , were determined for thiolysis and condensation reactions.

The potentiometric titration method was used for quantitative determination of germanium sulfide and germanium mercaptide evolved during the sol-gel processing of GeS_2 . The titrations were performed in 2-propanol or in a 50-50 vol % mixture of 2-propanol and toluene. The ion selective $\text{Ag}/\text{Ag}_2\text{S}$ electrode was used for equivalence point detection. Study of the Nernst equation shows that complexes were formed at the electrode surface. However, the titration equivalence point volume clearly demonstrates the formation of Ag_2S and $\text{Ge}(\text{SAg})_n$. In order to explain this discrepancy a new electrode reaction mechanism and a modified $\text{Ag}/\text{Ag}_2\text{S}$ electrode potential equation are proposed.

Effects of hydrogen sulfide and germanium ethoxide concentrations, the concentration ratio and temperature on the microstructure of the prepared GeS_2 gels were studied. It was found that the concentrations of the reactants have the most significant influence on gel structure.

ACKNOWLEDGMENTS

My profound gratitude goes to my supervisor, Dr. T.H. Etsell for providing me the opportunity and the guidance to complete the work in an interesting research area. My deep gratitude to former supervisor, Dr. A.C. Pierre, for giving me invaluable advice towards the realization of my initial research goals. My endless appreciation to Dr. R.J. Mikula for generous support for completion of this work.

I am grateful to CANMET, Fuel Processing Laboratory, Western Research Center, for their financial and technical support of the research.

I am also grateful to Mrs. C. Barker , Dr. S. Zang and Mr. S. Merali for the assistance they provided in scanning electron microscopy, infrared spectroscopy and x-ray powder diffraction analysis.

I am thankful to my friend and colleague, Dr. M. Baković for discussions about chemical kinetics and her encouragement.

And to all my friends from CANMET and the University of Alberta who made my stay worthwhile. Thank you.

TABLE OF CONTENTS

CHAPTER 1 INTRODUCTION

1.1 APPLICATIONS OF METAL SULFIDES.....	1
1.2 SOL-GEL PROCESSING.....	3
1.3 CONTROLLING THE MICROSTRUCTURE.....	8

CHAPTER 2 EXPERIMENTAL PROCEDURE

2.1 MATERIALS

2.1.1 Metal alkoxides.....	16
2.1.2 Toluene.....	17
2.1.3 Hydrogen sulfide.....	17
2.1.4 Titrants.....	17
2.1.5 Electrolyte.....	17

2.2 EQUIPMENT

2.2.1 Glove box.....	18
2.2.2 Down draft hood.....	18
2.2.3 Magnetic stirrer.....	18
2.2.4 Thermostat.....	19
2.2.5 Equipment for the emf measurements.....	19
2.2.6 Glassware.....	20

2.3 PURIFICATION OF CHEMICALS

2.3.1 H ₂ S drying.....	20
2.3.2 Toluene drying.....	21

2.4 SOL-GEL PROCESSING

2.4.1 GeS ₂ gels.....	21
2.4.2 The GeS ₂ -GeO _x gel mixture and sulfur.....	22
2.4.3 GeS ₂ gels at different C, R and T.....	22
2.4.4 Metal sulfides.....	24
2.4.5 Thin films.....	24

2.5 HEAT TREATMENT.....	26
-------------------------	----

2.6 POTENTIOMETRIC TITRATION.....	26
-----------------------------------	----

2.7 KINETICS.....	27
-------------------	----

2.8 CHARACTERIZATION METHODS	
2.8.1 X-ray diffraction (XRD).....	29
2.8.2 Infrared spectroscopy (IR).....	29
2.8.3 BET method (BET).....	29
2.8.4 Scanning electron microscopy (SEM).....	30
2.8.6 Energy dispersive spectrometry (EDS).....	30
2.8.6 Quantitative chemical analysis (EA).....	30

CHAPTER 3 RESULTS

3.1. CHARACTERIZATION OF GeS₂ AND THEIR HEAT TREATED PRODUCTS	
3.1.1 Sol-gel processing of GeS ₂ gels.....	31
3.1.2 X-ray diffraction analysis.....	33
3.1.3 Infrared analysis.....	33
3.1.4 Scanning electron microscope analysis.....	38
3.1.5 Chemical analysis.....	46
3.1.6 BET analysis.....	47
3.2 CHARACTERIZATION OF THE GeS_x-GeO_x GEL AND SULFUR MIXTURE AND THE HEAT TREATED PRODUCT	
3.2.1 X-ray analysis.....	48
3.2.2 Infrared analysis.....	48
3.2.3 Scanning electron microscope analysis.....	52
3.2.4 Chemical analysis.....	52
3.3. CHARACTERIZATION OF THE GeS₂ GELS PREPARED AT DIFFERENT C, R AND T	
3.3.1 Sol-gel processing.....	58
3.3.2 Scanning electron microscope analysis.....	62
a) Concentration.....	62
b) Ratio.....	67
c) Temperature.....	67
3.3.3 BET analysis.....	72
a) Concentration.....	72
b) Ratio.....	76
c) Temperature.....	78
3.3.4 XRD and infrared analyses.....	81

3.4.	CHARACTERIZATION OF METAL SULFIDES	
3.4.1	ZnS gel.....	83
3.4.2	Sol-gel products of tungsten sulfides.....	83
3.5.	CHARACTERIZATION OF THIN FILMS.....	91
3.6	POTENTIOMETRIC TITRATION	
3.6.1	Accuracy.....	94
3.6.2	Reproducibility.....	96
3.6.3	Selectivity.....	98
3.7	CHEMICAL KINETICS	
3.7.1	Kinetic data.....	106
3.7.2	Reaction mixture containing $[H_2S]_0/[Ge(OEt)_4]_0$ in ratio 9:1.....	106
3.7.3.	Reaction mixtures containing $[H_2S]_0/[Ge(OEt)_4]_0$ in ratio 1:1.2.....	114
3.7.4.	Reaction mixtures containing $[H_2S]_0/[Ge(OPr^i)_4]_0$ in ratio 2.25:1.....	118

CHAPTER 4 DISCUSSION

4.1	PREPARATION OF GeS_2 WITH LOW OXYGEN CONTENT	
4.1.1	Dried gels.....	130
4.1.2	Heat treated gels.....	135
4.2.	PREPARATION OF GeS_2 FROM THE MIXTURE OF GeS_x-GeO_x GEL AND SULFUR.....	137
4.3.	PREPARATION AND CHARACTERIZATION OF OTHER METAL SULFIDES	
4.3.1	Zinc sulfide gel.....	140
4.3.2	Colloidal tungsten sulfides.....	141
4.4.	PREPARATION OF THE THIN METAL SULFIDES FILMS.....	144

4.5 .	DETERMINATION OF SULFUR PRODUCTS IN THE SOL-GEL PROCESSING OF GeS₂ BY POTENTIOMETRIC TITRATION	
4.5.1	The method accuracy.....	145
4.5.2	The Ag/Ag ₂ S electrode response to the S ²⁻ and GeS ⁻ ions.....	149
4.5.3	Detection limits.....	151
4.5.4	The interference of the S ²⁻ and GeS ⁻ ions.....	152
4.6 .	CHEMICAL KINETICS STUDY OF THE SOL-GEL PROCESSING OF GeS₂	
4.6.1	Theoretical consideration.....	153
4.6.2	Reaction mixtures containing [H ₂ S] ₀ and [Ge(OEt) ₄] ₀ in ratio 9:1.....	163
4.6.3	Reaction mixtures containing [H ₂ S] ₀ and [Ge(OEt) ₄] ₀ in ratio 1:1.2.....	169
4.6.4	Reaction mixtures containing [Ge(OPr ⁱ) ₄] and [H ₂ S].....	171
4.6.5	Comparison of the Ge(OEt) ₄ and Ge(OPr ⁱ) ₄ chemical kinetics.....	175
4.7 .	INFLUENCE OF REACTION PARAMETERS ON THE MICROSTRUCTURE OF THE GeS₂ GEL	
4.7.1	Primary particle formation.....	179
4.7.2	Aggregation-gelation.....	184
4.7.3	Aging.....	187
4.7.4	Drying.....	189
CHAPTER 5	CONCLUSIONS	
5.1.	SUMMARY.....	191
5.2.	CONCLUSIONS.....	195
5.3.	FUTURE WORK.....	197
REFERENCES		199
APPENDIX I		208

LIST OF TABLES

Table 2.1	Alkoxides used for sol-gel synthesis of metal sulfides	16
Table 2.2	List of GeS ₂ gels produced by sol-gel processing	22
Table 2.3	Results of metal sulfides synthesis from various metal alkoxides	24
Table 2.4	Alkoxides and corresponding reaction solutions used for the thin film deposition	25
Table 2.5	The concentrations of reactants and their molar ratio used for reaction mixture preparation in the chemical kinetics study	28
Table 3.1.1	Content of S, O and Ge in the dried GeS ₂ gels determined using EDS analysis and S and O determined using EA analysis	47
Table 3.2.1	The XRD peak positions 2θ and d-spacing of the heat treated product and the standard GeS ₂ [77] shown along with their along deviations (Δ2θ)	51
Table 3.3.1	Influence of Ge(OEt) ₄ concentration on the microstructure of prepared GeS ₂ gels. The reactant ratio R was 2.5 for preparation of the gels	75
Table 3.3.2	Results of the BET analysis of gel IA aged 24 h and 30 days	76
Table 3.3.3	Influence of reactants ratio $R = [H_2S]/[Ge(OEt)_4]$ on the microstructure of GeS ₂ gels prepared at room temperature. The concentration of Ge(OEt) ₄ was 0.029 M for all prepared mixtures	78
Table 3.3.4	Influence of the reaction temperature on the microstructure of the	

GeS₂ gels prepared from [Ge(OEt)₄]₀=0.264 M and [H₂S]₀=	81
0.220 M	
Table 3.4.1 Tungsten sulfide sol-gel products	86
Table 3.6.1 Results of the electrode response to different ions obtained from	
the linear graphs in Fig 3.6.3	101
Table 3.6.2 Electrode response to GeS⁻ ions	103
Table 3.6.3 Selectivity coefficients obtained experimentally for different	
concentrations of pure primary GeS⁻ ion (C_{STH}) and mixtures	
of the primary (C'_{STH}) and interfering S²⁻ ion (C'_S)	105
Table 3.7.1 The thiolysis (k₁) and the condensation (k₃) rate constants	
obtained from apparent values k_{app}' and k_{app}'', respectively	
at different temperatures for the sol-gel process if [H₂S]₀/	
[Ge(OEt)₄]₀ is 9:1. The values are shown along with standard	
deviations (±σ)	113
Table 3.7.2 Activation energies, frequency factors, activation parameters and	
corresponding standard deviations (±σ) for the sol-gel reaction	
if [H₂S]₀/[Ge(OEt)₄]₀ is 9:1	114
Table 3 7.3 Thiolysis rate constants obtained at various temperatures for the	
sol-gel processing if [H₂S]₀/[Ge(OEt)₄]₀ is 1:1.2. The values are	
presented along with standard deviations (±σ)	118
Table 3.7.4 The thiolysis (k₁) and condensation (k₂) rate constants for the	
sol-gel process with [H₂S]₀/[Ge(OPrⁱ)₄]₀ ratio 2.25:1 at various	
temperatures. The constants are shown along with standard	

	deviations ($\pm\sigma$)	127
Table 3.7.5	Activation energy, frequency factor, activation parameters and standard deviations ($\pm\sigma$) for thiolysis and condensation when $\text{Ge(OPr}^i)_4$ is a precursor	127
Table A1	Concentration of H_2S and Ge(OEt)_2, the concentration ratio R and reaction temperatures used for study of their influence on the microstructure of GeS_2 gels. Corresponding gelation times are also shown along with these data	208
Table A2	The concentrations of sulfide (M) and mercaptide evolved in the sol-gel reaction, when $[\text{H}_2\text{S}]_0/[\text{Ge(OEt)}_4]_0$ is 9:1. The concentrations are in 10^{-3}M	209
Table A3	The concentrations of mercaptide (C) and sulfide (M) evolved in the sol-gel reaction for $[\text{H}_2\text{S}]_0/[\text{Ge(OEt)}_4]_0$ equal 1:1.2. The concentrations are in 10^{-3}M	210
Table A4	The concentrations of sulfide (M) and mercaptide (C) that appeared during sol-gel reaction of $\text{Ge(OPr}^i)_4$ and H_2S. The concentrations are in 10^{-3}M	211

LIST OF FIGURES

Fig. 3.1.1 XRD patterns of dried gels: a) 1A; b) 1B; c) 2; d) 3	32
Fig. 3.1.2 XRD patterns of heat treated gels: a) 1A; b) 1B; c) 2	34
Fig. 3.1.3 IR spectra of dried gels: a) 1A; b) 1B; c) 2; d) 3. Legend: ● (Ge-S-Ge); ▲ (Ge-O-Ge); ○ (Ge-OH); ◇ (Ge-SH); □ ethanol; □ toluene; ▣ toluene and ethanol	35
Fig. 3.1.4: IR spectra of heat treated gels: a) 1A; b) 1B; c) 2. Legend: ▲ GeS ₂ ; ○ GeO ₂	37
Fig. 3.1.5 Scanning electron micrographs of dried gels: a) 1A; b) 1B; c) 2; d) 3	39
Fig. 3.1.6 Scanning electron micrographs of heat treated gels: a) GeO ₂ crystal in 1A; b) GeO ₂ crystal in 1B; c) cross section of GeO ₂ crystal in 1A; d) cross section of GeO ₂ crystal in 1B; e) GeS ₂ phase in 1A; f) GeS ₂ phase in 1B; g) vermicular structure of 2	41
Fig. 3.1.7 Scanning electron micrographs of: a) gel 5 prepared upon the same same conditions as gel 2; b) gel 6 synthesized from Ge(OPr ⁱ) ₄ and all the other reaction conditions same as for gel 2	45
Fig. 3.2.1 XRD pattern of: a) the gel GeS _x -GeO _x ; b) monoclinic GeS ₂ obtained after heat treatment	49
Fig. 3.2.2 IR spectrum of: a) the gel GeS _x -GeO _x ; b) monoclinic GeS ₂ obtained after heat treatment of the gel	50
Fig. 3.2.3 Scanning electron micrographs of: a) the gel GeS _x - GeO _x ;	

- b) sulfur crystals deposited in the gel; c) sintered structure of monoclinic GeS_2 53
- Fig. 3.3.1 Observed changes in the sol-gel reaction mixture: a) Tyndall effect (gel IX); b) milky appearance of the mixture (gel XI); c) gelation (gel IA) 56**
- Fig. 3.3.2 Gels formed when $[\text{Ge}(\text{OEt})_4] \leq 0.044 \text{ M}$: a) gel III, $[\text{Ge}(\text{OEt})_4] = 0.044 \text{ M}$; b) gel V, $[\text{Ge}(\text{OEt})_4] = 0.022 \text{ M}$ 58**
- Fig. 3.3.3 Semi-transparent gel VI formed from $[\text{H}_2\text{S}] = 0.019 \text{ M}$ and $[\text{Ge}(\text{OEt})_4] = 0.029 \text{ M}$: a) gel monolith formed on the bottom of 250 mL flask; b) cracking of the monolith; c) pieces of dried gel VI occupy $\sim 5 \text{ cm}^2$ surface area 59**
- Fig. 3.3.4 Plot t_{gelation} vs. $[\text{Ge}(\text{OEt})_4]$ for $R=2.5$ 61**
- Fig. 3.3.5 Part of dried gel III is a typical structure formed during drying of all gels prepared from $[\text{Ge}(\text{OEt})_4] \leq 0.044 \text{ M}$ and $R=2.5$ 63**
- Fig. 3.3.6 Scanning electron micrographs of gels prepared from different concentrations of H_2S and $\text{Ge}(\text{OEt})_4$ and constant $R=2.5$: a) gel IA aged 24h, $[\text{Ge}(\text{OEt})_4] = 0.220 \text{ M}$; b) gel III, $[\text{Ge}(\text{OEt})_4] = 0.044 \text{ M}$; c) gel IV, $[\text{Ge}(\text{OEt})_4] = 0.029 \text{ M}$; d) gel V, $[\text{Ge}(\text{OEt})_4] = 0.022 \text{ M}$; e) gel IA aged 30 days 64**
- Fig. 3.3.7 Scanning electron micrographs of gels prepared with different ratios and $[\text{Ge}(\text{OEt})_4] = 0.029 \text{ M}$: a) gel XI, $R=0.93$; b) gel VII, $R=1.32$; c) gel VIII, $R=5$; d) gel IX, $R=10$ 68**
- Fig. 3.3.8 Scanning electron micrographs of gels synthesized at different**

temperatures: a) 30°C; b) 40°C; c) 45°C; d) 50°C	70
Fig. 3.3.9 BET adsorption-desorption isotherm of gel IV; insert presents pore size distribution obtained from the desorption branch of the isotherm	73
Fig. 3.3.10 Plot of surface area S_s vs. $[\text{Ge}(\text{OEt})_4]$ for $R=2.5$; particle radius r_p as a function of $[\text{Ge}(\text{OEt})_4]$ for $R=2.5$	74
Fig. 3.3.11 BET adsorption-desorption isotherm of gel XI; insert presents pore size distribution obtained from the desorption branch of the isotherm	77
Fig. 3.3.12 Plot of surface area $S_s=f(R)$ of gels prepared from $[\text{Ge}(\text{OEt})_4]=0.029 \text{ M}$ and $[\text{H}_2\text{S}]$; r_p vs. $R=[\text{H}_2\text{S}]/[\text{Ge}(\text{OEt})_4]_{\text{const.}}$	79
Fig. 3.3.13 BET isotherm of a gel prepared at 50°C; insert presents pore size distribution obtained from the desorption branch of the isotherm	80
Fig. 3.3.14 Plot of surface area $S_s=f(T)$ of gels prepared at various temperatures; average particle radius $r_p=f(T)$ of gels prepared at different temperatures	82
Fig. 3.4.1 XRD pattern of dried ZnS gel indicates the presence of β -ZnS	84
Fig. 3.4.2 Scanning electron micrograph of dried ZnS gel	85
Fig. 3.4.3 The IR spectrum of dried ZnS gel collected in the range from: a) 200-600 cm^{-1} ; b) 400-4000 cm^{-1}	86
Fig. 3.4.4 Scanning electron micrographs of tungsten sulfides : a) gel; b) powder	87

Fig. 3.4.5 XRD pattern of tungsten sulfide: a) gel; b) powder	89
Fig. 3.4.6 IR spectrum collected in the range from 400- 4000 cm⁻¹ of:	
a) tungsten sulfide gel; b) tungsten sulfide powder	90
Fig. 3.4.7 IR spectrum of tungsten sulfide powder collected in the range from	
200-600 cm⁻¹	92
Fig. 3.5.1 Scanning electron micrographs of the thin films: a) TF1, prepared	
from Ge(OEt)₄, solution 5; b) TF5, prepared from Zn(OBu^t)₂	93
Fig. 3.6.1 Potentiometric titration curves of the same samples of H₂S in toluene,	
titrated with:(○) 1x10⁻² M HgCl₂; (Δ) 1x10⁻² M AgNO₃.	95
Fig. 3.6.2 Potentiometric titration curves of the sample taken from the sol-gel	
reaction mixture after 3.5 h: a) 0.1 mL of the sample titrated with	
1x10⁻² M AgNO₃; b) 1 mL of the sample titrated with 1x10⁻² M	
AgNO₃ after removal of H₂S	97
Fig. 3.6.3 Electrode response to different ions plotted as E=f(logC_i). Graphs were	
obtained from data for: a) Fig. 3.6.1, part I, S²⁻ from H₂S titrated with	
HgCl₂ (□); Fig. 3.6.1, part I, S²⁻ from H₂S titrated with AgNO₃ (▲);	
Fig. 3.6.2, part I, S²⁻ from GeS₂ and GeS⁻ were present in the solution	
(Δ); Fig. 3.6.2, part II, only GeS⁻ was in the solution (●); b) Fig. 3.6.2a,	
part III, Ag⁺ from the excess AgNO₃ in the solution	100
Fig. 3.7.1 Potentiometric titration curves of samples undergoing the sol-gel	
reaction performed at 30°C with Ge(OPrⁱ)₄, titrated with AgNO₃.	
The samples were taken : 1) 0.5h; 2) 1.5h; 3) 2.5h; 4) 3.5h; 5) 4.5h;	
6) 5.5h, from the beginning of the reaction	107

Fig. 3.7.2 Concentration as a function of time for: M - sulfide ($\equiv\text{GeSGe}\equiv$);
 C - mercaptide ($\equiv\text{GeSH}$); A - ethoxy group ($\equiv\text{GeOEt}$), for the sol-gel
 reaction if $[\text{H}_2\text{S}]_0/[\text{Ge}(\text{OEt})_4]_0$ is 9:1. The reaction was performed
 at 50°C 108

Fig. 3.7.3 Plots of $-\ln([A]/[A]_0)$ as a function of time for various
 temperatures when $[\text{H}_2\text{S}]_0/[\text{Ge}(\text{OEt})_4]_0$ is 9:1 110

Fig. 3.7.4 Plots of reaction rate of sulfide formation $\Delta[M]/\Delta t$ as a function
 of mercaptide concentration [C] at various temperatures for the
 sol-gel process when $[\text{H}_2\text{S}]_0/[\text{Ge}(\text{OEt})_4]_0$ is 9:1 111

Fig. 3.7.5 Influence of the reaction temperature on the thiolysis (k_1) and the
 condensation (k_3) rate constants: a) Arrhenius plot, $\ln k$ vs. $(1/T)$;
 b) transition-state theory plot, $\ln(k/T)$ vs. $(1/T)$, for the sol-gel
 process if $[\text{H}_2\text{S}]_0/[\text{Ge}(\text{OEt})_4]_0$ is 9:1 112

Fig. 3.7.6 Mass balance as a function of time for the sol-gel process if $[\text{H}_2\text{S}]_0/$
 $[\text{Ge}(\text{OEt})_4]_0$ is 1:1.2. The concentrations of sulfide M and mercaptide
 C were determined experimentally, while the concentrations of ethoxy
 group A and hydrogen sulfide B were calculated. The reaction was
 performed at 50°C. 116

Fig. 3.7.7 Plot of $-\ln([Y]/[Y]_0)$ as a function of time if Y is: ethoxide group
 concentration [A]; hydrogen sulfide concentration [B]. The reaction
 was performed at 50°C with the $[\text{H}_2\text{S}]_0/[\text{Ge}(\text{OEt})_4]_0$ ratio 1:1.2. 117

Fig. 3.7.8 Plots of $\frac{1}{[B]_0 - [A]_0} \ln \frac{[A]_0[B]}{[B]_0[A]}$ as functions of time made for the induction

period at different reaction temperatures and a $[\text{H}_2\text{S}]_0/[\text{Ge}(\text{OEt})_4]_0$

ratio 1:1.2

119

Fig. 3.7.9 Functional relationship of the thiolysis constant (k_1) with temperature: a) Arrhenius plot, $\ln k$ vs. $(1/T)$; b) transition-state theory plot, $\ln(k/T)$ vs. $(1/T)$, for the sol-gel process with $[\text{H}_2\text{S}]_0/[\text{Ge}(\text{OEt})_4]_0$ ratio 1:1.2

120

Fig. 3.7.10 Mass balance of components present in the sol-gel process reaction mixture containing the $[\text{H}_2\text{S}]_0/[\text{Ge}(\text{OPr}^i)_4]_0$ in ratio 2.25:1 : M- sulfide; C- mercaptide; A-isopropoxide group concentrations. The reaction was performed at 40°C

123

Fig. 3.7.11 Determination of the reaction order of the sol-gel process with $[\text{H}_2\text{S}]_0/[\text{Ge}(\text{OPr}^i)_4]_0$ ratio 2.25:1, performed at 40°C. Plots $-\ln([Y]/[Y]_0)=f(t)$ for: ethoxide group (A); hydrogen sulfide (B)

124

Fig. 3.7.12 Plots of $\frac{1}{[B]_0 - [A]_0} \ln \frac{[A]_0[B]}{[A][B]_0}$ as a function of time for various reaction temperatures. The slopes of the plots are assigned to k_1

125

Fig. 3.7.13 Plots of concentration of sulfide $[M]$ as a function of the mercaptide concentration-time integral, $\int_0^t [C]^2 dt$, for various temperatures. The slopes of these lines are assigned to the constant k_2

126

Fig. 3.7.14 Influence of reaction temperature on the thiolysis (k_1) and condensation (k_2) rate constants: a) Arrhenius plot, $\ln k$ vs. $(1/T)$;

b) transition-state theory plot, $\ln(k/T)$ vs. $(1/T)$ 128

Fig. 4.6.1 Free energy-reaction coordinate diagram for the sol-gel processing of GeS_2 when $[\text{H}_2\text{S}]/[\text{Ge}(\text{OEt})_4]_0$ is 9:1 168

Fig. 4.6.2 Free energy-reaction coordinate diagram for the sol-gel process if $[\text{H}_2\text{S}]/[\text{Ge}(\text{OPr}^i)_4]_0$ is 2.25:1 176

SYMBOLS AND ABBREVIATIONS

SYMBOL	QUANTITY	SI UNITS
A	frequency factor for second order reaction	$(M \cdot s)^{-1}$
A	constant in Debye-Hückel equation	$\text{mole}^{-1/2}$
a_i	ion activity	M
B	constant in Debye-Hückel equation	$\text{mole}^{-1/2}\text{cm}^{-1}$
cm^{-1}	wave number	-
E	electrode potential	V
$E^{\circ'}$	apparent standard electrode potential	V
E_a	activation energy	kJmole^{-1}
E_g	band gap, 1.602×10^{-19}	$\text{CV}(=eV)$
F	Faraday's constant, 9.648×10^4	Cmole^{-1}
h	time, 3600	s (1 hour)
h	Planck's constant, 6.626×10^{-34}	J s
I	ionic strength	M
k	Boltzmann's constant, 1.381×10^{-23}	JK^{-1}
$K_{\text{Ag}_2\text{S}}$	solubility product of Ag_2S	-

k_{app}	apparent reaction rate constant for the pseudo first order reaction	s^{-1}
k_n	$n=1,2,3$, reaction rate constant for second order reaction	$(M \cdot s)^{-1}$
K_S	solubility product for silver sulfide complex	-
K_{SH}	solubility product for silver mercaptide complex	-
$k_{SH,S}^{pot}$	selectivity coefficient	-
M	molar concentration	$mol\,dm^{-3}$
N	normal concentration	$equivalent\,dm^{-3}$
n	number of electrons involved in electrochemical reaction	-
N_A	Avogadro's number, 6.022×10^{23}	$mole^{-1}$
nm	length, nanometre	$10^{-9}m$
p	stoichiometric coefficient for electrode reaction, $1/n$	-
q	stoichiometric coefficient for electrode reaction, $1/n$	-
R	gas constant, 8.314	$JK^{-1}mole^{-1}$
r'	nucleus radius	$10^{-9}m$
R_p	average pore radius	$10^{-9}m$
r_p	average particle radius	$10^{-9}m$
S_a	specific surface area	$10^{-3}m^2kg^{-1}$ ($=m^2/g$)
torr	pressure, 133.32	Pa

W^*	energetic barrier for spherical nucleus formation during sintering	kJmole^{-1}
wt%	concentration, weight percentage	-
vol%	concentration, volume percentage	-
$Z_{+(-)}$	ion charge	-
γ_i	activity coefficient	-
γ_{SL}	solid-liquid surface tension	kJmole^{-1}
ΔG°	standard free energy of compound formation	kJmole^{-1}
ΔG^\ddagger	standard free energy of activation complex formation	kJmole^{-1}
ΔG_V	volume free energy of spherical nucleus formation	kJmole^{-1}
ΔG^*	standard free energy for spherical nucleus formation in homogeneous nucleation	kJmole^{-1}
ΔH	reaction enthalpy	kJmole^{-1}
ΔH^\ddagger	standard free enthalpy of activation complex formation	kJmole^{-1}
ΔS^\ddagger	standard free entropy of activation complex formation	$\text{JK}^{-1}\text{mole}^{-1}$
ϵ_r	dielectric constant	-
ρ	density	$10^3\text{kgm}^{-3}(=\text{g/cm}^3)$
η	viscosity	$\text{Pa} \cdot \text{s}(=10\text{poises})$

ABBREVIATION**NAME**

(A)	alkoxide group (OEt) or (OPr ⁱ)
Al(OBu ^s) ₃	aluminum sec-butoxide, Al(OC ₄ H ₇ ^s) ₃
(B)	hydrogen sulfide, H ₂ S
BET isotherm	Brunauer, Emmett and Teller isotherm
(BzS) ₂ S	dibenzyl trisulfide, (C ₆ H ₅ CS) ₂ S
C	concentration
(C)	mercaptide, SH
(D)	alcohol, EtOH or Pr ⁱ OH
EDS	energy dispersive spectrometry
E _N 2	bimolecular nucleophilic elimination reaction
Et ₂ Zn	zinc ethyl, (C ₂ H ₅) ₂ Zn
Ge(OEt) ₄	germanium ethoxide, Ge(OC ₂ H ₅) ₄
Ge(OPr ⁱ) ₄	germanium isopropoxide, Ge(OC ₃ H ₇ ⁱ) ₄
HPLC	high performance liquid chromatography
IR spectroscopy	infrared spectroscopy
M-O	metal-oxygen bond
M(OR) _n	metal alkoxides
NIR spectroscopy	near infrared spectroscopy
NMR	nuclear magnetic resonance
O	oxide, O ²⁻
OR	alkoxide group

Pr	2-propanol
2-PrOH	2-propanol (isopropyl alcohol), $\text{C}_3\text{H}_7\text{OH}$
R	ratio of the molar concentrations of reactants, $[\text{H}_2\text{O}]/[\text{alkoxide}]$ or $[\text{H}_2\text{S}]/[\text{alkoxide}]$
SEM	scanning electron microscopy
$\text{S}_{\text{N}}2$	bimolecular nucleophilic substitution reaction
T	toluene
T	temperature, K or $^{\circ}\text{C}$
TFN	thin film N=1-6
TOES	tetraethoxysilane, $\text{Si}(\text{OC}_2\text{H}_5)_4$
TS1	transition state of thiolysis
TS2	transition state of condensation
$\text{W}(\text{OEt})_6$	tungsten ethoxide, $\text{W}(\text{OC}_2\text{H}_5)_6$
$\text{WCl}_2(\text{OEt})_3$	tungsten dichloride ethoxide, $\text{WCl}_2(\text{OC}_2\text{H}_5)_3$
V_{eq}	volume of titrant at equivalence point
XRD	x-ray diffraction
$\text{Zn}(\text{O}i\text{Bu})_2$	zinc tert-butoxide, $\text{Zn}(\text{OC}_4\text{H}_7)_2$

CHAPTER 1

INTRODUCTION

1.1. APPLICATIONS OF METAL SULFIDES

In 1880. Alexander Graham Bell invented the photophone, a device which transformed sound into light and transmitted the light to a detector[1]. The photophone was the beginning of the information transmission era which today utilizes more complicated electro-optical systems so called Integrated Optics[1]. Tendency is to use CO and CO₂ lasers operating in the middle and far infrared spectral ranges as the light sources in these systems today.

Semiconductor materials, such as the sulfides of group II-IV elements, are promising materials for infrared operating Integrated Optical systems. These materials have band gaps $E_g > 2\text{eV}$ [2] and thus they are transparent to wavelengths from 2-15 μm . They also have low intrinsic transmission losses in this spectral region. These characteristics qualify them for applications such as infrared lenses, windows and optical fibres. For instance,

germanium disulfide has ten times lower absorption than silica in the far IR region[3] and is an excellent material for the CO₂ laser beam delivery optical fibre.

Moreover, some metal sulfides (ZnS, CdS, Ag₂S) are photoconducting due to high efficiency in producing the excess of current carriers when the valence electrons are optically excited. The potential applications of these metal sulfides are as solar cell materials and photodetectors. Zinc sulfide is also a photo and electroluminescent material and thus a good photo/ electro converting material. Because of this property it can be applied as a coating on fluorescent lamps, colour television screens and light-emitting diodes. Transition metal sulfides are very interesting materials for technical applications. For instance, tungsten disulfide can be used as a lubricant due to its layered structure [4]. Also, it is a photoconductive material suitable for photovoltaic applications [5,6] as well as a catalyst [7]. The electronic and optical properties of semiconductors are strongly affected by impurities and inhomogeneity in the material, most of which are a result of the preparation process. For instance, impurities can change the nature of the conducting process of a semiconductor or decrease its light and electron conductivity. The best material for electro-optical applications would be a monocrystal. Since it is very difficult to produce a monocrystal and to control its properties (band gap and refractive index) glasses are used to overcome these shortcomings. Moreover, high quality monocrystals are virtually impossible to produce by high temperature methods[8]. Instead, by using an appropriate synthesis method, the transmission losses of the prepared material could be minimized to the level of intrinsic losses based on the pure material properties. The

sol-gel process is a method providing a homogeneous product with a low level of impurities, a controlled structure and stoichiometry.

1.2. SOL-GEL PROCESSING

The sol-gel processing represents the chemical synthesis of ceramics in solutions at low temperature wherein the reaction products such as colloidal powders or gels can be prepared[9]. There are numerous advantages of this process. For example, the product purity can be controlled by using refined precursors as well the low processing temperature which inhibits the precursor reaction with reactor walls. Additionally, the homogeneity of solution is achieved at the molecular level. Since the sol-gel product is prepared by chemical synthesis, its microstructure can be controlled by the chemical reaction parameters. The products of the sol-gel processing having high surface areas can be densified by sintering at much lower temperatures than in conventional preparations. The sol-gel processing has been extensively studied for the preparation of advanced oxide ceramics. However, it has also great potential for metal sulfide synthesis.

The first attempt to synthesize a colloidal metal sulfide was reported in 1982 by Matijević and Wilhelmy[10]. They synthesized monodispersed CdS particles, using $\text{Cd}(\text{NO}_3)_2$ and hydrolysed thioacetamide. By controlling the reaction conditions, including pH, concentration, temperature, and the nature of the anions, particle nucleation and growth was controlled in order to obtain a monodispersed CdS sol.

In 1984, Melling[11] explained the first effort to synthesize metal sulfides from metal alkoxides and H₂S. He produced GeS₂ by reacting Ge(OEt)₄ dissolved in toluene with H₂S gas bubbled through the solution. Since alkoxides easily hydrolyze, Melling had previously purged the reaction apparatus with inert gas. The reaction product was a GeS₂-gel with significant GeO₂ impurities. Seddon et al.[12] repeated Melling's[11] experiment and proved by IR spectroscopy that the reaction product was not pure GeS₂, but a mixture of GeS₂ and GeO₂. They proposed that water impurity was the reason for GeO₂ formation during GeS₂ synthesis.

Johnson et al.[13], also used sol-gel synthesis for metal sulfide production. They used organometallic compounds of Zn, Al, and Mg, and H₂S as precursors and obtained metal sulfide particle aggregates.

An attempt to synthesize a lanthanum metal sulfide by bubbling H₂S through the metal alkoxide solution was made by Kumta and Risbud[14]. They used lanthanum alkoxide and hydrogen sulfide as precursors, and dry benzene as a solvent. They heat treated the powder in H₂S, finally producing single-phase La₂S₃. The most recent sol-gel synthesis of a metal sulfide was carried out by Sriram and Kumta[15]. They synthesized amorphous, monodispersed particles by reacting Ti(OC₃H₇)₄ and H₂S gas. They heat treated the powder in flowing H₂S producing crystalline TiS₂.

Various methods have been successfully employed for zinc sulfide powder synthesis in solutions[16-25]. From aqueous solutions [16-20], the ZnS powder was precipitated using zinc containing salts such as zinc sulfate[16-18], zinc nitrate [18,19], zinc chloride [18] and zinc tetramine chloride[20], and sulfur donating compounds

thioacetamide[17,18,20], hydrogen sulfide[17] and ammonium sulfide[20]. However, for the synthesis of ZnS in nonaqueous solutions[21-25], usually organometallics were used as the zinc sources and either hydrogen sulfide gas[21-25] or dibenzyl trisulfide[21] were employed as the sulfur sources. Not only ZnS was precipitated, but also a ZnS gel was obtained[25].

This short review shows that considerable success has been achieved in terms of sol-gel synthesis of metal sulfides. Any inorganic or organic compound containing metal or sulfide ion of the future metal sulfide can be used as precursor. The precursors of the cation and sulfide must be soluble in a mutual solvent and react easily at chosen temperature. Metal alkoxides[26] are the precursors very often used in sol-gel synthesis due to their reactivities and ease of purification. Metal alkoxides with general formula $M(OR)_n$ are considered as alcohol derivatives. They involve polarized $M^{\delta+}-O^{\delta-}-C$ bonds whose degree of polarization depends on the electronegativity of the metal atom. Alkoxides are covalent compounds consisting of volatile monomers if prepared from electronegative elements like silicon and germanium. However, they are electrovalent polymeric solids such as in the case of electropositive alkali and alkaline earth metals. For the same metal atom, the covalent character of the M-O bond increases with the greater inductive effect of the alkyl group. Thus, the alkoxide with tertiary carbon (3°) atoms in the bonded alkyl groups has higher covalent character in comparison to those alkyl groups containing only primary (1°) carbon atoms.

Metal alkoxides are generally very reactive compounds due to the presence of the polarized M-O bond. It makes metal atoms very susceptible to nucleophilic attack.

Moreover, the alkoxy group is a strong base. It is able to react as a nucleophile in substitution reactions or as a base in elimination reactions. Which type of reaction will occur depends on the reaction parameters such as concentration of precursors, structure of alkoxide (1°, 2° or 3°), solvent and reaction temperature.

Although the idea of chemical synthesis of metal sulfide compounds using alkoxides and H₂S originates in the sol-gel preparation of oxides from alkoxides and H₂O, it is important to recognize that there are significant difference in the chemical properties of oxygen and sulfur that may influence these reactions. Perhaps the most important is lower electro-negativity of sulfur which causes that the sulfide compounds are more covalent and less susceptible to hydrogen bonding. In addition, the bigger covalent radius and the same charge as that of an oxygen ion makes H₂S a stronger acid than water. The diffuse electrons in the valence shell also cause H₂S to have a weaker dipole moment than water.

Since H₂S has free electron pairs located in two sp³ hybrid orbitals it is able to donate them to free electron orbitals in the metal atoms of alkoxides. However, if water is present in the same reaction system then it will react with alkoxide instead of hydrogen sulfide as the stronger base. Then the reaction product is a mixture of both metal oxide and metal sulfide. This indicates that further precautions are needed to eliminate water. Therefore, in order to get pure metal sulfides, additional conversion reactions under H₂S have to be undertaken[14,15]. An unhygroscopic solvent such as toluene, is an appropriate liquid medium for the sol-gel processing of metal sulfides from metal alkoxides since they easily hydrolyse. Moreover, it is a common solvent for both metal

alkoxides and hydrogen sulfide.

I believed that the first step in successful metal sulfide preparation by this reaction would be the findings of the oxide formation cause. Therefore, the germanium disulfide gel was prepared directly by the methods previously reported in [11] and [12], but with special precautions to protect the reaction mixture from exposure to any water impurity. It was concluded that the main source of water was the H₂S gas[27]. The reaction conditions used for the synthesis of the pure germanium sulfide were applied for the synthesis of other metal sulfides. Thus, in the present study, tungsten sulfide colloidal powder was obtained from WCl₂(OEt)₃, while a gel was prepared from W(OEt)₆[28]. Also, zinc sulfide gel was synthesized from zinc tert-butoxide, Zn(OBu^t)₂[29].

Moreover, an original approach to metal sulfide synthesis is demonstrated by the example of monoclinic germanium disulfide, which was produced by reduction of the sol-gel product with elemental sulfur[30]. Sulfur was produced by oxidizing H₂S in the presence of concentrated sulfuric acid, per the following reaction:



Sulfur made a colloidal suspension in sulfuric acid, and it was extracted and homogeneously distributed in the toluene solution of germanium ethoxide by the H₂S gas flow. The sol-gel reaction product was characterized by various methods before and after heat treatment.

1.3. CONTROLLING THE MICROSTRUCTURE

Sol-gel processing of ceramics materials consists of chemical changes succeeded by phase transformations, dictated by the chosen reaction conditions. One of the most important advantages of the sol-gel process is that it provides an opportunity to dictate the microstructure of the future ceramics during chemical reaction. For example, if structural ceramics are required, then monodispersed powders are prepared. If the ceramics is to be used as catalyst, then colloidal particles with rough surface are required. If thin films are to be prepared, then polymeric gels are necessary. Therefore, the proper understanding of the phase transformation mechanism and how it can be controlled by reaction conditions are essential to the generation of the desired materials.

Due to its importance, this area of the sol-gel science attracted almost every scientist involved. The list of people who successfully obtained materials under defined reacting conditions and explained the phase transformation mechanism is long[9,31]. However, from this extensive body of literature, there are few papers which can be chosen for comparison because similar chemical systems involving alkoxide precursors in nonaqueous solvents were treated.

A widely used method for preparing spherical monodispersed silica particles was developed by Stöber, Fink and Bohn[32] from TEOS in a basic solution of water and alcohol. They examined the influence of H₂O and NH₃ concentrations on the sizes of prepared particles when the concentration of TEOS was 0.28 M. They found out that the size of the silica spheres increased for all concentrations of NH₃ up to 7M. They

prepared silica sols for a concentration ratio R ranging from 20 to 50.

Performing the reaction originally proposed by Stöber et al.[32] at low temperature and using tetrapentylorthosilicate as precursor, Tan et al.[33] prepared larger silica colloids, size $\sim 2 \mu\text{m}$.

Fegley and Barringer[34] synthesized amorphous monodispersed spherical colloidal powders of TiO_2 , ZrO_2 , SiO_2 and $\text{ZrO}_2\text{-Al}_2\text{O}_3$ from corresponding alkoxides. Subsequently, they studied of the influence of alkoxides on the particle monodispersity and sphericity[35]. They found that non-agglomerated ZrO_2 monodispersed spheres could be made from Zr n-propoxide but not from Zr isopropoxide. Also, agglomerated particles were generated if isopropanol was the solvent. Narrower particle distribution were obtained by Ogihara et al.[36] from Zr butoxide in ethanol when the influence of concentration and ratio of Zr butoxide and water were studied.

The discovery of Yoldas[37,38] that alumina gel monolith can be prepared by hydrolysis and condensation of aluminum alkoxides started a new era in the sol-gel research. Yoldas obtained fibrillar boehmite from $\text{Al}(\text{O}^i\text{Bu})_3$ and large excess of water ($R = 100\text{-}200$) in the temperature range $80\text{-}100^\circ\text{C}$. Adding acid yielded a stable sol. When hydrolysis was performed at room temperature, an amorphous precipitate was prepared, that converted into crystalline bayerite upon aging. Gelation was achieved by concentrating the sol via boiling or evaporation. The influences of the concentration ratio R, acid content and temperature on the microstructure of alumina gel were studied by Chane-Ching and Klien[39,40].

Yolads[41] investigated the preparation of ZrO_2 by hydrolysis and condensation of

alkoxides and the parameters that affected their morphology. He showed that it is possible to prepare clear gels only if the acid catalysts are HNO_3 or HCl and the $[\text{acid}]/[\text{alkoxide}]$ ratio is less than 0.3.

Komarneni et al.[42] prepared titania gels by controlling the ratio R , $[\text{H}_2\text{O}]/[\text{alkoxide}]$ and the reactant concentrations. They prepared polymeric titania gel from titanium isopropoxide and for $R < 1$.

Preparation of tungsten oxide gels from different alkoxides and at different temperatures was performed by Yamaguchi et al.[43]. They obtained amorphous polymeric WO_3 gel at 20°C .

Silica gels can also be prepared from silicon alkoxides by varying reaction conditions. Thus, using acidic conditions and an $[\text{H}_2\text{O}]/[\text{TEOS}]$ ratio 10, Nogami and Moriia[44] prepared polymeric silica gel. Brinker et al.[45] obtained silica gels by performing two step hydrolysis. In the first step they used a concentration ratio, $[\text{H}_2\text{O}]/[\text{TEOS}]$, $R=1.1$ and acid conditions. The second step varied. If $3[\text{H}_2\text{O}]/[\text{TEOS}]$ was added under acidic conditions, a polymeric silica gel was formed. However, when $4[\text{H}_2\text{O}]/[\text{TEOS}]$ was added under basic conditions, colloidal silica gel was obtained.

Klein et al.[46] studied the influence of $[\text{H}_2\text{O}]/[\text{TEOS}]$ molar ratio on gel structure, using HCl or NH_4OH as catalyst. They concluded that reaction rates of hydrolysis and condensation determine resulting dried microstructure. Catalyst concentration and water level were varied in the TEOS -water-ethanol system. Increased water level increased the rate of hydrolysis in both cases. Increasing the base addition decreases surface area and porosity. Acid-catalyzed solutions give transparent gels, while base-catalyzed result in

translucent or opaque gels.

Fahrenholtz and Smith[47] used mixtures of TEOS and methyl-substituted silicon alkoxides for the silica gel preparation. For base catalyzed reactions, gel surface area, pore volume and density dramatically decreased with use of the modified alkoxide. Mechanical strength of the gels prepared by acid catalyzed reactions dropped proportionally to the methyl content.

In this work, a study of the influence of reaction conditions on the structure of GeS_2 gel synthesized by the sol-gel processing from H_2S and $\text{Ge}(\text{OEt})_4$ in toluene is presented[48]. The parameters studied were reactant concentrations, concentration ratio R and reaction temperature. It is demonstrated that the main influence on the structure of the GeS_2 gels is exerted by the concentrations of H_2S and $\text{Ge}(\text{OEt})_4$.

In order to interpret the results correctly, the chemical kinetics of the sol-gel reaction was examined[49,50]. The connection between the sol-gel process kinetics and the product microstructure can be illustrated by the following sequence[9]:

solvolysis (hydrolysis, thiolysis) → condensation → nucleation →
growth → aggregation

The chemical reactions, hydrolysis or thiolysis, and condensation are succeeded by the phase transformation, nucleation, growth and aggregation giving the connection between reaction chemistry and product structure.

In the sol-gel literature numerous publications concerning the process of hydrolysis

and condensation of silicon alkoxides exist. These investigations show that under well defined conditions detailed statements about reaction mechanism can be made. The following brief review of research on the kinetics of the sol-gel processing of silica illustrates the most important achievements in the investigations of the most frequently studied sol-gel prepared materials.

One of the earliest attempts at a theoretical explanation of the polymerization mechanism of silicic acid on the basis of donor-acceptor properties was made by Strelko[51]. McNeilet et al.[52] determined the apparent hydrolysis reaction constants of tris(2-methoxyethoxy)-phenyl silane at different temperature. The importance of this work is that for the first time reaction of the silica precursors was studied in a purely aqueous medium and activation parameters were determined.

Assink and Kay[53] introduced proton nuclear magnetic resonance (^1H NMR) spectroscopy in investigations of both the temporal and chemical nature of sol-gel reactions. One of their first studies was sol-gel kinetics of the functional groups in the acid catalyzed reaction of $\text{Si}(\text{OCH}_3)_4$ and H_2O [54]. Their work continued to a theoretical kinetic formalism which specifically treats the evolution of various transient groups at a silicon atom undergoing hydrolysis and condensation[54-57].

The kinetics of $\text{Si}(\text{OC}_2\text{H}_5)_4$ sol-gel polymerization using ^{29}Si NMR spectroscopy was studied by Pouxviel et al.[58]. They used mathematical simulations of the reaction mechanism in order to predict the size of the colloidal particles formed[59].

In order to explore the possibility of reducing gelation time without affecting the characteristics of the resulting gel, Artaki et al.[60] investigated the influence of pressure

on the polymerization kinetics of $\text{Si}(\text{OCH}_3)_4$ in an acid catalyzed reaction. However, Ro et al.[61] examined the acid catalytic reactions of $\text{Si}(\text{OC}_2\text{H}_5)_4$ by measuring temperature profile during hydrolysis.

A new method, cylindrical attenuated total reflectance infrared spectroscopy, for monitoring in-situ kinetics of the sol-gel process of acidic $\text{Si}(\text{OC}_2\text{H}_5)_4$ and $\text{Al}(\text{NO}_3)_3 \cdot 9\text{H}_2\text{O}$ ethanol-water solutions was employed for the first time by Kline et al.[62]. They determined the reaction rate constants at various temperatures and did computer modelling on the experimental results of concentration as a function of time[63].

The effect of various base catalysts on the reaction kinetics of $\text{Si}(\text{OC}_2\text{H}_5)_4$ in ethanol-water solutions was studied by Sanchez et al.[64]. They obtained apparent activation energies from simplified kinetics model.

Liu et al.[65] reported results of ^1H and ^{13}C NMR characterizations performed on a system of methyl-threemethoxysilane as the precursor and ethanol as the solvent. Their results revealed complicated structures of the reaction intermediates.

The present study of the chemical kinetics of the sol-gel processing of GeS_2 from different germanium alkoxides and hydrogen sulfide in toluene solution contributed to a new era of the sol-gel processing of metal sulfides. The study shows that the reaction mechanism of this chemical process is complex consisting of thiolysis and condensation reactions. It is expected that thiolysis products are intermediates, germanium mercaptides, $\text{Ge}(\text{OR})_{4-n}(\text{SH})_n$, which upon further reaction yield sulfide species $\text{Ge}(\text{SH})_{4-n}\text{S}_n$, where n could be from 1 - 4.

For measurements of reaction parameters, rate constants and activation energies,

physicochemical methods are usually employed, such as light or mass spectroscopy, nuclear magnetic resonance, gas chromatography and conductometry. There were numerous limitations in choosing an appropriate method for determination of the time evolution of functional group concentrations during sol-gel processing of GeS_2 . Some of them are due to an inability to prepare a standard $\text{Ge}(\text{SH})_n$ solution for IR spectroscopy, or to detect the ethyl alcohol that forms at concentrations less than 10^{-2} M by near infrared (NIR) spectroscopy. Moreover, nuclear magnetic resonance requires very high reactant concentrations, $\approx 2\%$, which cause high reaction rates making measurements of reaction rate constants difficult. Thus, potentiometric titration with the ion selective electrode $\text{Ag}/\text{Ag}_2\text{S}$ was chosen for determination of H_2S , germanium disulfide (GeS_2) and mercaptide (GeSH) present in the reaction mixture[66]. The $\text{Ag}/\text{Ag}_2\text{S}$ electrode was equally suitable for potentiometric titration of both sulfide and mercaptide.

Extensive research on the suitability and applicability of the $\text{Ag}/\text{Ag}_2\text{S}$ electrode was performed in the sixties and seventies in its diverse applications in the pulp industry [67-70], pharmacology[71-74], petrochemistry[75-79] and pollution[80,81].

In this work, quantitative determination of germanium disulfide and mercaptide by potentiometric titration is demonstrated using the following electrochemical cell:



It also describes the optimum conditions for quantitative measurements of metal sulfide and mercaptide in the presence of each other. Existing standard methods[82,83] for H_2S

elimination from the sample were not applicable due to the solubility of germanium sulfide and germanium mercaptide in water. Therefore, an original way of eliminating the H_2S gas from the titration mixture was demonstrated. In addition, a different approach was used for the reaction scheme at the electrode interface. Furthermore, a modified equation for the ion selective Ag/Ag_2S electrode potential dependence on mixed ion concentrations was proposed, which agreed with experimental results.

Knowledge and understanding of this sol-gel reaction mechanism helped to interpret the results. They indicate that the primary particles grow by a monomer-cluster reaction-limited mechanism, whereas the gels were formed by reaction-limited cluster-cluster mechanism.

CHAPTER 2

EXPERIMENTAL PROCEDURE

2.1. MATERIALS

2.1.1. Metal alkoxides

List of metal alkoxides used for the sol-gel processing of metal sulfides is presented in Table 2.1. The alkoxides were used as received, with no additional purification.

Table 2.1: Alkoxides used for the sol-gel synthesis of metal sulfides

N°	Chemical formula	Concentration	Supplier
1	$\text{Ge}(\text{OC}_2\text{H}_5)_4$	99.99 % in ethanol	ALDRICH
2	$\text{Ge}(\text{OC}_3\text{H}_7)_4$	99.99 % in isopropanol	PROCHEM
3	$\text{SrTi}(\text{OC}_3\text{H}_7)_4$	5 g/100 mL isopropanol	CHEMAT
4	$\text{W}(\text{OC}_2\text{H}_5)_6$	10 g/100 mL ethanol	CHEMAT
5	$\text{WCl}_2(\text{OC}_2\text{H}_5)_3$	20 g/100 mL ethanol	CHEMAT
6	$\text{Zn}(\text{OC}_4\text{H}_9)_2$	10g/100mLtert.butanol	CHEMAT
7	$\text{Si}(\text{OC}_2\text{H}_5)_4$	98.00 % in ethanol	ALDRICH
8	$\text{Zr}[\text{O}(\text{CH}_2)\text{CH}_3]_4$	80 g/100g butanol	ALDRICH

2.1.2. Toluene

In the sol-gel processing toluene was used as a solvent. It was supplied by Fisher Scientific, HPLC grade. Even though the toluene had a low water content, (<0.02%), it was dried prior to use in order to get a water free reaction.

2.1.3. Hydrogen sulfide

The hydrogen sulfide gas, used in the sol-gel processing was supplied by Linde Canada (99.6% H₂S). Hydrogen sulfide was dried before it was introduced into the pure toluene or the alkoxide solution in toluene.

2.1.4. Titrants

Silver nitrate 0.01 N solution was prepared by dissolving AgNO₃ (Fisher Scientific, 99.99 %) in 2 mL distilled water and then by diluting to 1 L with 2-propanol (BDH, 99.8 %). It was standardized with 0.01 N NaCl (Fisher Scientific, 99.99 %) potentiometrically using the same instrument set up. Lower concentration AgNO₃ solutions used for titrations were prepared by diluting the base solution with 2-propanol to 1x10⁻³ N and 1x10⁻⁴ N. Mercury (II) chloride was prepared similarly from reagent grade HgCl₂ also supplied by Fisher Scientific.

2.1.5. Electrolyte

The electrolyte was prepared from sodium acetate (Fisher Scientific, 99.99 %) dissolved in 5 mL of distilled water and then in 2-propanol to make 1 L of 0.005 M

solution. The pH of the electrolyte was ≈ 8.6 .

2.2. EQUIPMENT

2.2.1. Glove box

Since the metal alkoxides are water sensitive compounds, all manipulations with them and the sol-gel reaction products were performed under a dried nitrogen atmosphere in a glove box.

The glove box consists of two chambers: transfer and main. The transfer chamber serves for transport of glassware and chemicals in and out of the main chamber. After every opening and air entry the transfer chamber was purged with nitrogen.

Before manipulation with the alkoxides and the sol-gel reaction products, the main chamber was purged with nitrogen, also dried by passing the flow through a column filled with CaSO_4 desiccant.

2.2.2. Down draft hood

Since hydrogen sulfide is an extremely poisonous gas, heavier than air, the down draft hood was used for all the experiments with the H_2S gas. In addition, the hydrogen sulfide detector was a necessary device for safety precautions.

2.2.3. Magnetic stirrer

A laboratory magnetic stirrer was used to improve the mixing of chemicals during titrations and sol-gel reactions, and the dissolution of H₂S in toluene.

2.2.4. Thermostat

A constant-temperature bath HAAK 20 was used to maintain the reaction temperature during the chemical kinetics measurements. The thermostat was filled with ethylene glycol and provided with both heating and cooling systems. The temperature of the reaction mixtures placed in the bath was held constant within $\pm 0.1^{\circ}\text{C}$ by circulating the bath liquid.

2.2.5. Equipment for the emf measurements

All the cell emf measurements were taken with an Accumet, model 55, pH/ion conductivity meter. The Ag/Ag₂S ion selective electrode was the ORION 94-16A electrode. The reference electrode was a Fisher Scientific saturated calomel electrode. Connection between the reference electrode and the test solution was made with a constrained-diffusion junction (porous diaphragm) filled with 0.1M KNO₃ solution. For pH measurement, an ORION glass electrode was used connected to the same Accumet 55 meter.

2.2. Glassware

Hydrogen sulfide was introduced into toluene or the alkoxide-toluene solutions through a glass tube dispenser (Fisher Scientific 12C). The various sizes (20, 50, 150, 250 and 1000 mL) of the glass erlenmeyers with side arms were used for this purpose. However, ordinary erlenmeyers of different sizes were employed for the preparation of reaction mixtures from the H₂S-toluene solution already made. A 50 mL glass cylinder capped with a rubber septum was used for the chemical kinetics measurement reaction.

Liquids were roughly measured by graduated cylinders (10, 25 and 50 mL). For more precise measurements glass pipets and syringes were used. For preparation of standard solutions, volumetric flasks were employed.

A 50 mL burette, graduated in 0.1 mL intervals was used for addition of titrant. The potentiometric titration was performed in 100 mL glass beakers.

For toluene purification a glass reflux and a water condenser, size 24/40, were used. The toluene and metal sodium mixture was heated in a 1 L round bottom flask. The condensate was collected in a 0.5 L Winchester bottle.

2.3. PURIFICATION OF CHEMICALS

2.3.1. H₂S drying

To prevent water contamination of the reaction solution, hydrogen sulfide was passed through the column containing the CaSO₄ desiccant before it entered the toluene

passed through the column containing the CaSO_4 desiccant before it entered the toluene or the alkoxide-toluene solution.

2.3.2. Toluene drying

A chemical method was applied for toluene drying. This method consists of three steps. First, CaCl_2 is added to toluene to partially absorb water. After filtration toluene is refluxed over Na metal for 24 h. To get pure toluene for the experiments, it is distilled after refluxing.

2.4. SOL-GEL PROCESSING

2.4.1. GeS_2 gels

The germanium ethoxide and toluene were mixed under a dried nitrogen atmosphere in a glove box. A glass erlenmeyer with side arm was used as the reactor. The H_2S gas was bubbled through the ethoxide-toluene solution until gelation occurred. Reaction parameters were changed for each experiment. Table 2.2 lists all of the produced GeS_2 gels along with experimental conditions. Gels 1A and 1B were produced from the same reaction mixture with undried H_2S . They were obtained by splitting the gel product according to colour: the top of the gel was yellow (1A), while the bottom was white (1B).

Gel 2 was synthesized with H_2S dried using a CaSO_4 desiccant and a lower (10x)

concentration of $\text{Ge}(\text{OEt})_4$ than in 1A and 1B. The same reaction conditions were used for the preparation of gel 3, with the only difference that air leaked into the reaction mixture during synthesis. The flow rate of the H_2S gas was constant for all the experiments. The gels, enclosed in the reactor, were aged for 24 hours. Samples for analysis were dried in a vacuum oven at room temperature.

Table 2.2: List of GeS_2 gels produced by sol-gel processing

Gel	Toluene/Alkoxide (%)	H_2S drying agent	Colour
1A	50 : 50	none	yellow
1B	50 : 50	"	white
2,5	95 : 5	CaSO_4	"
3*	95 : 5	"	"
6	95 : 5	"	"

* air leaked into the reaction mixture.

In order to check the reproducibility of the method, gel 5 was synthesized using the same reaction conditions as for the preparation of gel 2. Moreover, germanium isopropoxide was employed instead of germanium ethoxide to prepare gel 6, keeping all the other reaction parameters unchanged.

2.4.2. The GeS_2 - GeO_x gel mixture and sulfur

The germanium ethoxide and toluene were mixed under a dried nitrogen atmosphere of a glove box. The toluene/ethoxide ratio was 95:5 vol%. Before the H_2S gas was introduced into the solution, it was passed through concentrated sulfuric acid.

The gas carrying elemental sulfur was bubbled through the toluene/ethoxide solution until complete gelation has occurred. The obtained gel enclosed in the reactor was aged for 24 h at room temperature. Samples for analysis were dried in a vacuum oven at room temperature.

2.4.3. GeS₂ gels at different C, R and T

The concentrations of precursors used for preparation of all reaction mixtures are listed in Appendix I, Table A1. The mixtures were prepared in the following way. First, a solution of hydrogen sulfide in toluene was prepared by purging. After the concentration was determined, a certain volume of the solution was pipetted, placed into the reaction vessel and diluted by toluene to the required concentration. Then, the proper volume of alkoxide was taken by syringe and injected into the H₂S solution under a nitrogen atmosphere in a glove box. The vessel was capped and the reaction occurred.

For the study of reactant concentrations and their ratio on gel structure, the synthesis was performed at room temperature. However, the temperature influence was studied at 30, 40, 45 and 50°C.

The appearance of the solid gel was taken as the gelation time. After gelation, the gels enclosed in reaction vessels were aged for 24 h at room temperature. After samples for analysis were taken, gel IA was additionally aged for 30 days also at room temperature. All gels were dried in a vacuum oven at room temperature.

2.4.4. Metal sulfides

For preparation of other metal sulfides, the same reaction as that used for the synthesis of gel 2 was employed. Results of the synthesis along with alkoxide and toluene concentrations are shown in Table 2.3.

Table 2.3 Results of metal sulfide syntheses from various metal alkoxides.

Alkoxide	Toluene (vol %)	Alkoxide (vol %)	Product	Colour
Zn(OC ₄ H ₉) ₄	95	5	gel	yellow
W(OC ₂ H ₅) ₆	95	5	gel	black
WCl ₂ (OC ₂ H ₅) ₃	75	25	sol	black
SrTi(OC ₃ H ₇) ₆	95	5	none	-
Zr[O(CH ₂) ₃ CH ₃]	95	5	none	-
Si(OC ₂ H ₅) ₄	50	50	none	-

The zinc and tungsten alkoxides were the only alkoxides which reacted with H₂S at room temperature. The reaction products were aged for 24 h and dried in a vacuum oven at room temperature before characterization.

2.4.5. Thin films

Preparation of the sulfide thin films was performed by the sol-gel dip process. The glass slides were dipped into the solutions of the metal sulfides prepared by the sol-gel

processing. In Table 2.4 the alkoxides used for the thin film deposition are listed along with reaction parameters and solution numbers. These solutions were prepared in the same way as those for metal sulfide synthesis. However, the H₂S gas was introduced into the solutions only until Tyndall effect appeared. The dipping was done under a nitrogen atmosphere in a glove box. Fast drying of solutions 5, 6, and 7 caused gelation on the slides. They covered the slides more uniformly than solutions 8 and 9 which had completed gel/sol formation before dipping. The dried films were kept in a desiccator until characterization.

Table 2.4 Alkoxides and corresponding reaction solutions used for the thin film deposition.

Solution	Film	Alkoxide	Number of dippings
5	TF1	Ge(OC ₂ H ₅) ₄	1
6	TF2 and TF6	Ge(OC ₃ H ₇) ₄	1 and 2
7	TF5	Zn(OC ₄ H ₉) ₂	1
8	TF3	W(OC ₂ H ₅) ₆	1
9	TF4	WCl ₂ (OC ₂ H ₅) ₃	1

2.5. HEAT TREATMENT

The GeS_2 gels 1A, 1B, 2, 3 and the $\text{GeS}_x\text{-GeO}_x$ gel and sulfur mixture were heat treated isothermally in a furnace at 630°C , after being placed into quartz ampoules at 10^{-4} torr pressure. They were homogenized for 24 h, and then the ampoules were quenched to room temperature in water. The cooling rate was $> 17^\circ\text{C/s}$.

2.6. POTENTIOMETRIC TITRATION

The concentration of H_2S solution in toluene was determined by potentiometric titration, taking 0.1 mL of solution and dissolving it in 50 mL of the electrolyte. For kinetics measurement an exact amount of the H_2S /toluene solution was mixed with germanium ethoxide and dry toluene and left to react at constant temperature. One mL aliquots were taken from the mixture with a syringe at uniform time intervals. They were diluted in 25 mL of toluene and quenched at -95°C . The sample solution was then purged with nitrogen gas in order to remove hydrogen sulfide. It was mixed with 25 mL of electrolyte for titrating both $\text{Ge}(\text{SH})_x$ and GeS_x (henceforth simply written as GeS_2 and GeSH). For determination of $\text{Ge}(\text{SH})_x$ and GeS_x in the presence of H_2S , 0.1 mL samples were taken and mixed with 50 mL of the electrolyte.

The solutions were stirred during titrations. Titrations were performed at room temperature (20°C). In order to protect the solutions from heating, a piece of styrofoam

was placed between the glass beaker and the stirrer. Before mixing with a sample, each aliquot of electrolyte was deaerated by purging with nitrogen gas for several minutes. Titrations of samples containing H₂S were performed in a closed down draft hood. The electrode was equilibrated in the sample solution before titration. The concentration of titrant was chosen based on expected concentrations of sulfides and mercaptide. Titrant was added in volume increments small enough to change the potential no more than 10 mV. After each titrant addition the potential was recorded when a constant reading was reached. The Ag/Ag₂S electrode was polished with ORION polishing strips before each measurement and conditioned in 1x10⁻² N AgNO₃ solution.

The potential readings were plotted as a function of the added reagent volume. The inflection point of the potentiometric curve, indicating the equivalence point, was first roughly located from the curve. In order to eliminate human error, the equivalence point was then calculated from the point where $\Delta^2E/\Delta V^2$ becomes zero. That is, $V_{eq,p}$ was calculated as a mean value of volumes corresponding to the second derivatives of $E=f(V)$ where the function changed sign from + to -.

2.7. KINETICS

The reaction mixtures were prepared in the following way. First, toluene was saturated with the H₂S gas for several hours. The concentration of the solution obtained was determined by potentiometric titration. The proper volume of this solution was

placed in the 50 mL reaction vessel by pipetting and diluted to the desired H₂S concentration with toluene. After this the reaction vessel was capped with a rubber septum and placed in a constant temperature bath (HAAK 20). The H₂S solution was thermostated for ~0.5 h prior to addition of germanium alkoxide.

Desired volumes of germanium alkoxide were added via a syringe into the solution and mixed by shaking. The reaction mixture concentrations are listed in Table 2.5. The mixtures were thermally equilibrated ($\pm 0.1^\circ\text{C}$) for 0.5 h or 1 h. At proper intervals (0.5 h or 1 h), 1-mL aliquots were removed by syringe from the mixture. They were injected into 100-mL flasks containing 25 mL of toluene, agitated and cooled to $\sim -95^\circ\text{C}$. Unreacted H₂S was quickly purged from the flasks by nitrogen. Then, the samples were carefully analyzed by potentiometric titration with the Ag/Ag₂S ion selective electrode.

In studying the temperature effect on the reaction constants 30, 40, 45 and 50°C were used when the reactant was Ge(OEt)₄. However, the temperatures were changed to 25, 30, 35 and 40°C for the same study of Ge(OPrⁱ)₄.

Software Enzfitter, version 1.05 EGA (Elsevier Biosoft, Cambridge, UK, 1987) was used for plotting graphs and calculation of standard deviations by linear regression analysis.

Table 2.5: The concentration of reactants and their ratios used for reaction mixtures preparations in the chemical kinetics study.

Alkoxide	[Ge(OEt) ₄] ₀ (M)	[H ₂ S] ₀ (M)	[H ₂ S] ₀ /[Ge(OEt) ₄] ₀
Ge(OEt) ₄	0.044	0.400	9.00 : 1.0
Ge(OEt) ₄	0.264	0.220	1.00 : 1.2
Ge(OPr ⁱ) ₄	0.046	0.104	2.25 : 1.0

2.8. CHARACTERIZATION METHODS

2.8.1. X-ray diffraction (XRD)

The samples were analyzed by x-ray diffraction on a Rigaku RU-200B automated powder diffractometer with $\text{CuK}\alpha$. The system uses a horizontal goniometer equipped with graphite crystal diffracted beam monochromator with a rotating anode and copper target. The samples were run at 40kV, 80mA, 2°/min. The samples were mounted on glass slides using dry toluene or vaseline.

2.8.2. Infrared spectroscopy (IR)

The IR spectra were collected in the wave number range from 400-4000 cm^{-1} by Fourier transform infrared (FTIR) spectrometer Bruker IFS 113V, equipped with a photoacoustic cell (Princeton Applied Research, model 6003 EG&G). The dried powdered samples were mixed with KBr to make 2 % mixtures for the analysis.

2.8.3. BET method (BET)

The specific surface area and the pore volume of the dried gels were determined by the Brunauer, Emmett and Teller (BET) method in two different instruments: a Quantachrome Instruments Autosorb-1 sorption system and an Omnisorp 360. The measurements were performed at liquid nitrogen temperature and with nitrogen gas.

2.8.4. Scanning electron microscopy (SEM)

The morphology of the samples was examined on a scanning electron microscope Hitachi S-2700. The samples were mounted on carbon holders. Prior to analysis, they were carbon coated. The examination was performed in the secondary electron mode.

2.8.5. Energy dispersive spectrometry (EDS)

Microanalysis of the germanium, sulfur and oxygen content in the samples was done with a Link analytical eXL energy dispersive x-ray spectrometer, on the S-2700 electron microscope. The analysis was performed at 20 kV and working distance of 12 mm. The microanalysis of oxygen content was done by the windowless technique.

2.8.6. Quantitative chemical analysis (EA)

Quantitative chemical analysis of samples for sulphur and oxygen content was performed using a Carlo-Erba CHNS-O EA 1108 elemental analyzer based on combustion analysis.

CHAPTER 3

RESULTS

3.1. CHARACTERIZATION OF GeS₂ GELS AND HEAT TREATED PRODUCTS

3.1.1. Sol-gel processing of GeS₂ gels

The reaction of germanium alkoxides with hydrogen sulfide was performed in toluene at room temperature. The solutions gelled after different times. The formed gels had different colour and appearance (Table 2.2). Gels 1A and 1B were produced from solution which contained 50 vol% of germanium ethoxide. After 15 min of passing H₂S through the solution the Tyndall effect appeared and gel lumps formed after 20 min. The solution completely gelled after 30 min. During synthesis of gels 2 and 3 the Tyndall effect appeared 10 min after the beginning of the H₂S introduction. The gel lumps appeared within additional 10-20 min, while gelation occurred 3.5 h. After drying in a vacuum oven, the homogeneous mass of the gels cracked into small solid pieces.

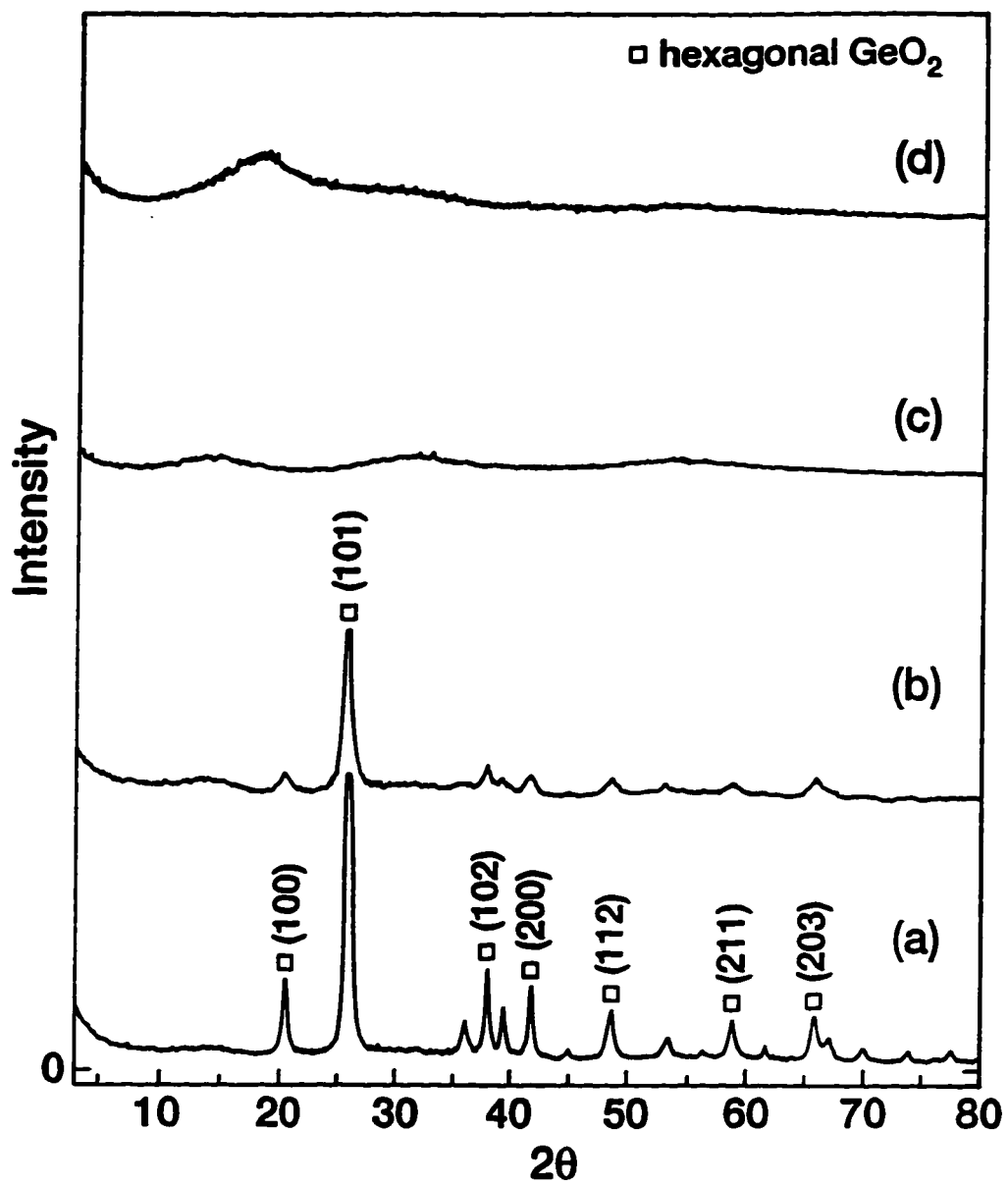


Fig. 3.1.1 XRD patterns of dried gels: a) 1A; b) 1B; c) 2; d) 3.

3.1.2. X-ray diffraction analysis

The XRD patterns of gels 1A and 1B, shown in Fig. 3.1.1a and b, indicate the presence of a crystalline phase, which was identified as hexagonal GeO_2 [84]. However, XRD peaks in the 1B gel pattern are broader than the ones for gel 1A. In addition, there is a broad, low intensity peak at $\approx 15^\circ 2\theta$, which appears in the XRD patterns of both the 1A and 1B gels. Gels 2 and 3 have an amorphous structure as is shown in Fig. 3.1.1c and d. The XRD patterns of gel 5 and gel 6 are identical to the pattern of gel 2.

The XRD patterns of the heat treated gels 1A and 1B (Fig. 3.1.2a,b) match tetragonal GeO_2 . Their XRD patterns also show the existence of an amorphous phase, since the broad peak at $\approx 15^\circ 2\theta$ is evident here as well. The XRD pattern of the heat treated gel 2 (Fig. 3.1.2c) matches monoclinic GeS_2 [85].

3.1.3. Infrared analysis

The gel IR spectra collected in the range from $400\text{--}4000\text{ cm}^{-1}$ are shown in Fig. 3.1.3. In the range $400\text{--}450\text{ cm}^{-1}$, the gels 1A, 1B and 3 have similar IR spectra with shoulders at ≈ 405 and $\approx 436\text{ cm}^{-1}$, assigned to vitreous GeS_2 [86]. Since the IR spectrum of gel 2 was collected from 450 cm^{-1} , it was not possible to identify Ge-S vibrations.

The IR spectrum of gel 1A has the vibrational absorption triplet of hexagonal GeO_2 at 515 , 555 , and 587 cm^{-1} [87]. It also has a strong absorption band at $\approx 885\text{ cm}^{-1}$, assigned to asymmetric stretching of Ge-O-Ge[87], which confirms the presence of

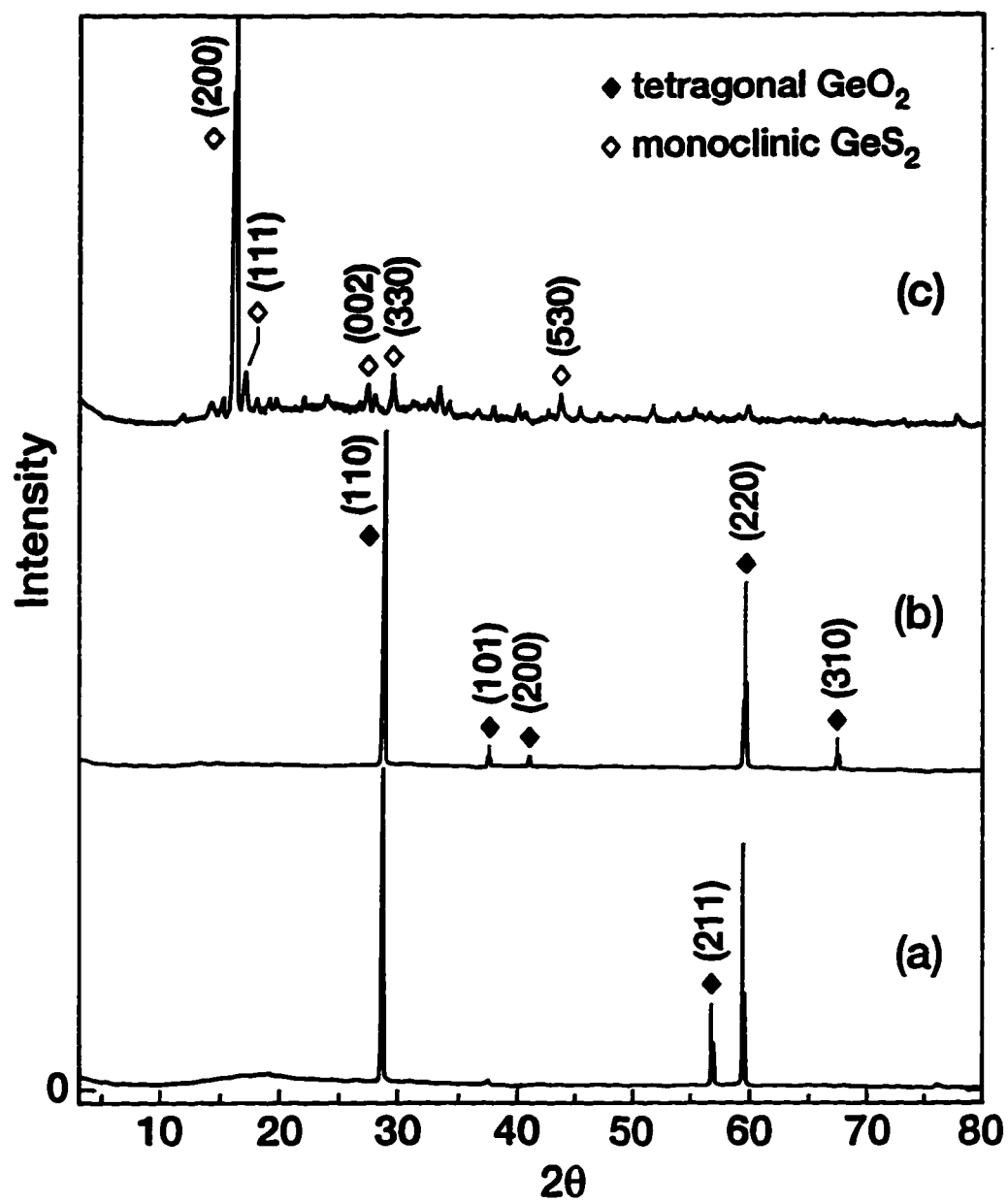


Fig. 3.1.2 XRD patterns of heat treated gels: a) 1A; b) 1B; c) 2.

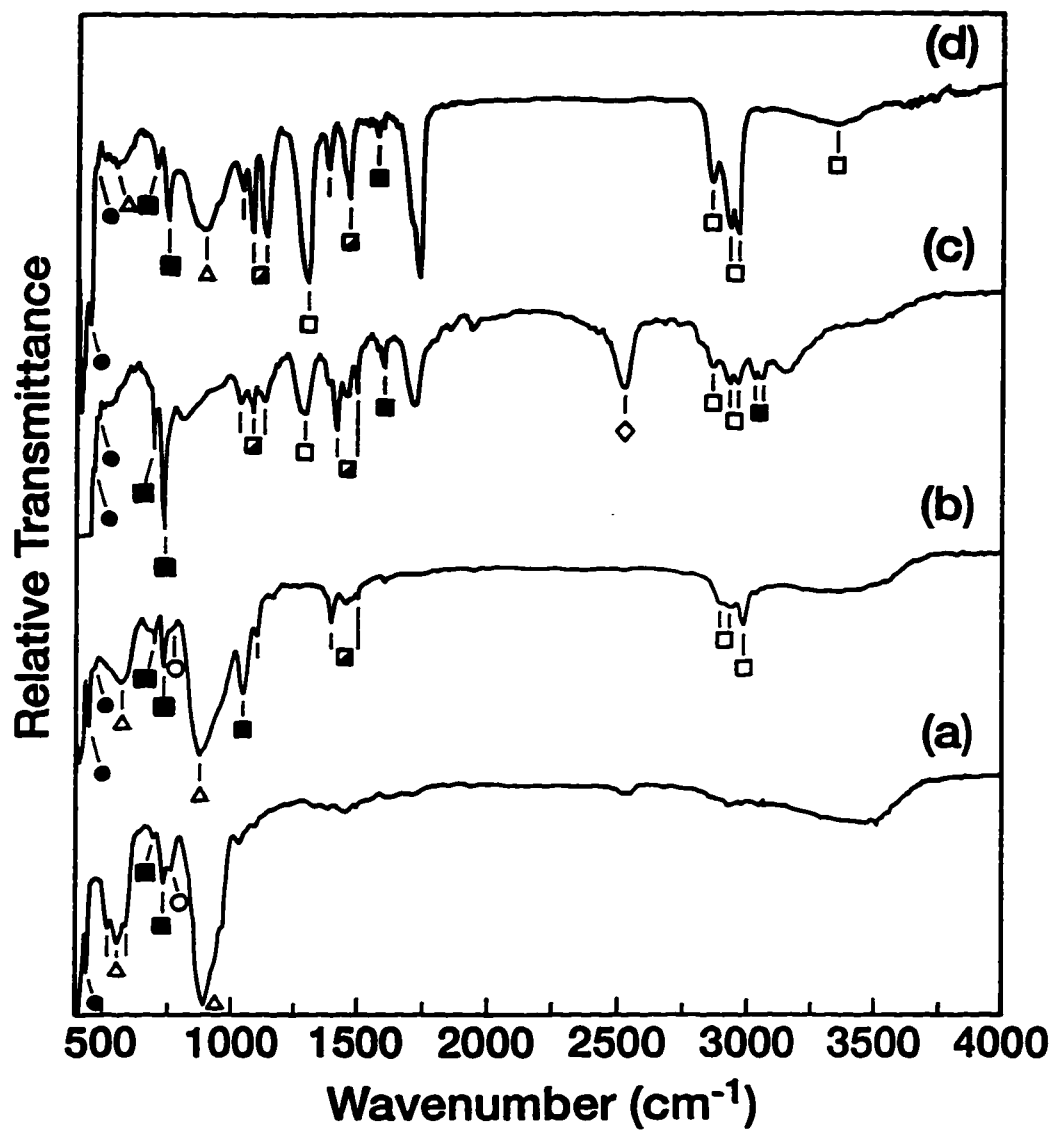


Fig. 3.1.3 IR spectra of dried gels: a) 1A; b) 1B; c) 2; d) 3.
 Legend: • (Ge-S-Ge); Δ (Ge-O-Ge); \circ (Ge-OH); \diamond (GeS-H);
 \square ethanol; \blacksquare toluene; \blacksquare toluene and ethanol.

hexagonal GeO_2 . All these strong peaks are replaced by broad bands at ≈ 570 and ≈ 880 cm^{-1} in the spectra of gels 1B and 3. The broad, weak absorption band at 780 cm^{-1} in the infrared spectra of gels 1A, 1B and 3 suggests existence of GeO-H vibration[87].

The strong absorption peaks at 694 and 728 cm^{-1} are characteristic peaks of toluene and they appeared in the spectrum of each gel due to retained toluene[88]. Toluene absorption peaks were also identified in the range from 1000 - 4000 cm^{-1} . Peaks at ≈ 1124 , 1280 , 1713 , 2860 , 2930 and 3144 cm^{-1} indicate the presence of ethanol. A strong absorption peak at 2516 cm^{-1} in the spectrum of gel 2 could be assigned to a GeS-H vibration.

The infrared spectra of heat treated gels 1A, 1B and 2, collected in the IR range from 400 - 4000 cm^{-1} , are shown in Fig. 3.1.4. In the range 400 - 450 cm^{-1} , IR spectra of the heat treated gels 1A and 1B indicate the presence of amorphous GeS_2 [86]. The bands at 801 cm^{-1} and 1070 cm^{-1} in the spectrum of 1A and the band at 820 cm^{-1} in the spectrum of 1B could be assigned to tetragonal GeO_2 . The IR spectrum of the heat treated gel 2 indicates the presence of monoclinic GeS_2 , with sharp absorption peaks at ≈ 410 , 433 , and 454 cm^{-1} .

In the range 400 - 4000 cm^{-1} , the IR spectra of gel 5 and 6 are the same as the IR spectrum of gel 2. The IR spectra of both gels indicate the presence of amorphous GeS_2 . In addition, the IR spectra evidence the presence of a GeS-H vibrational band at ≈ 2500 cm^{-1} , the same as the IR spectrum of gel 2. While the IR spectrum of gel 5 indicates the presence of ethanol, the IR spectrum of gel 6 shows the presence of isopropyl alcohol.

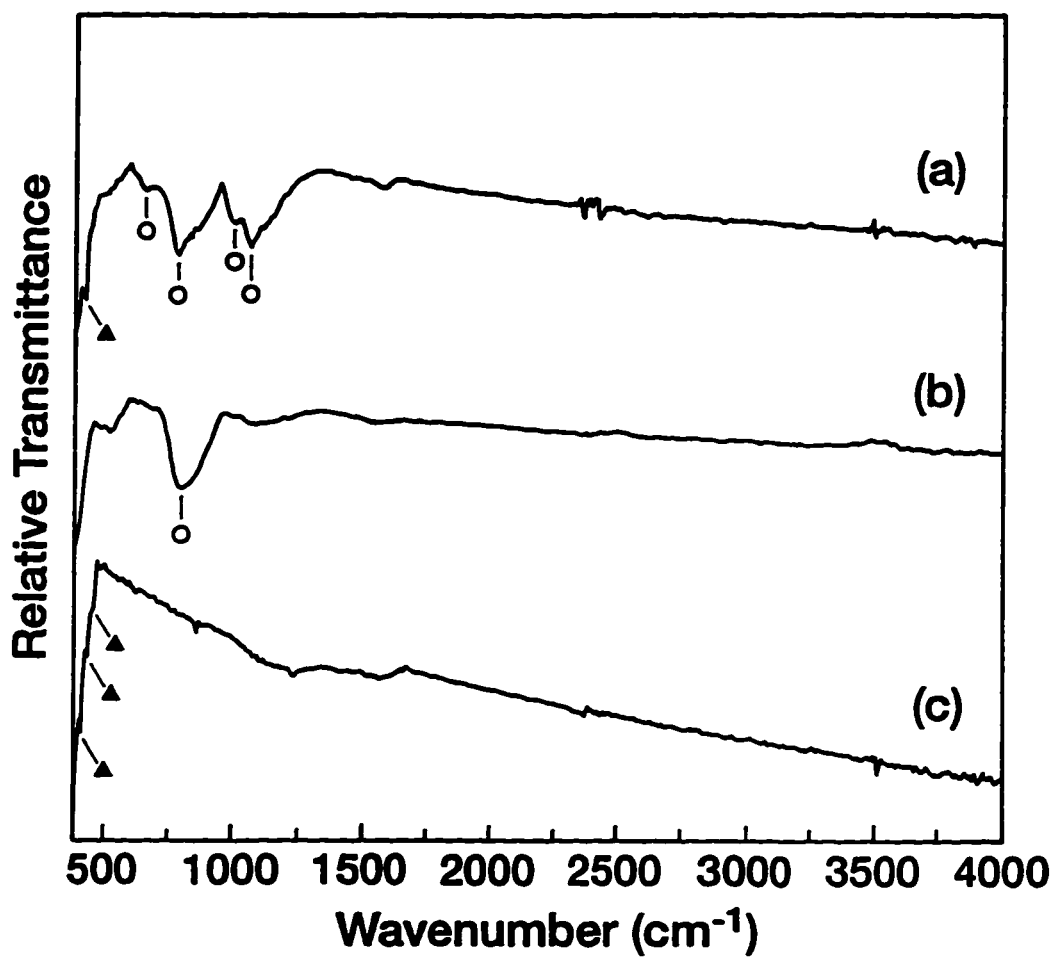


Fig. 3.1.4: IR spectra of heat treated gels: a) 1A; b) 1B; c)2.
Legend: ▲ GeS₂; ○ GeO₂.

3.1.4. Scanning electron microscope analysis

The scanning electron micrographs of the dried gels 1A, 1B, 2 and 3, shown in Figure 3.1.5, reveal that they are colloidal xerogels, i.e., the gels were formed by linking of spherical colloidal particles into a porous network. The size of particles depends on the gel, but in each gel the size distribution is relatively narrow. From the micrographs, it is evident that particles agglomerated and that they are linked by necks.

After heat treatment, the microstructure of gels 1A, 1B and 2 changed. The micrographs are shown in Fig. 3.1.6. The microstructure of the heat treated gels 1A and 1B has two phases. One of them consists of large tetragonal crystals of size $60\mu\text{m}$ (Fig. 3.1.6a,b). Examination of their cross-section shows a very porous internal structure (Fig. 3.1.6c,d). A second phase was identified in both gels 1A and 1B (Fig. 3.1.6e,f). SEM examination of this phase reveals that sintering has occurred but has not been completed. Macropores are evident in the structure, especially in gel 1B. The SEM analysis of the heat treated gel 2 indicates formation of vermicular grains (Fig. 3.1.6g).

In Fig. 3.1.7a, the SEM micrograph shows the structure of gel 5 after drying in the vacuum oven at room temperature. It consists of connected spherical particles.

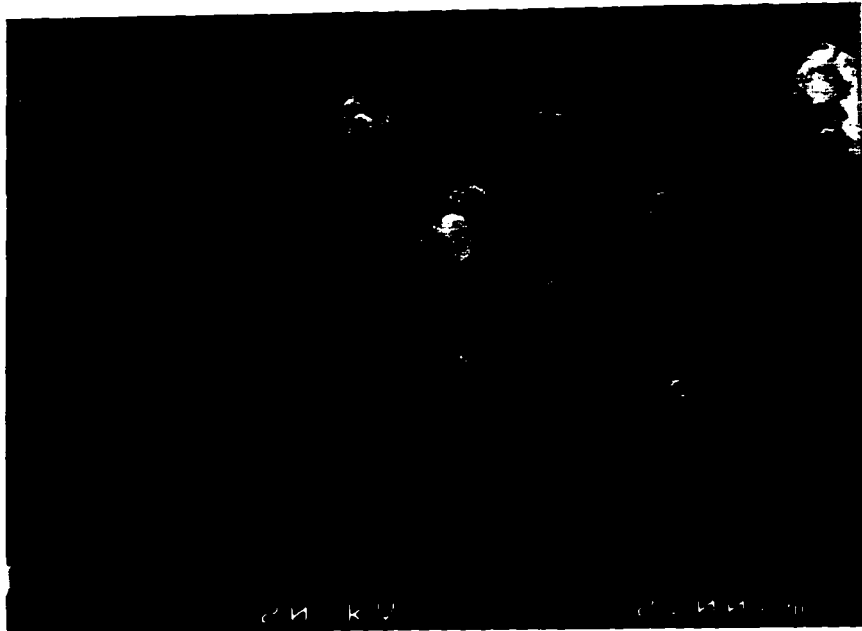


Fig. 3.1.5 Scanning electron micrographs of dried gels: a) 1A; b) 1B;

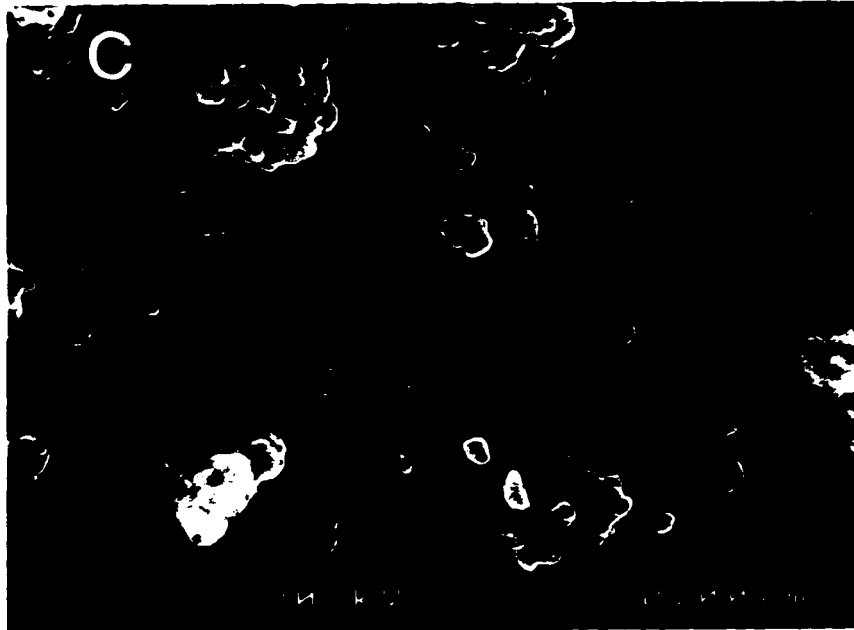


Fig. 3.1.5. c) 2; d) 3.

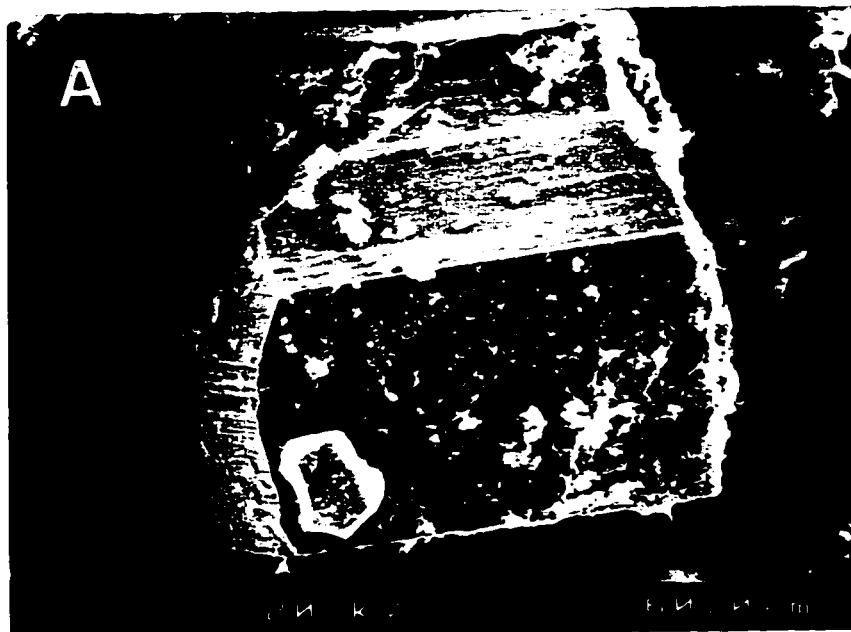


Fig. 3.1.6 Scanning electron micrographs of heat treated gels: a) GeO_2 crystal in 1A; b) GeO_2 crystal in 1B;



Fig. 3.1.6

c) cross section of GeO_2 crystal in 1A; d) cross section of GeO_2 crystal in 1B;

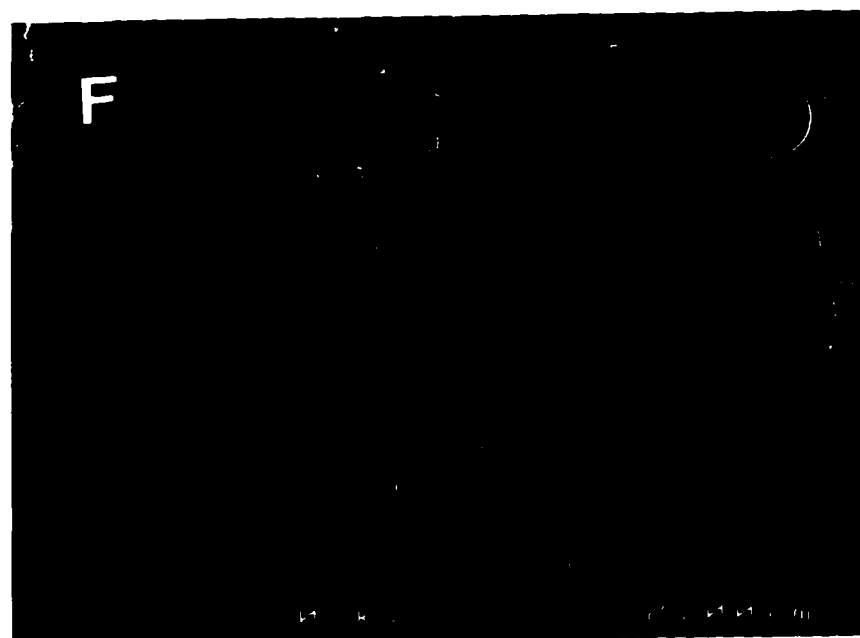
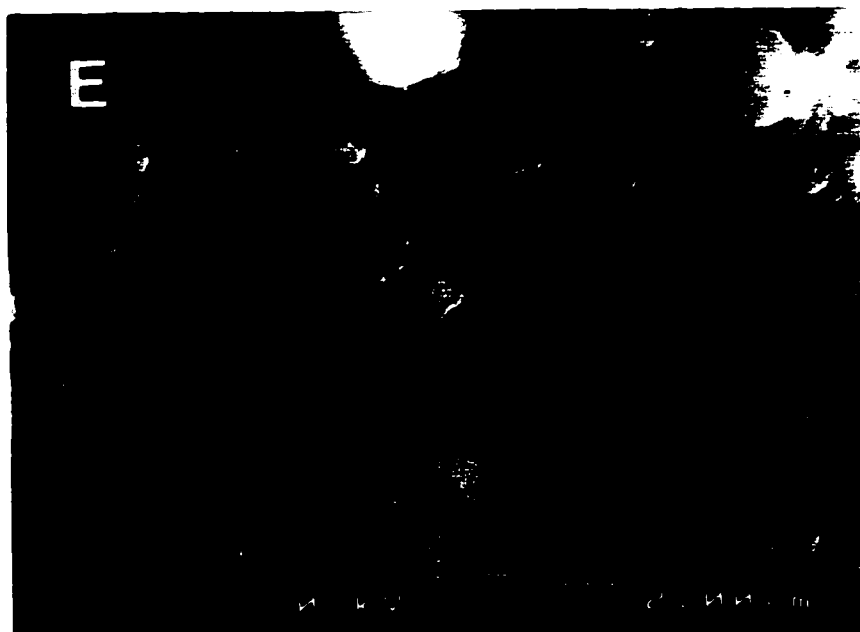


Fig. 3.1.6

e) GeS_2 phase in 1A; f) GeS_2 phase in 1B;

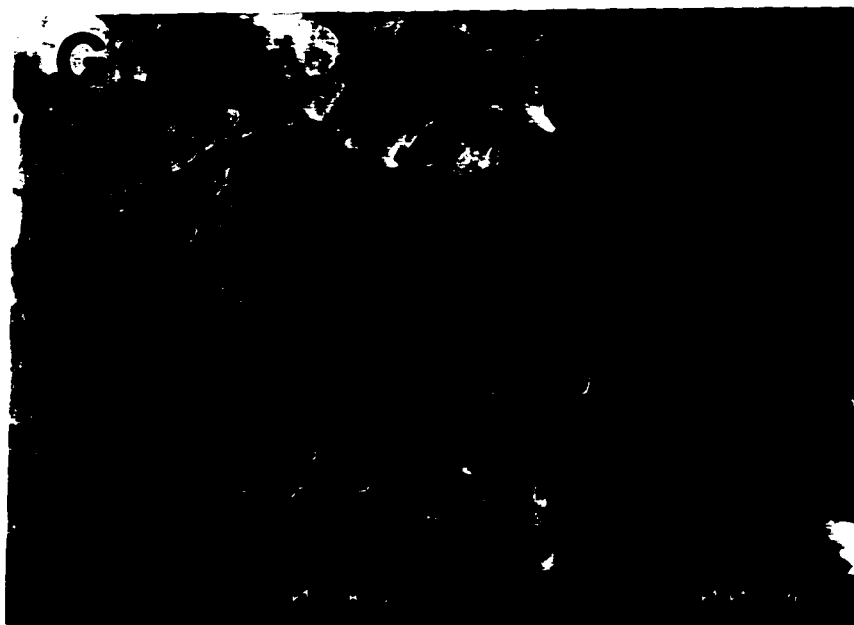


Fig. 3.1.6. **g) vermicular structure of 2.**



Fig. 3.1.7

Scanning electron micrographs of: a) gel 5 prepared upon the same conditions as gel 2; b) gel 6 synthesized from $\text{Ge}(\text{OPr})_4$, and all the other reaction conditions same as for gel 2.

The estimated particle size is $0.1\mu\text{m}$. The scanning electron micrograph of gel 6 is shown in Fig. 3.1.7b. It is evident that this gel also belongs to the group of colloidal gels, since it consists of linked spherical particles size $< 0.1\mu\text{m}$.

3.1.5 Chemical analysis

Energy dispersive spectrometry (EDS) shows that dried gels 1A and 1B have apparent Ge/S atomic ratios 1:0.3 and 1:0.7, while gels 2 and 3 have 1:1.8 and 1:1.6, respectively. The ratios deviated very little at different spots on the samples.

EDS analysis confirmed that after heat treatment gels 1A and 1B were two phase systems. The large tetragonal crystals revealed by SEM in the heat treated products 1A and 1B (Fig. 3.1.6a,b) are GeO_2 , whereas the small grain phase is GeS_2 . For gel 2, the atomic percentage of determined sulfur increased so that the Ge/S ratio was 1:2.3.

The content of sulfur and oxygen in gels 1B and 2 was determined quantitatively by combustion analysis. The results, shown in Table 3.1.1, are close to those obtained by EDS, even for oxygen. Thus, quantitative chemical analysis confirmed that gel 2, prepared using dried H_2S , had an oxygen content approximately ten times less than gel 1B synthesized with undried H_2S .

Table 3.1.1 Content of S,O and Ge in the dried GeS₂ gels determined using EDS analysis and S and O determined using EA analysis.

GEL	EDS (wt%)			EA (wt %)	
	S	O	Ge	S	O
1A	7.50	6.32	86.18	-	-
1B	22.64	3.56	73.80	22.53	3.52
2	41.94	<0.17	58.06	41.64	0.35
3	33.92	1.35	64.74	-	-
5	42.83	<0.18	56.63	-	-
6	42.91	<0.16	57.09	-	-

3.1.6. BET analysis

The BET analysis of the dried gels 1A, 1B and 2, yielded specific surface areas of 86.6, 48.6 and 227.4 m²/g, respectively. The isotherms were type IV, which indicates that the gels contain mostly mesopores. Calculated values for mesopore content in gels 1A, 1B and 2 are 62.5, 74 and 97% of total pore volume. The micropores, which are attributed to the internal particle structure, occupy 3.5% of total pore volume in gel 1A, 4.8% in gel 1B and 3% in gel 2. The average pore radius in gels 1A, 1B and 2 is similar, \approx 12.5nm (mesopore range). The isotherms had the A type of hysteresis loop, which is usually associated with cylindrical pores[89].

3.2 CHARACTERIZATION OF THE GeS_x-GeO_x GEL AND SULFUR MIXTURE AND THE HEAT TREATED PRODUCT

3.2.1. X-ray analysis

The obtained gel had a smooth appearance and a yellow colour. The XRD pattern of the gel (Fig. 3.2.1a) evidences the presence of two crystalline phases. One of them was identified as hexagonal GeO₂[84], while the second phase was detected as orthorhombic sulfur[90]. The XRD pattern of the gel after heat treatment (Fig. 3.2.1b) is identical to that of monoclinic GeS₂[85].

The peak positions from this XRD pattern were matched with standard[85] using software PDF-2 Database sets 1-42. The results of 2θ and d-spacing for the heat treated product and standard are shown in Table 3.2.1 along with their absolute deviations $\Delta 2\theta$.

3.2.2. Infrared analysis

The gel IR spectrum from 400-1000 cm⁻¹ is shown in Fig. 3.2.2a. In the range 400-450 cm⁻¹ shoulders at ≈ 405 , 415 and 430 cm⁻¹ can be assigned to Ge-S vibrational absorption by vitreous GeS₂[86]. The IR spectrum of the gel shows the vibrational absorption triplet of hexagonal GeO₂ at 515, 555 and 587 cm⁻¹[87]. It also has a strong absorption peak at ≈ 885 cm⁻¹, assigned to asymmetric stretching of Ge-O-Ge[87], which confirms the presence of hexagonal GeO₂. A shoulder at 780 cm⁻¹

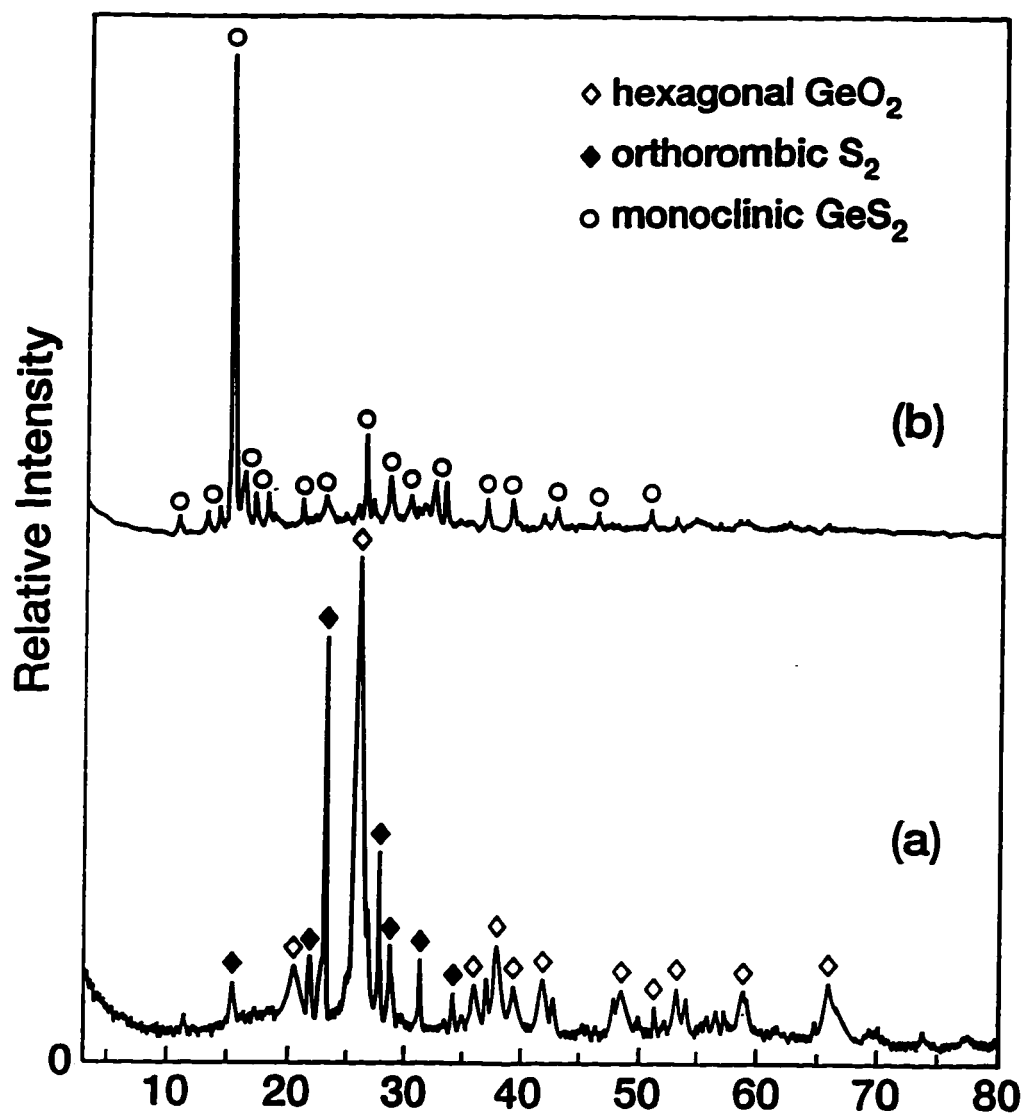


Fig. 3.2.1 XRD pattern of: a) the gel $\text{GeS}_x\text{-GeO}_x$; b) monoclinic GeS_2 obtained after heat treatment.

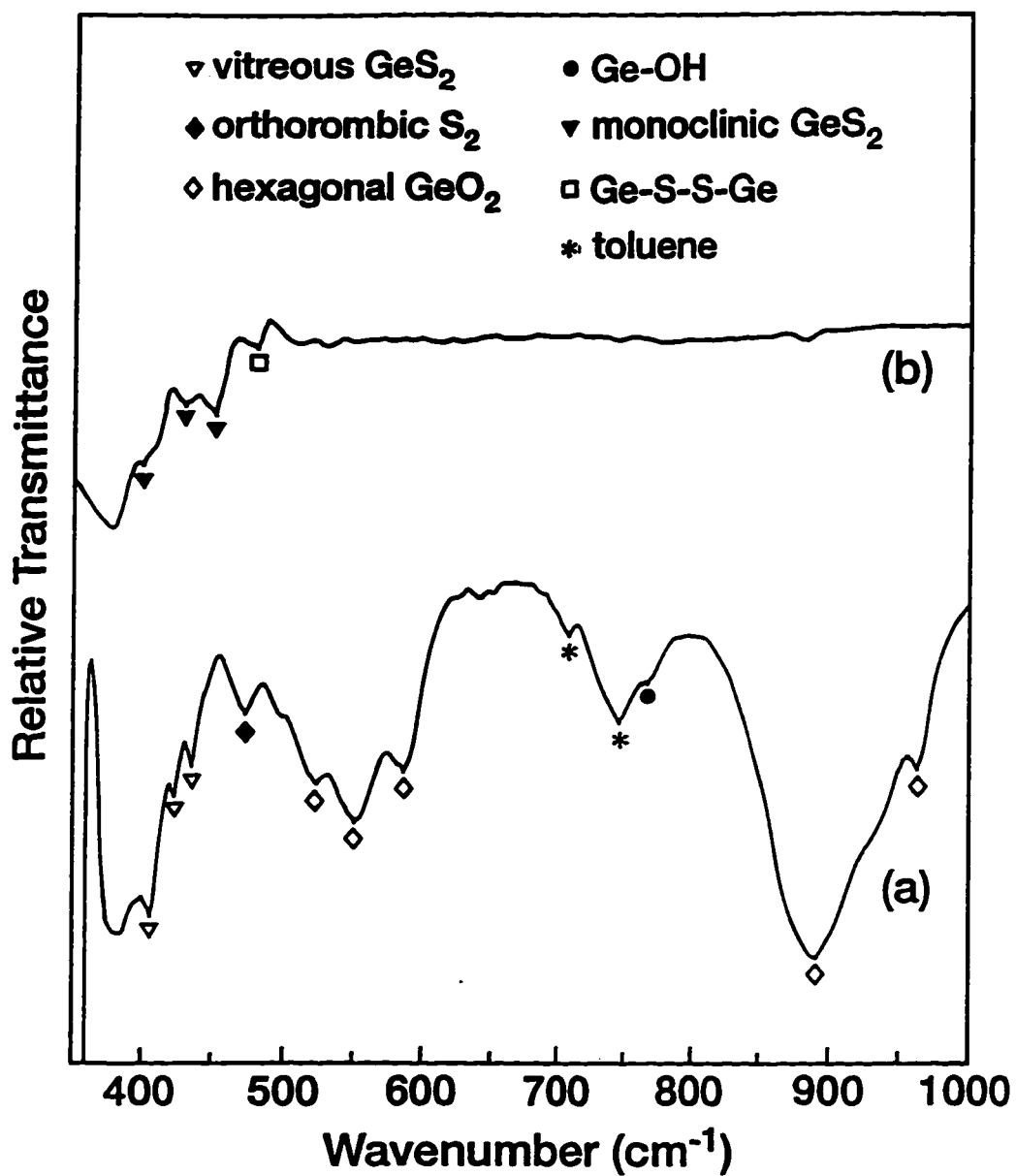


Fig. 3.2.2 IR spectrum of: a) the gel GeS_x-GeO_x; b) monoclinic GeS₂ obtained after heat treatment of the gel.

Table 3.2.1 The XRD peak positions 2θ and d-spacing of the heat treated product and the standard GeS_2 [85] shown along with their absolute deviations ($\Delta 2\theta$).

hkl	$2\theta(^{\circ})$			d(Å)		
	Standard GeS_2	Heat treated product	$\Delta 2\theta$	Standard GeS_2	Heat treated product	Δd
(200)	15.479	15.477	-0.002	5.7200	5.7208	0.0008
(111)	16.372	16.377	0.005	5.4100	5.4082	-0.0018
(211)	21.239	21.245	0.006	4.1800	4.1788	-0.0012
(002)	26.555	26.551	-0.004	3.3540	3.3544	0.0004
(151)	31.832	31.839	0.007	2.8090	2.8084	-0.0006
(260)	36.978	36.975	-0.003	2.4290	2.4292	0.0002
(-332)	39.223	39.228	0.005	2.2950	2.2947	-0.0003

suggests existence of a GeO-H vibration[87]. An absorption band at 473 cm^{-1} is characteristic of S-S vibrational absorption by elemental sulfur[88]. In this spectrum, absorption peaks of toluene have been also recorded at ≈ 694 and 730 cm^{-1} [88].

The IR spectrum of the heat treated gel is shown in Fig. 3.2.2b. It has absorption peaks close to that of monoclinic GeS_2 at ≈ 405 , 430 , and 450 cm^{-1} [86]. Furthermore, the absorption band at 483 cm^{-1} can be assigned to S-S vibrational absorption.

3.2.3. Scanning electron microscope analysis

The scanning electron micrograph of the dried gel, shown in Fig. 3.2.3a, reveals that the gel is a colloidal gel, i.e., it was formed by linking of spherical colloidal particles into a porous network. From the micrographs, it is evident that particles of $\approx 0.4\mu\text{m}$ were linearly linked by necks. Besides the gel network, the micrograph of the gel obtained at lower magnification, shown in Fig. 3.2.3b, reveals large crystals $\approx 60\mu\text{m}$. The morphology of the heat treated gel is presented in Fig. 3.2.3c. It indicates a fused structure with large grains and no macropores.

3.2.4. Chemical analysis

Energy dispersive spectrometry (EDS) shows that particles have a Ge/S atomic ratio 1:3.7. However, the big crystals have the ratio 1:46.5, which indicates that they are almost pure sulfur.

The microstructure changed after heat treatment. The sulfur crystals completely disappeared and a homogeneous structure formed. EDS revealed that the atomic ratio Ge/S was constant when measured at different spots on the sample; the values did not deviate from the average value 1:2.9.



Fig. 3.2.3 Scanning electron micrographs of: a) gel $\text{GeS}_x\text{-GeO}_x$; b) sulfur crystals deposited in the gel;



Fig. 3.2.3. c) sintered structure of monoclinic GeS₂ (630°C for 24 h).

3.3. CHARACTERIZATION OF THE GeS₂ GELS PREPARED AT DIFFERENT C, R AND T

3.3.1. Sol-gel processing

During sol-gel processing of GeS₂, the reaction mixtures changed from clear liquid to white or semi-transparent gel. There are three stages which differ visually and are typical for all the prepared gels. The first noticeable change in the reacting solution is the appearance of the Tyndall effect, shown in Fig. 3.3.1a. It is assigned to the formation of colloidal particle agglomerates of ~ 300 nm size [91]. This is followed by the solution taking on a milky appearance (Fig. 3.3.1b). This stage is indicative of stable agglomerates, size > 300 nm, scattering visible light.

After this stage, gelation occurs. If the initial concentration of Ge(OEt)₄ is high, > 0.044 M, aggregates are connected into a 3-D solid network within the entire liquid present in the reaction vessel. There is no more liquid meniscus and the solution turns into a white, low viscosity substance (Fig. 3.3.1c). However, if the concentration of Ge(OEt)₄ is < 0.044 M, the gel precipitates, as demonstrated in Fig. 3.3.2a,b, for gels III and V, respectively. The gels formed are opaque. A semi-transparent gel was formed when the concentration of H₂S was 0.019 M and the concentration of Ge(OEt)₄ was 0.029 M (Fig. 3.3.3a).

The concentrations of precursors drastically affected the gelation time. In Fig. 3.3.4 plot t_{gelation} versus [Ge(OEt)₄] for the ratio, $R = [\text{H}_2\text{S}]/[\text{Ge}(\text{OEt})_4]$, 2.5 is shown. However, when the gels were synthesized at various temperatures, gelation occurred

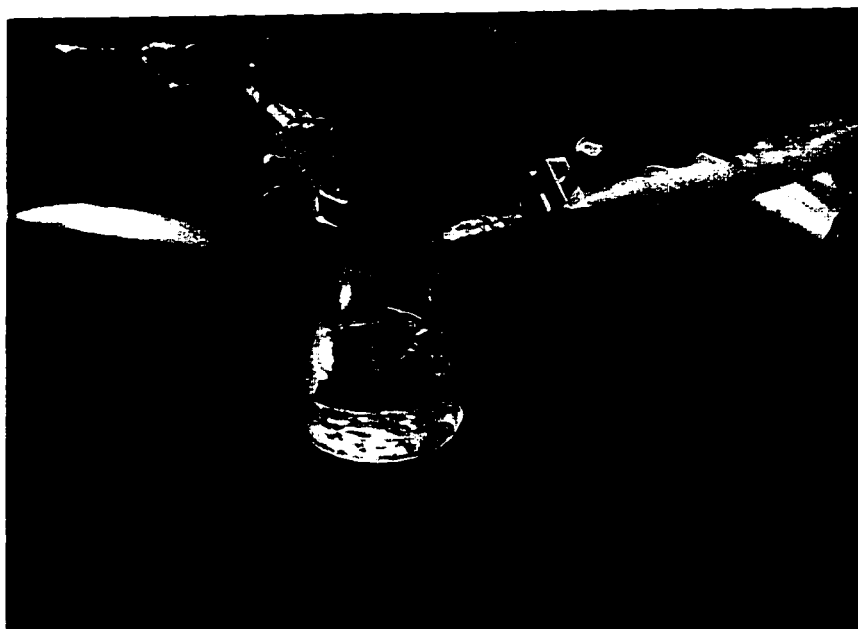


Fig. 3.3.1 Observed changes in the sol-gel reaction mixture: a) Tyndall effect (gel IX); b) milky appearance of the mixture (gel XI);

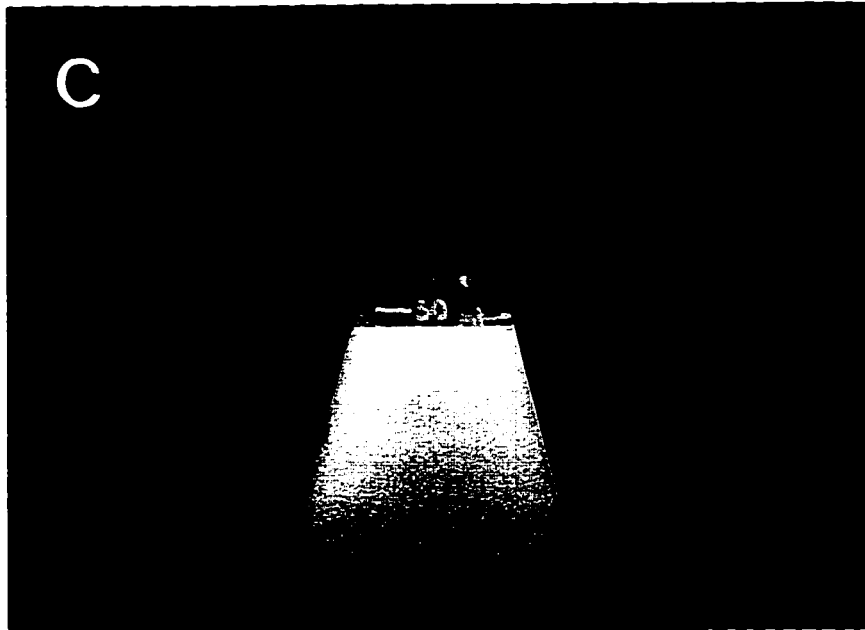


Fig. 3.3.1 c) gelation (gel IA).

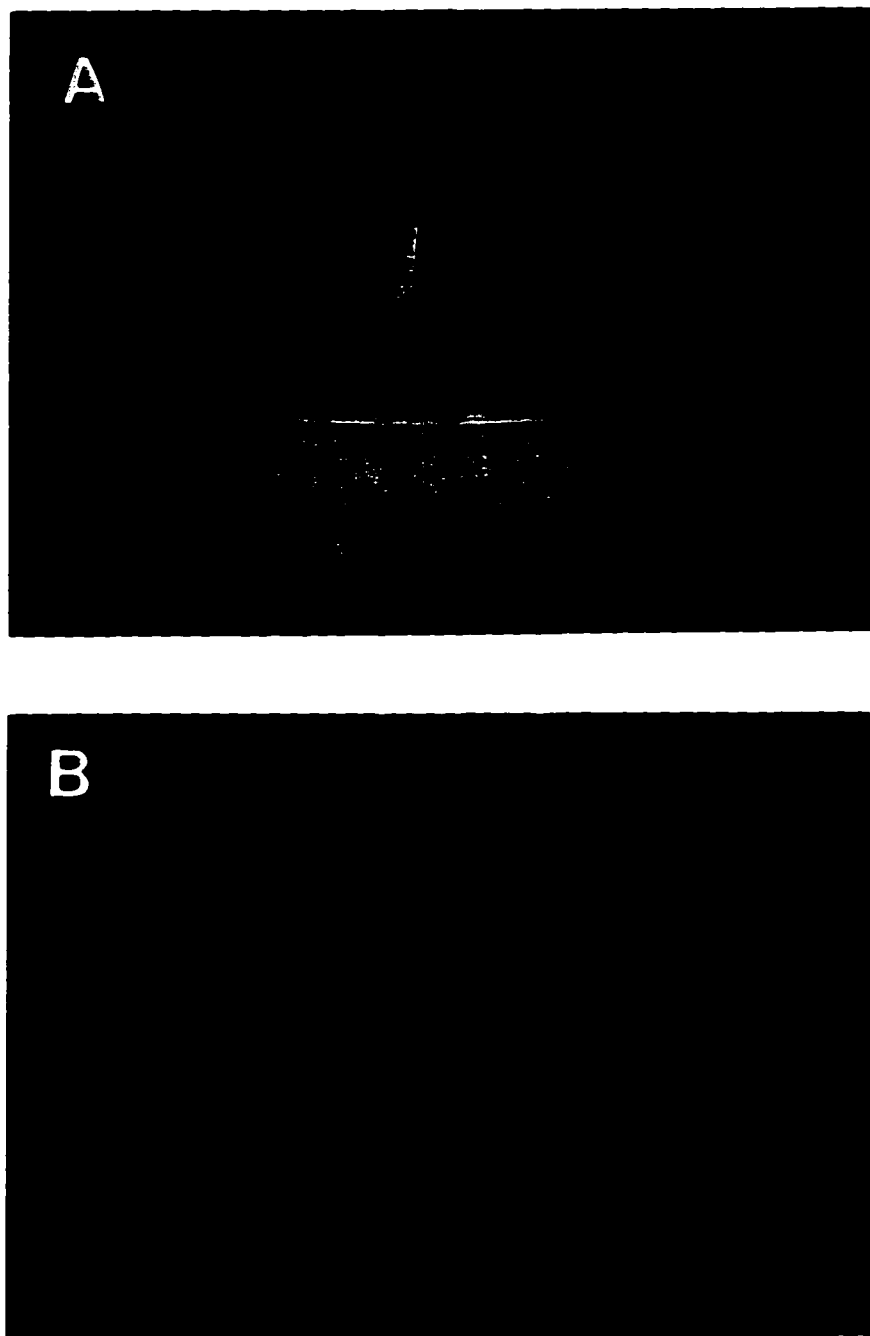


Fig. 3.3.2

Gels formed when $[\text{Ge}(\text{OEt})_4] \leq 0.044 \text{ M}$: a) gel III, $[\text{Ge}(\text{OEt})_4] = 0.044 \text{ M}$; b) gel V, $[\text{Ge}(\text{OEt})_4] = 0.022 \text{ M}$.

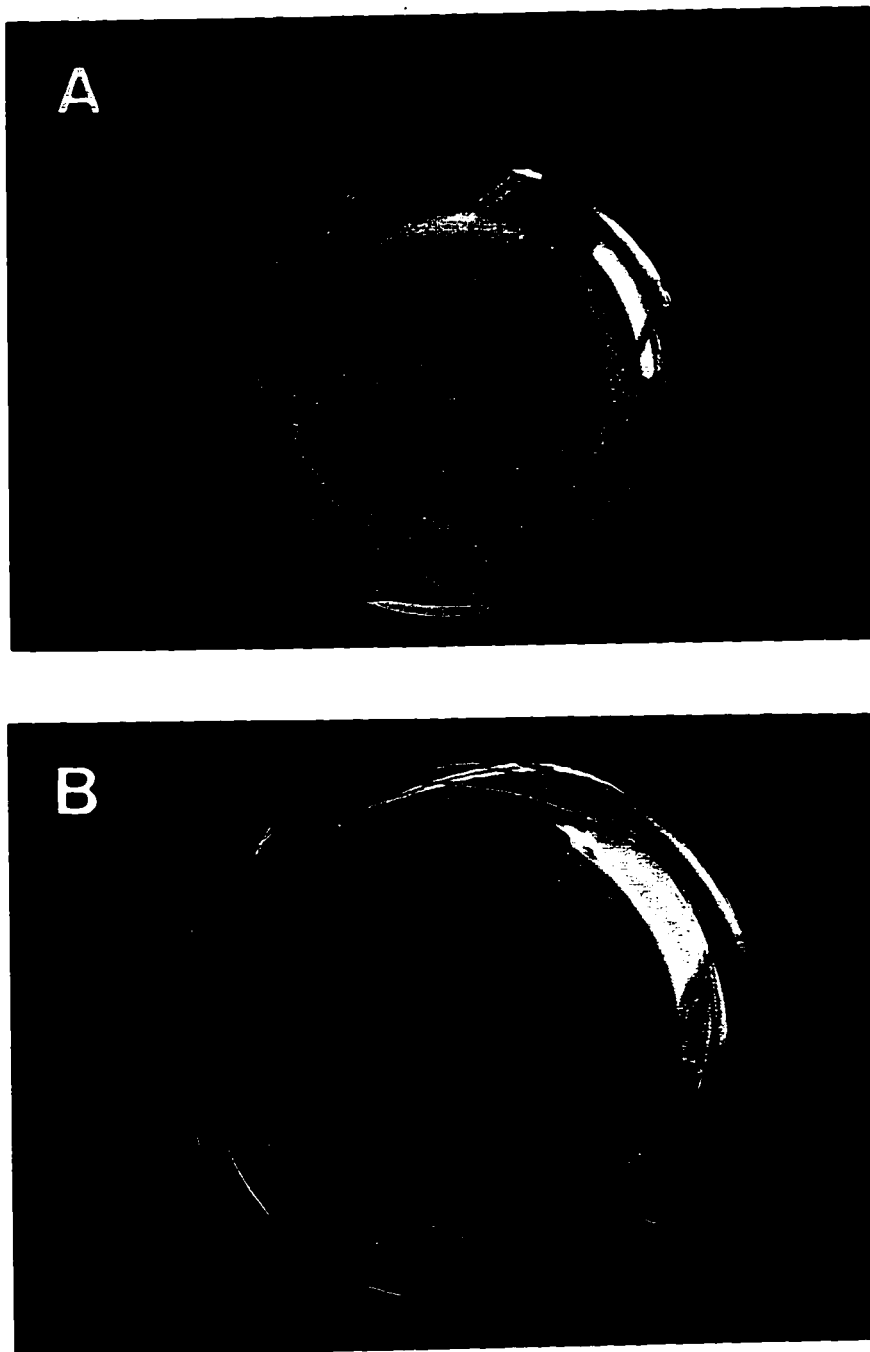


Fig. 3.3.3 Semi-transparent gel VI formed from $[H_2S]=0.019M$ and $[Ge(OEt)_4] = 0.029 M$: a) gel monolith formed at the bottom of 250 mL flask; b) cracking of the monolith;

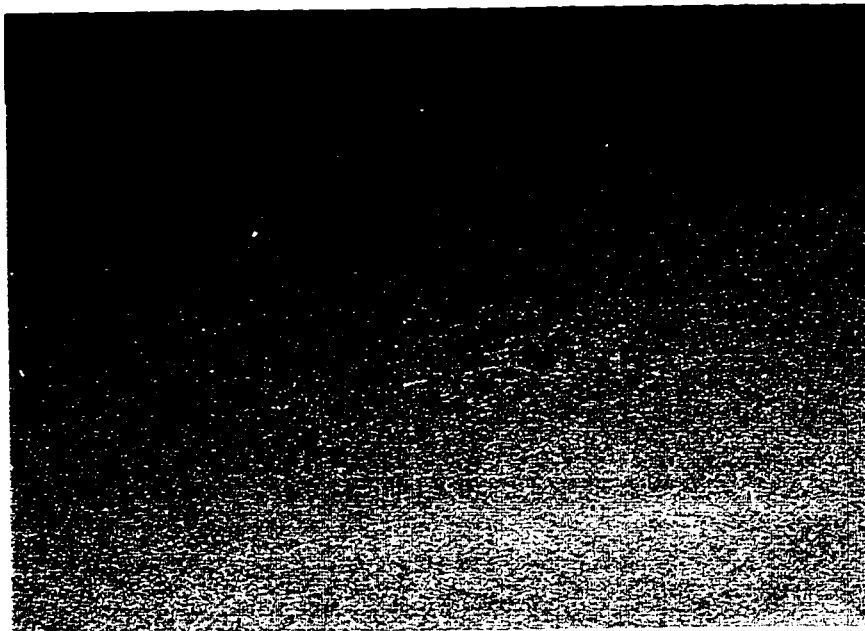


Fig. 3.3.3 c) pieces of dried gel VI occupy $\sim 5\text{cm}^2$ surface area.

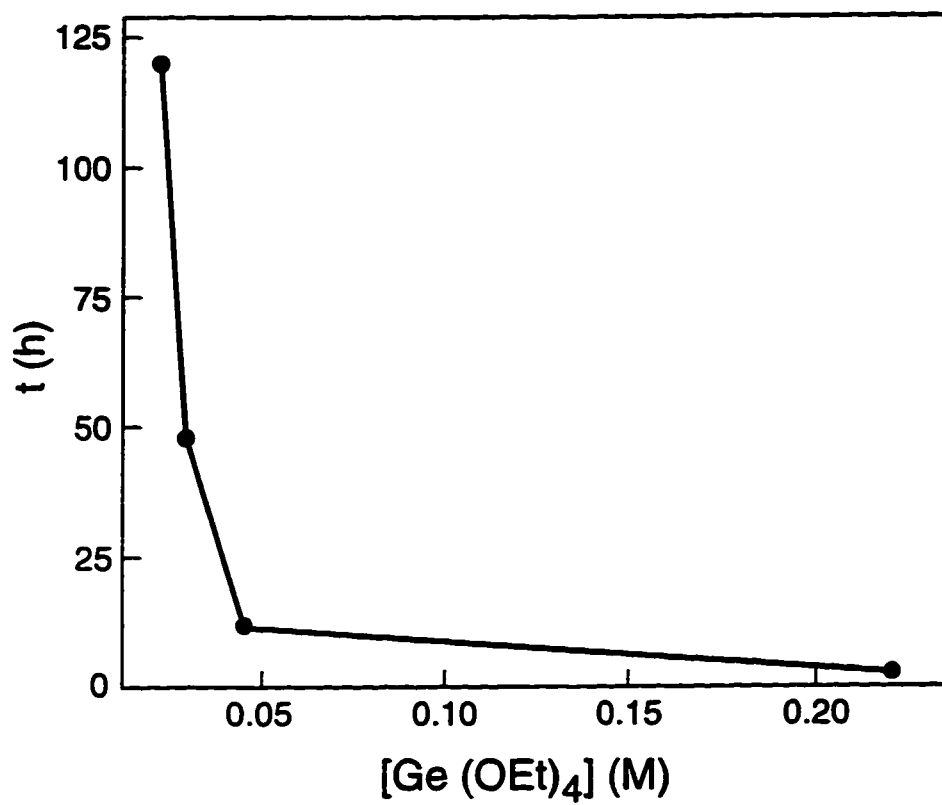


Fig. 3.3.4 Plot t_{relation} vs. $[\text{Ge}(\text{OEt})_4]$ for $R=2.5$.

at approximately the same time, as seen from the data in Appendix I, Table A1. Data in Table A1 show that gelation time is very long, even 6 months, if the ratio R is low, 0.66. When R is ~ 2 , gelation time radically decreased and stays almost constant regardless of further change to R.

During drying, the gels cracked into small pieces. The process is illustrated in Fig. 3.3.3b,c by the behaviour of gel VI. Moreover, in Fig. 3.3.5, pieces of dried gel III are shown, typical for all gels prepared from low concentrations of $\text{Ge}(\text{OEt})_4$ and $R = 2.5$.

3.3.2. Scanning electron microscope analysis

a) Concentration

In Fig. 3.3.6 scanning electron micrographs of GeS_2 gels IA, III, IV and V are presented. They were prepared with various concentrations and the constant ratio $R = 2.5$ of H_2S and $\text{Ge}(\text{OEt})_4$. The micrographs reveal that gels IA, III and IV (Fig. 3.3.6a,b,c, respectively) consist of spherical colloidal particles, diameter $\sim 0.1 \mu\text{m}$, connected into irregularly shaped agglomerates. The size of the agglomerates varied from coarse in gel IA (Fig. 3.3.6a) to fine in gel IV (Fig. 3.3.6c). However, gel V (Fig. 3.3.6d) is formed from large agglomerates, which seem to have a layered structure. The building particles of these agglomerates are indistinguishable in the micrograph.

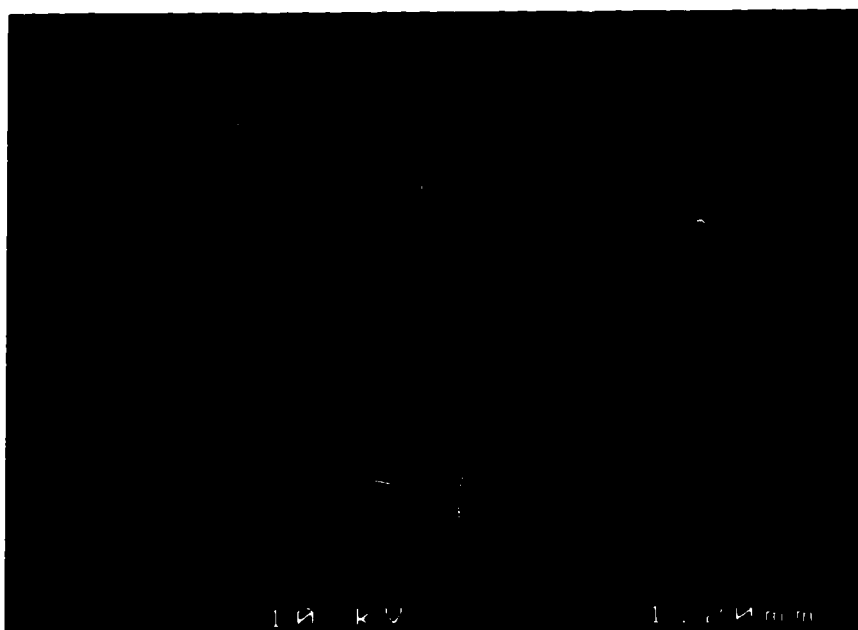


Fig. 3.3.5 Part of dried gel III is a typical structure formed during drying of all gels prepared from $[\text{Ge}(\text{OEt})_4] \leq 0.044 \text{ M}$ and $R=2.5$.



Fig. 3.3.6 Scanning electron micrographs of gels prepared from different concentrations of H_2S and $Ge(OEt)_4$ and constant $R=2.5$: a) gel IA aged 24h, $[Ge(OEt)_4]=0.220$ M; b) gel III, $[Ge(OEt)_4]=0.04$ M;

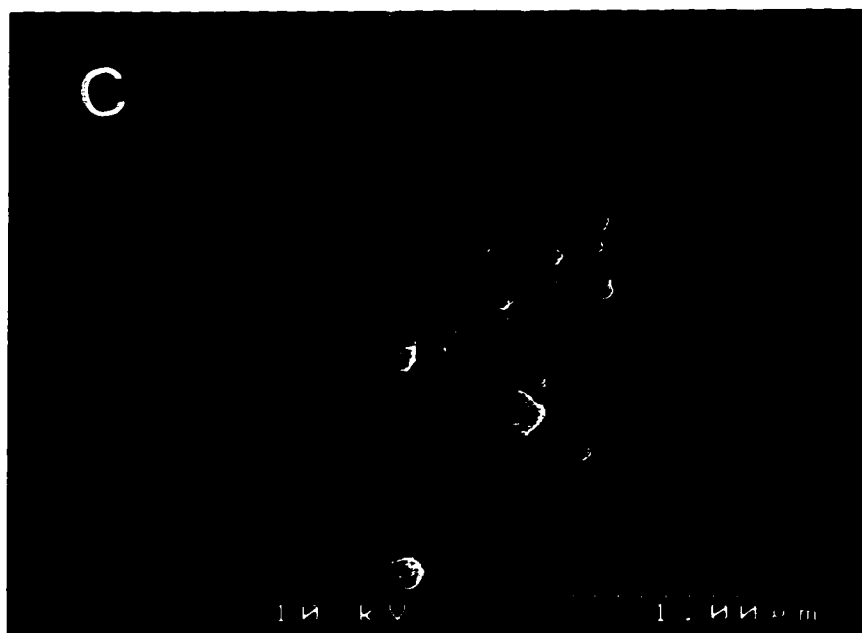


Fig. 3.3.6 c) gel IV, $[\text{Ge}(\text{OEt})_4]=0.029 \text{ M}$; d) gel V, $[\text{Ge}(\text{OEt})_4]=0.022 \text{ M}$;

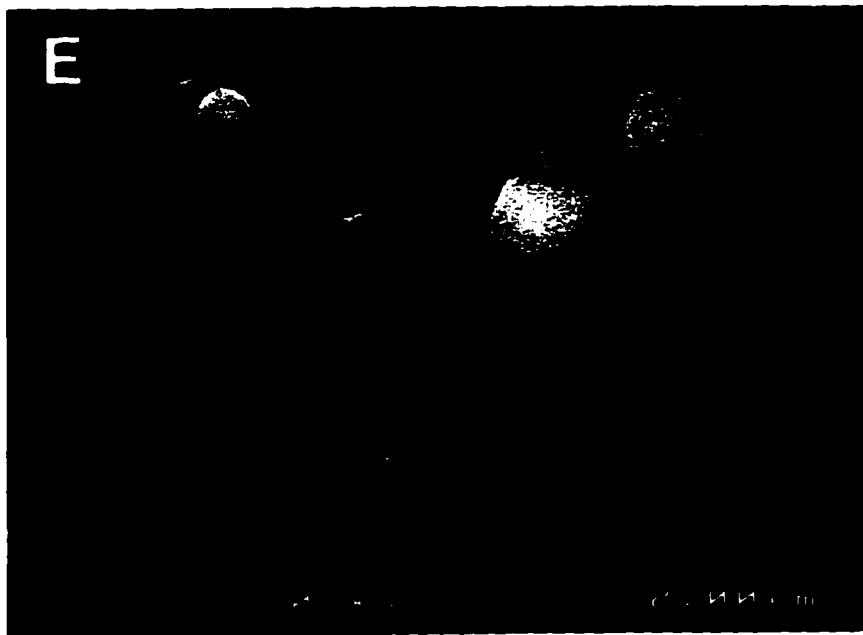


Fig. 3.3.6 e) gel IA aged 30 days.

b) Ratio

The microstructures of GeS₂ gels prepared with ratios $R < 2$ (gels XI and VII) are represented in Fig. 3.3.7 a,b, whereas of those prepared with $R > 2$ (gels VIII and IX) are shown in Fig. 3.3.7c,d. They consist of colloidal particles linked into agglomerates, as perceived in the micrographs. The appearance of the agglomerates is different for gels prepared with $R > 2$ and $R < 2$. Estimated diameter of the colloidal particles forming gels XI and VII from the micrographs is ~ 50 nm. They are connected into agglomerates ~ 0.2 μm , laterally or linearly.

The smallest particles observed in gels VIII and IX (Fig. 3.3.7c,d) have diameters ~ 0.1 μm . In gel VIII they are more linearly connected, while in gel IX they are connected into granular, ~ 0.3 μm large agglomerates. These agglomerates are subsequently linked into a 3-D porous gel network.

c) Temperature

The microstructures of the gels synthesized at different temperatures from the same concentration and ratio of the precursors are shown in Fig. 3.3.8. Characteristic of all structures is that the diameter of the smallest particle observed in the micrographs is ~ 0.1 μm . The particles are connected into different size agglomerates. Thus, the agglomerates are fine in gels synthesized at 30 and 40°C (Fig. 3.3.8a,b) and coarse in gels prepared at 45 and 50°C (Fig. 3.3.8c,d).

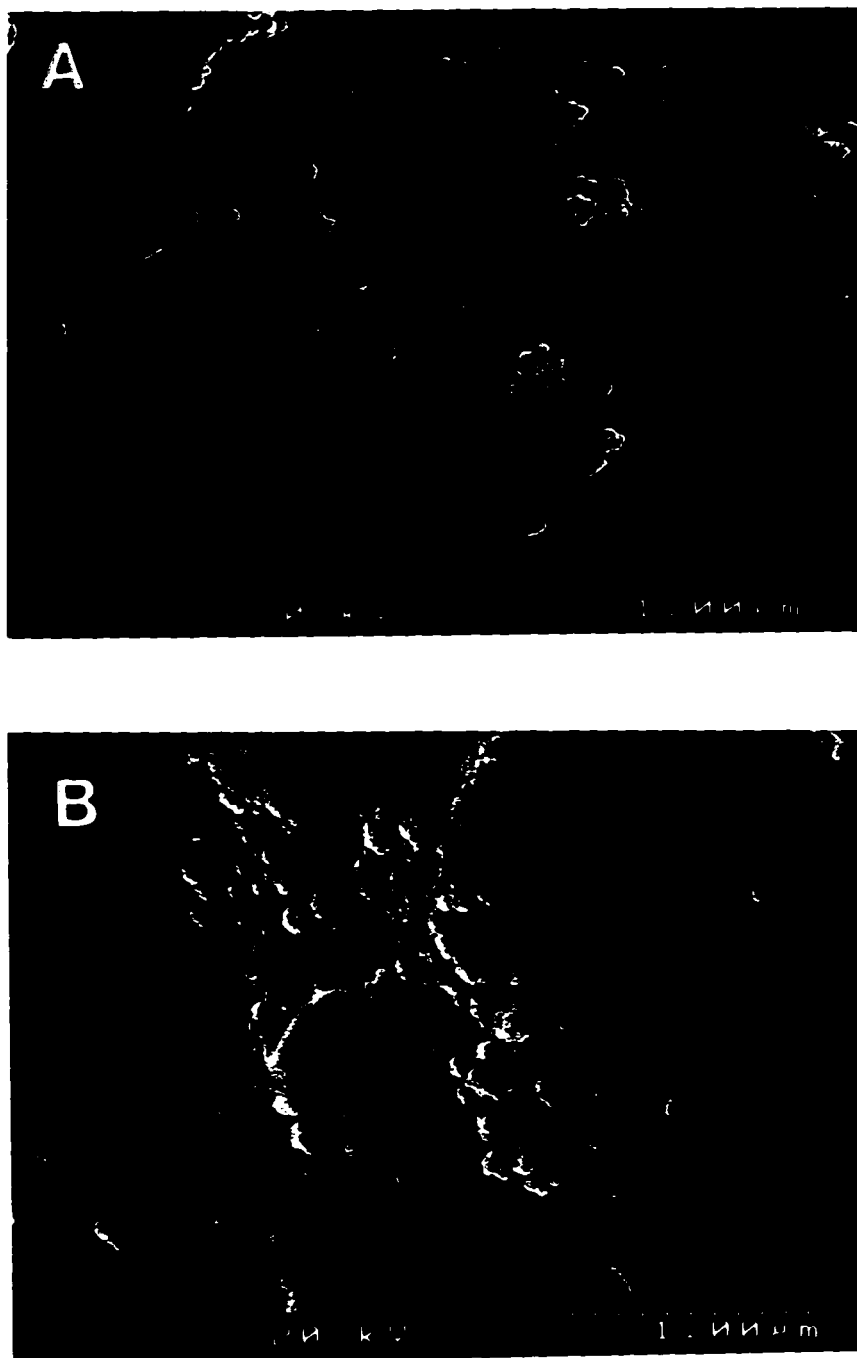


Fig. 3.3.7

Scanning electron micrographs of gels prepared with different ratios and $[\text{Ge}(\text{OEt})_4]=0.029 \text{ M}$: a) gel XI, $R=0.93$; b) gel VII, $R=1.32$;



Fig. 3.3.7 c) gel VIII, R=5; d) gel IX, R=10.

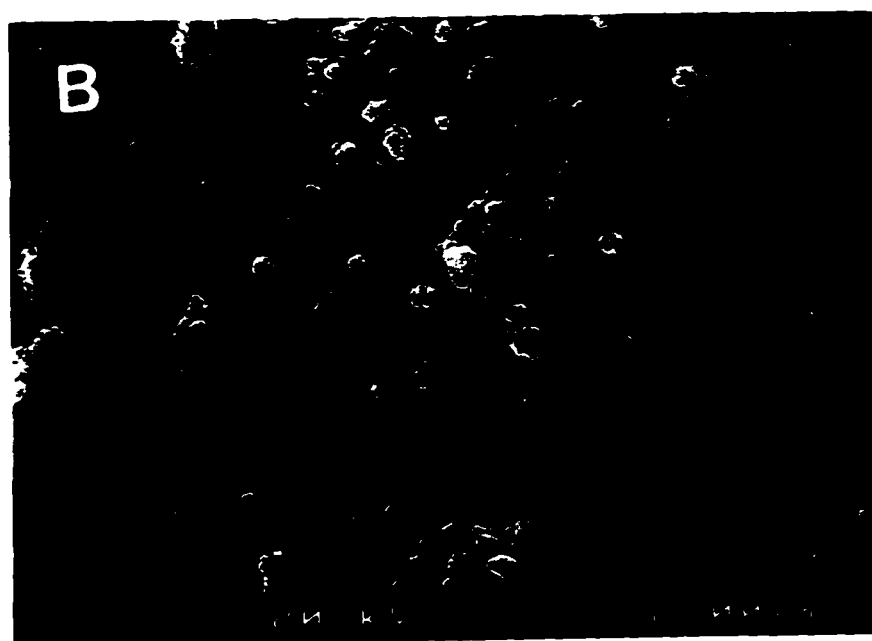


Fig. 3.3.8 Scanning electron micrographs of gels synthesized at different temperatures: a) 30°C; b) 40°C;

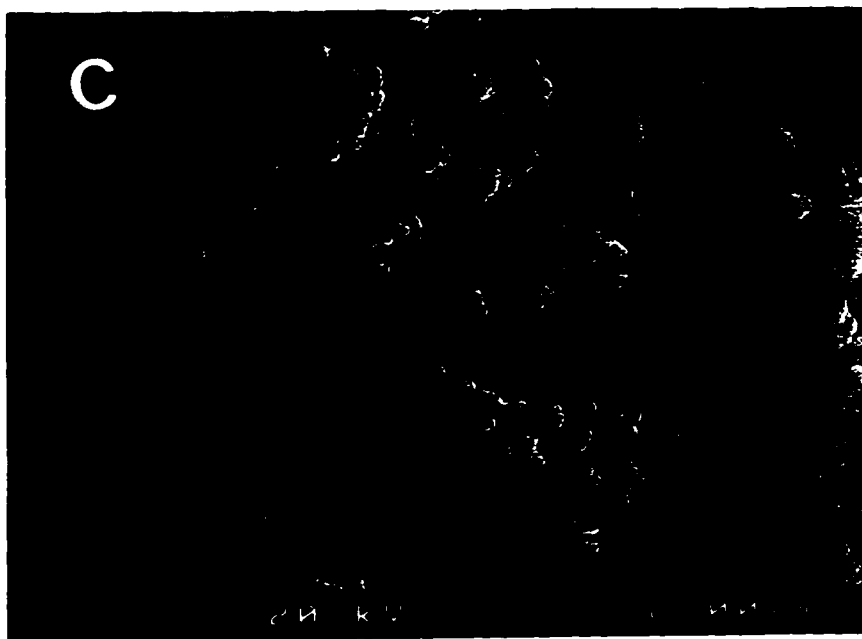


Fig. 3.3.8 c) 45°C; d) 50°C.

3.3.3. BET analysis

a) Concentration

A typical adsorption-desorption isotherm for GeS₂ gels prepared with different concentrations of H₂S and Ge(OEt)₄ is shown in Fig. 3.3.9a for gel IV. The isotherm is type IV according to the BDDT classification[92]. It exhibits hysteresis at high nitrogen partial pressures. The hysteresis loop of the isotherms is A type[89], attributed to cylindrical pores. According to the pore size distribution (Fig. 3.3.9 insert) obtained from the desorption branch of the isotherm, the pores are non-uniformly distributed within the mesopore range (1nm < R_p < 25nm).

The specific surface areas S_a of the dried gels, measured by N₂ BET adsorption, are listed in Table 3.3.1. These S_a values are plotted vs. the concentration of Ge(OEt)₄, shown in Fig. 3.3.10. The graph demonstrates that the specific surface area decreases if the concentration of Ge(OEt)₄ increases.

The average particle radius r_p was calculated from the measured specific surface area S_a and the density of monoclinic GeS₂, ρ=2.94 g/cm³, using the following formula[91]

$$r_p = \frac{3}{\rho \cdot S_a} \quad (3.3.1)$$

In Fig. 3.3.10 particle radius r_p is also plotted vs. the concentration of Ge(OEt)₄. The graph demonstrates that the particle radius increases if the concentration of Ge(OEt)₄

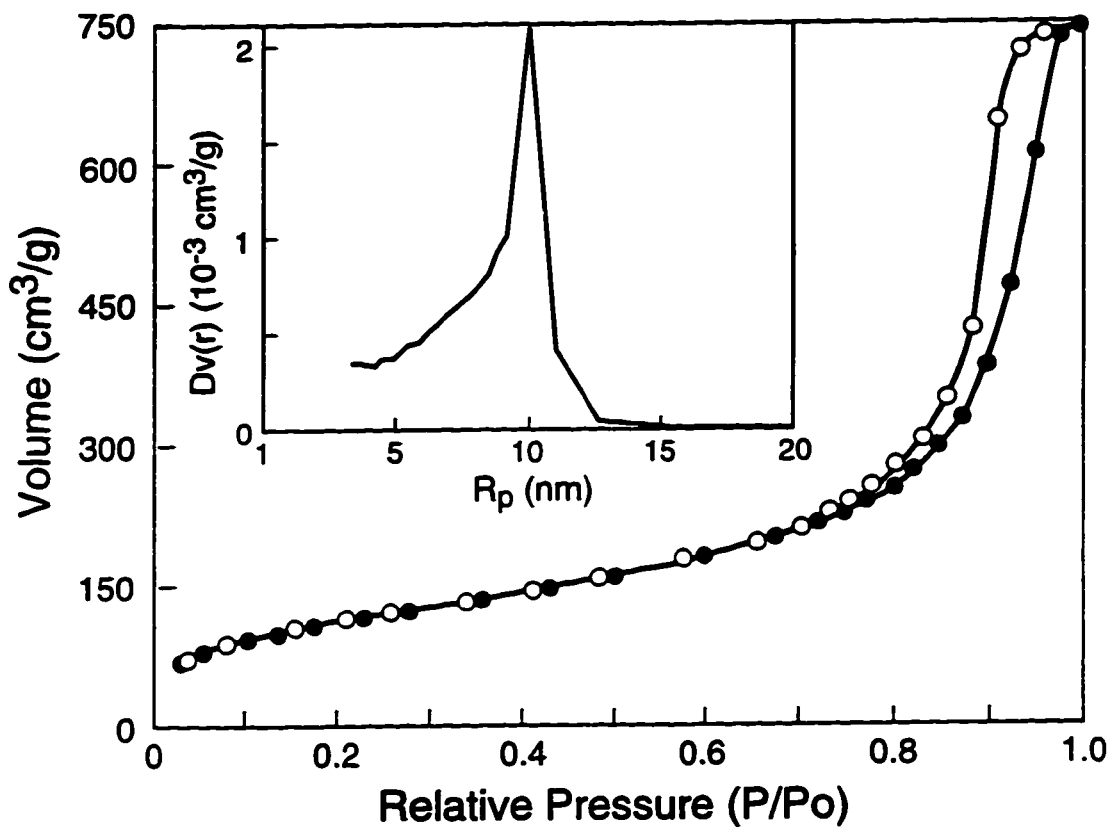


Fig. 3.3.9 BET adsorption-desorption isotherm of gel IV; insert presents pore size distribution obtained from the desorption branch of the isotherm.

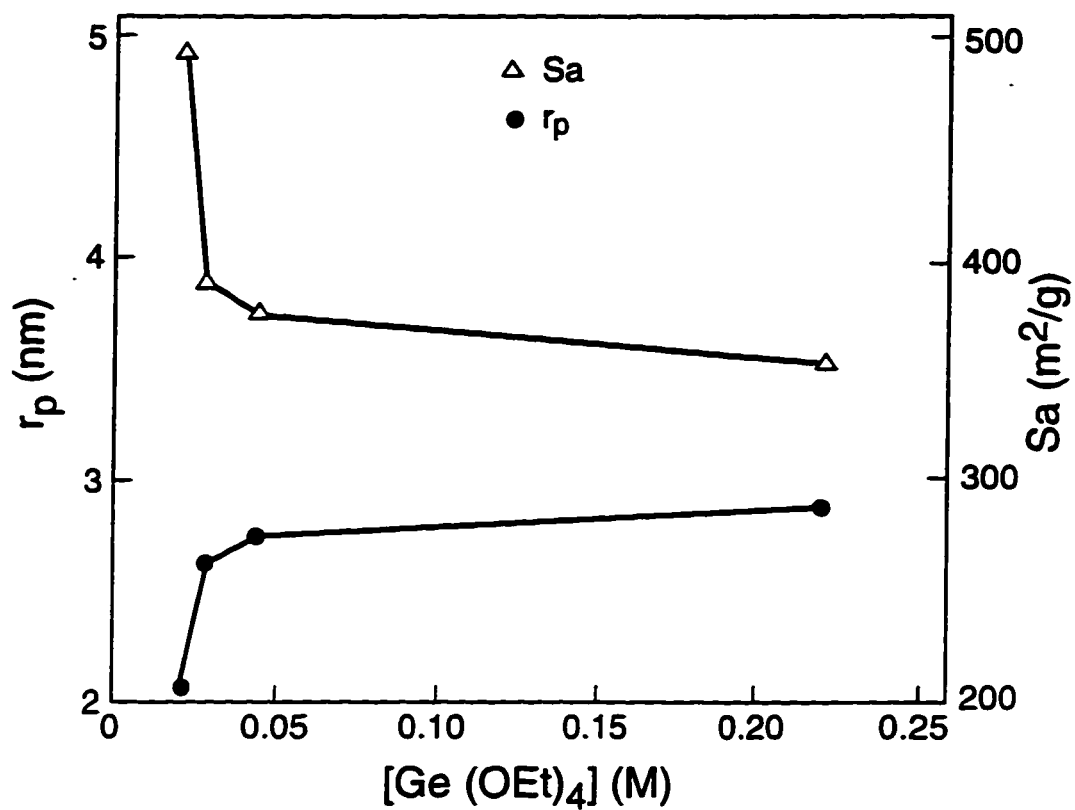


Fig. 3.3.10 Plot of surface area S_a vs. $[\text{Ge}(\text{OEt})_4]$ for $R=2.5$; particle radius r_p as a function of $[\text{Ge}(\text{OEt})_4]$ for $R=2.5$.

increases.

In Table 3.3.1 the average pore radii R_p of the gels are listed. They were calculated from the following equation[93]

$$R_p = \frac{2V_{TOT}}{S_a} \quad (3.3.2)$$

where V_{TOT} is the total pore volume measured by N_2 BET adsorption. Results indicate that the pore radius is affected by the precursor concentration more than the particle radius. The radii belong to the mesopore range. The total pore volume consists of micropores ($R_p < 1$ nm), mesopores and macropores (150 nm $> R_p > 50$ nm). Results show that GeS_2 gels include mostly mesopores. The micropore volume increases if the reactant concentration decreases, as indicated by the results presented in Table 3.3.1.

Table 3.3.1 Influence of $Ge(OEt)_4$ concentration on the microstructure of prepared GeS_2 gels. The reactants ratio R was constant 2.5 for preparation of all gels.

Gel	$[Ge(OEt)_4]$ (M)	S_a (m^2/g)	r_p (nm)	V_{tot} (cm^3/g)	V_{micro} (%)	V_{meso} (%)	V_{macro} (%)	R_p (nm)
IA	0.220	352.9	2.88	1.53	7.3	79.7	13.0	8.68
III	0.088	373.0	2.74	1.06	9.8	91.0	0.0	5.67
IV	0.029	388.1	2.63	1.16	9.2	92.3	0.0	5.97
V	0.022	491.2	2.08	0.85	15.8	77.5	6.5	3.44

BET analysis results for gel IA aged 24 h and 30 days are listed in Table 3.3.2. They indicate that the surface area of the gel is drastically reduced by aging. In addition, the average particle size increases, whereas the micropore volume decreases.

Table 3.3.2 Results of the BET analysis of gel IA aged 24 h and 30 days.

Aging	S_s	r_p	V_{tot}	V_{micro}	V_{meso}	V_{macro}	R_p
	(m^2/g)	(nm)	(cm^3/g)	(%)	(%)	(%)	(nm)
24h	352.9	2.89	1.53	7.3	79.7	13.0	8.7
30 days	60.4	17.00	0.92	2.8	73.5	23.8	30.6

b) Ratio

Fig. 3.3.11 shows an adsorption-desorption isotherm of gel XI, Appendix I, Table A1. It is a type IV isotherm with type A hysteresis [89]. Regardless of the concentration ratio R , isotherms of all GeS_2 gels were of the same type. The hysteresis appeared at high nitrogen partial pressures. The pore size distribution determined from the desorption branch of the isotherm is shown in Fig. 3.3. 11 insert. Specific surface area S_s and total pore volume V_{tot} determined from the isotherm are listed in Table 3.3.3. The results indicate that S_s increases if the ratio R increases and $R < 2$. Once R exceeds stoichiometric ($R > 2$), the specific surface area begins to decrease. Consequently, the average particle radius r_p , calculated from eq.(3.3.1), behaves contrary to S_s as a function

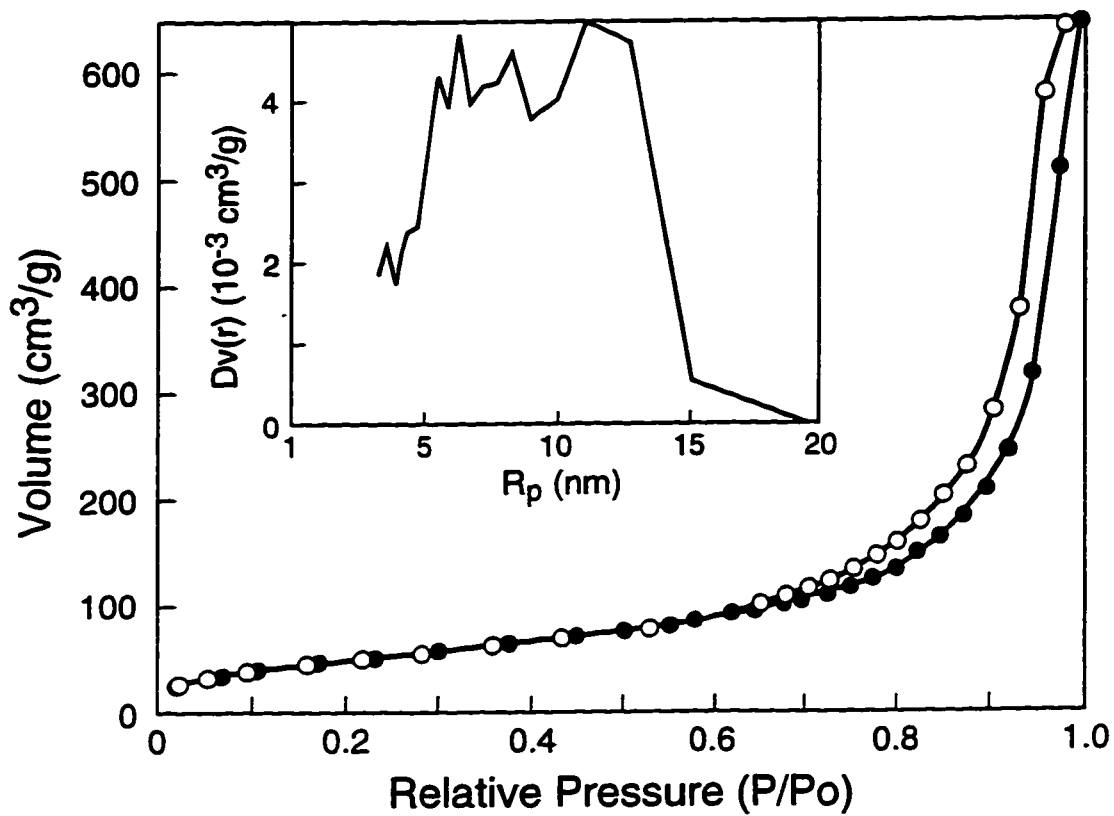


Fig. 3.3.11 BET adsorption-desorption isotherm of gel XI; insert presents pore size distribution obtained from the desorption branch of the isotherm.

of R. The plots $S_a=f(R)$ and $r_p=f(R)$ are both presented in Fig. 3.3.12.

The average pore radii R_p , calculated from eq.(3.3.2) are listed in Table 3.3.3. They are from the mesopore range. The total pore volume mostly consists of the mesopores (Table 3.3.3). When the ratio increased to $R = 5$ or greater, the macropores appeared.

Table 3.3.3 Influence of reactants ratio $R=[H_2S]/[Ge(OEt)_4]$ on the microstructure of the GeS_2 gels prepared at room temperature. The concentration of $Ge(OEt)_4$ was 0.029 M for all prepared mixtures.

Gel	R	S_a (m^2/g)	r_p (nm)	V_{tot} (cm^3/g)	V_{micro} (%)	V_{meso} (%)	V_{macro} (%)	R_p (nm)
XI	0.93	180.7	5.65	1.00	3.4	96.6	0	11.12
VII	1.32	255.6	3.97	0.21	7.0	93.0	0	1.62
IV	2.50	388.1	2.63	1.16	9.2	92.3	0	5.97
VII	5.00	363.5	2.81	0.57	15.8	76.4	7.8	3.12
IX	10.00	316.4	3.22	1.15	9.2	72.3	18.5	7.30

c) Temperature

In Fig. 3.3.13a an adsorption-desorption isotherm of a gel prepared at 50°C is typical for all the other gels synthesized at different temperatures. This isotherm belongs to type IV linked to porous materials. The type A hysteresis loop of the isotherm appears for high nitrogen partial pressures. The pore size distribution is shown in Fig. 3.3.13 insert. It is apparent, the pores are broadly distributed mesopores. The calculated average pore radii of the gels are listed in Table 3.3.4.

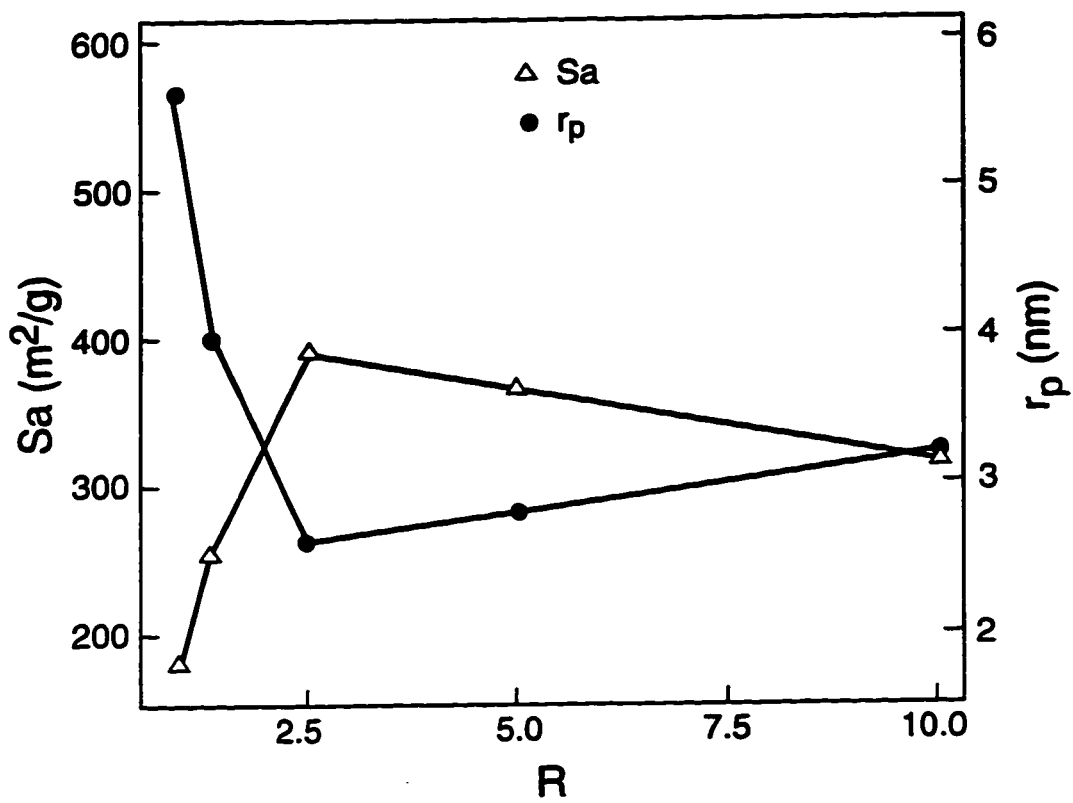


Fig. 3.3.12 Plot surface area $S_a=f(R)$ of gels prepared from $[\text{Ge}(\text{OEt})_4]=0.029 \text{ M}$ and $[\text{H}_2\text{S}]$; r_p vs. $R=[\text{H}_2\text{S}]/[\text{Ge}(\text{OEt})_4]_{\text{const.}}$.

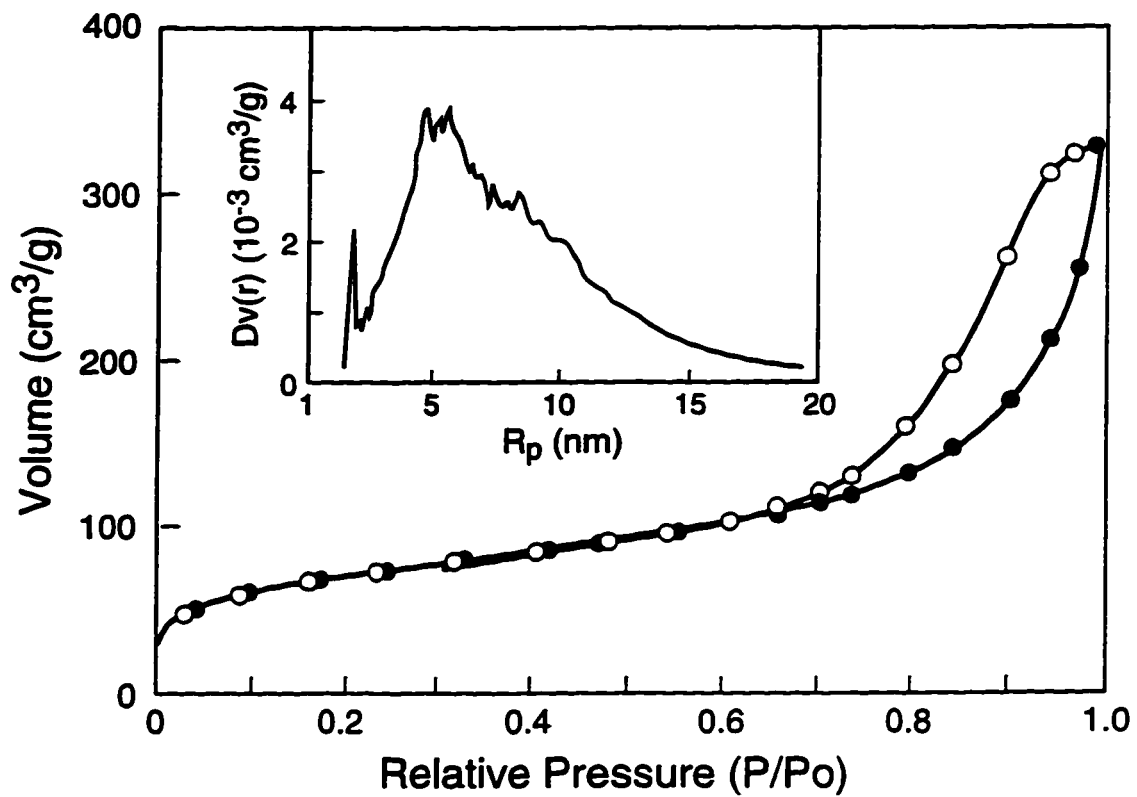


Fig. 3.3.13 BET isotherm of a gel prepared at 50°C; insert presents pore size distribution obtained from the desorption branch of the isotherm.

The total pore volume involves micro, meso and macropores. The micropore content decreased when gels were prepared at higher temperatures. The mesopores are the main element constituting the total pore volume in these gels.

Specific surface areas and particle radii are presented in Table 3.3.4. The graphs $S_s=f(T)$ and $r_p=f(T)$ are shown in Fig. 3.3.14. They reveal that S_s and r_p are opposite functions of temperature.

Table 3.3.4 Influence of the reaction temperature on the microstructure of the GeS_2 gels prepared from $[\text{Ge}(\text{OEt})_4]=0.264 \text{ M}$ and $[\text{H}_2\text{S}]=0.220\text{M}$.

T (°C)	S_s (m^2/g)	r_p (nm)	V_{tot} (cm^3/g)	V_{micro} (%)	V_{meso} (%)	V_{macro} (%)	R_p (nm)
30	429.9	2.37	0.689	5.4	83.1	11.5	3.2
40	385.4	2.65	0.693	2.6	87.2	10.2	3.6
45	285.6	3.57	0.603	2.1	88.1	9.8	4.2
50	248.9	4.10	0.514	1.6	88.4	10.1	4.1

3.3.4. XRD and infrared analyses

All synthesized gels were amorphous regardless of the reaction conditions (Appendix I, Table A1). A typical XRD pattern is represented by the graph of gel 2 (Fig. 3.1.1c).

The IR spectrum collected in the range $400\text{--}4000\text{cm}^{-1}$ for gel 2 (Fig. 3.1.3c) is also representative of the gels listed in Appendix I, Table A1.

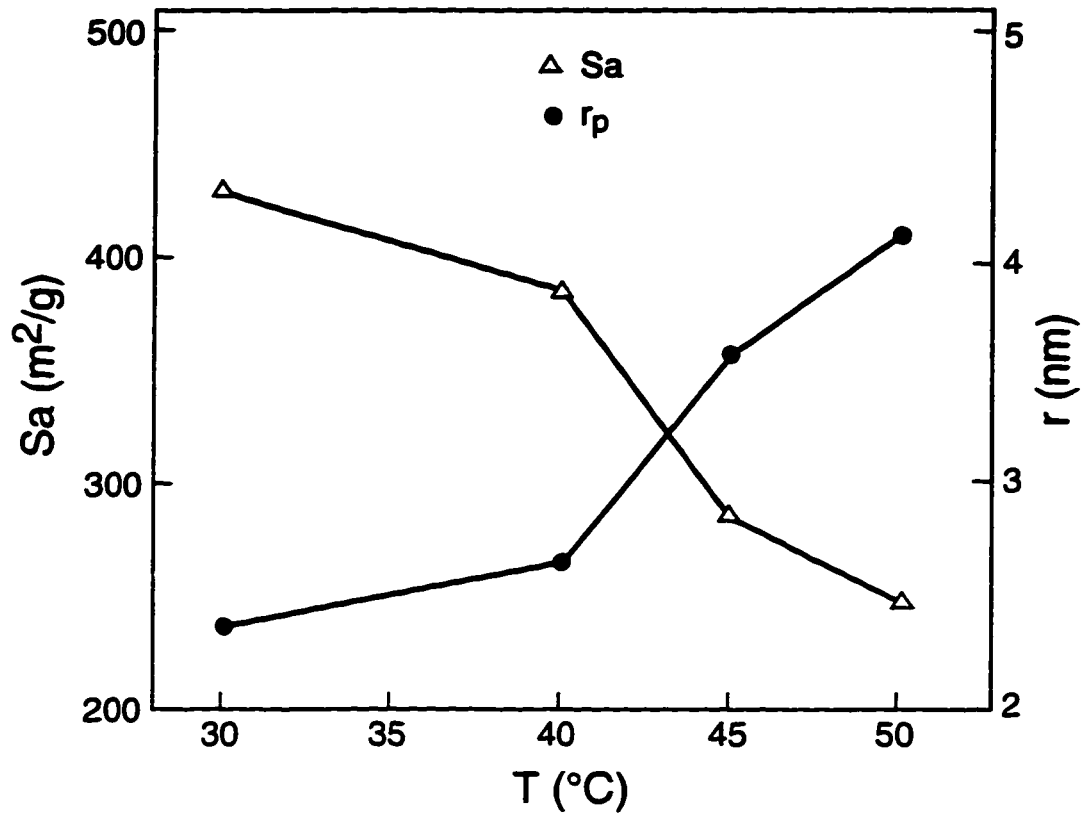


Fig. 3.3.14 Plot of surface area $Sa=f(T)$ of gels prepared at various temperatures; average particle radius $r =f(T)$ of gels prepared at different temperatures.

3.4. CHARACTERIZATION OF METAL SULFIDES

3.4.1. ZnS gel

The reaction of $\text{Zn}(\text{OC}_4\text{H}_9)_2$ and H_2S in toluene yielded a yellow, semi-transparent gel. After solvent evaporation in a vacuum oven, the gel dried into a transparent reddish-orange solid. The gel shrunk during drying; thus the solid cracked into pieces $\approx 2 \times 2$ mm.

The x-ray diffraction pattern shown in Fig. 3.4.1 indicates the presence of β -ZnS[94], the most stable allotrope at room temperature. The average crystallite size calculated from x-ray line widths by the Sherrer equation [95] is ≈ 10 nm. The scanning electron micrograph of a dried gel (Fig. 3.4.2) reveals that the gel is colloidal, formed by the linking of spherical particles $\approx 0.1 \mu\text{m}$ in size. The IR spectrum in the range from 200 - 600 cm^{-1} (Fig. 3.4.3a) has an absorption peak at 350 cm^{-1} which could be assigned to Zn-S-Zn vibration mode[88]. Moreover, the spectrum in the range from 400 - 4000 cm^{-1} (Fig. 3.4.3b) indicates only the presence of absorbed toluene and tert-butanol left in the gel after drying. A peak at $\approx 1700 \text{ cm}^{-1}$ could be assigned to absorbed water. Energy dispersive spectrometry (EDS) shows that the dried gel has a Zn/S atomic ratio $\approx 1:1$.

3.4.2. Sol-gel products of tungsten sulfides

Reactions of $\text{W}(\text{OEt})_6$ and $\text{WCl}_2(\text{OEt})_3$ began instantly with H_2S introduction into the solutions. Black precipitates were formed with both alkoxides. After aging and drying, the reaction product of $\text{W}(\text{OEt})_6$ appeared to be a brown black, highly viscous

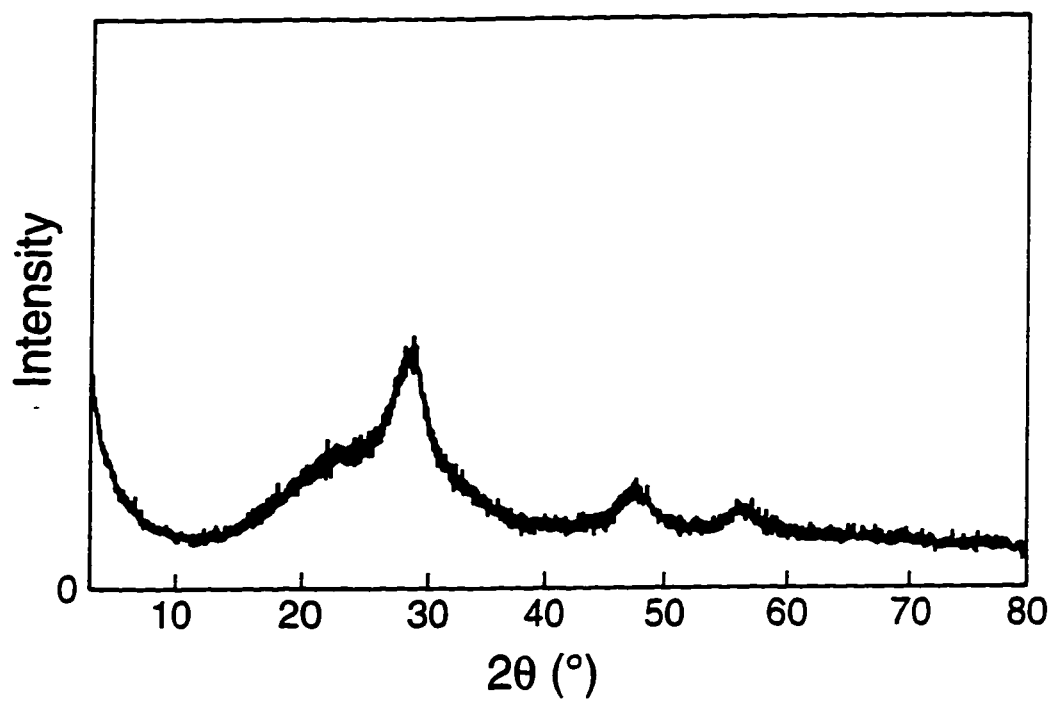


Fig. 3.4.1 XRD pattern of dried ZnS gel indicates the presence of β -ZnS.



Fig. 3.4.2 Scanning electron micrograph of dried ZnS gel.

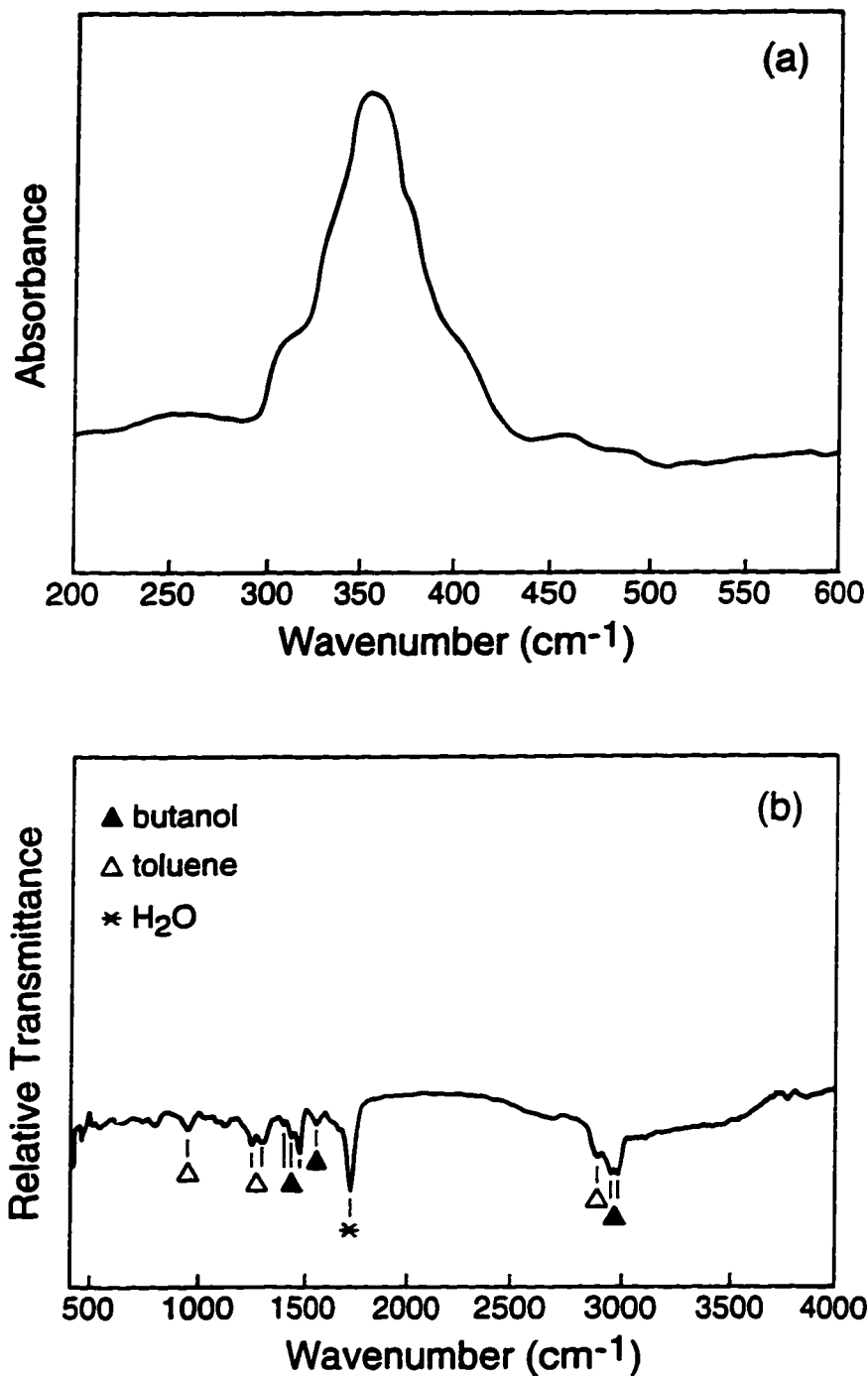


Fig. 3.4.3 The IR spectrum of dried ZnS gel collected in the range from: a) 200-600 cm⁻¹; b) 400-4000 cm⁻¹.

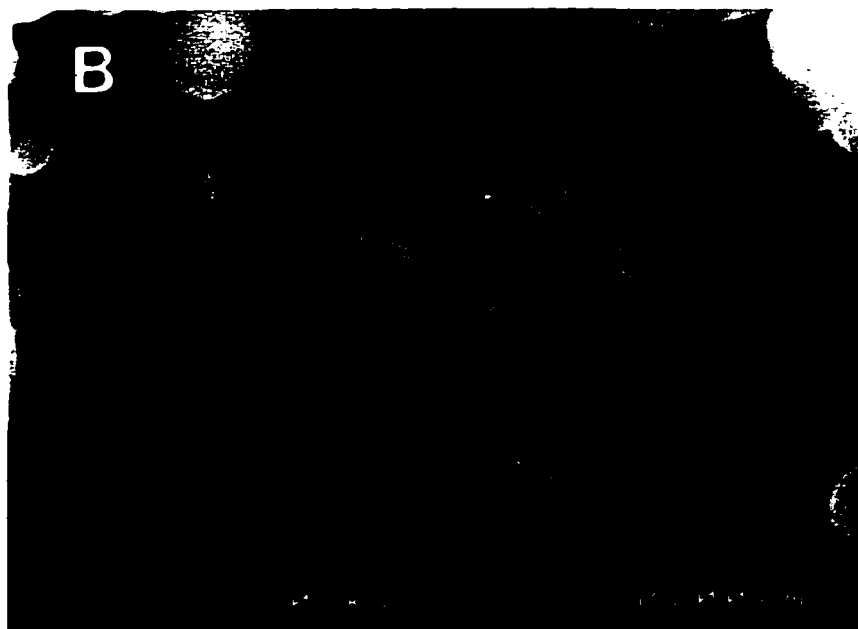
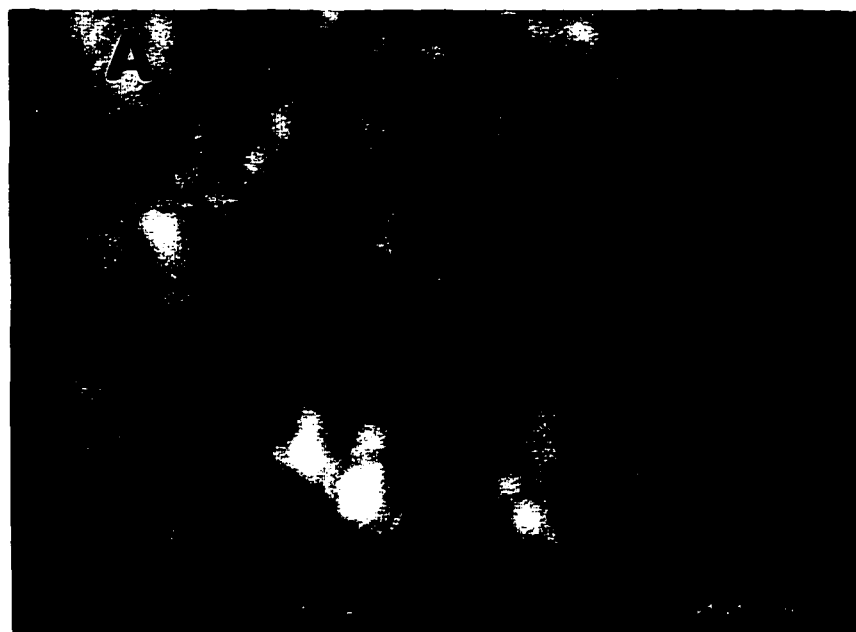


Fig. 3.4.4 Scanning electron micrographs of tungsten sulfide: a) gel; b) powder.

liquid (Table 3.4.1, Product 1). However, the precipitate formed in the reaction of $WCl_2(OEt)_3$ was a brown-black powder (Table 3.4.1, Product 2).

Table 3.4.1 Tungsten sulfide sol-gel products

Product	Type	Alkoxide	Concentration (10^3M)
1	gel	$W(OEt)_6$	14
2	powder	$WCl_2(OEt)_3$	68

Examination by the scanning electron microscope indicates that Product 1 is a gel formed from spherical colloidal particles connected into a 3-dimensional network (Fig. 3.4.4a). Nonetheless, SEM examination reveals that Product 2 is a powder which consists of loose colloidal particles whose radii are in the range of $0.5 < r < 1\mu m$ (Fig. 3.4.4b).

The XRD patterns of Product 1 and 2, shown in Fig. 3.4.5a and b, indicate that both products have amorphous structures. The amorphous halo of Product 1 appeared at $\approx 23^\circ 2\theta$, while Product 2 has two broad peaks at $\approx 16^\circ$ and $36^\circ 2\theta$.

The IR spectra of Products 1 and 2 collected in the range from $400-4000\text{ cm}^{-1}$ are represented in Fig. 3.4.6. The strong absorption peaks at ≈ 694 and 728 cm^{-1} are characteristic peaks of toluene and they appeared in the spectrum of each product due to retained toluene [88]. Toluene absorption peaks were also identified at $\approx 1081, 1380, 1495$ and 2860 . Peaks at ≈ 880 (identified in Fig. 3.4.6b), 1050 (identified in Fig. 3.4.6a), $1120, 1274, 2975$ and 3331 cm^{-1} indicate the presence of ethanol [88].

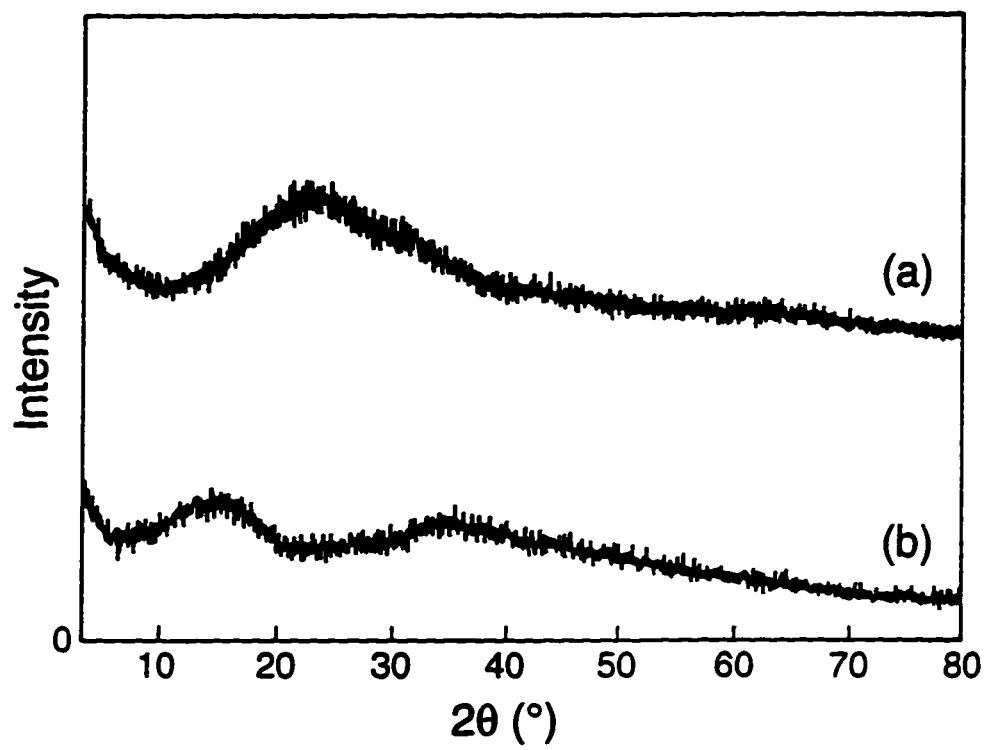


Fig. 3.4.5 XRD pattern of tungsten sulfide: a) gel; b) powder.

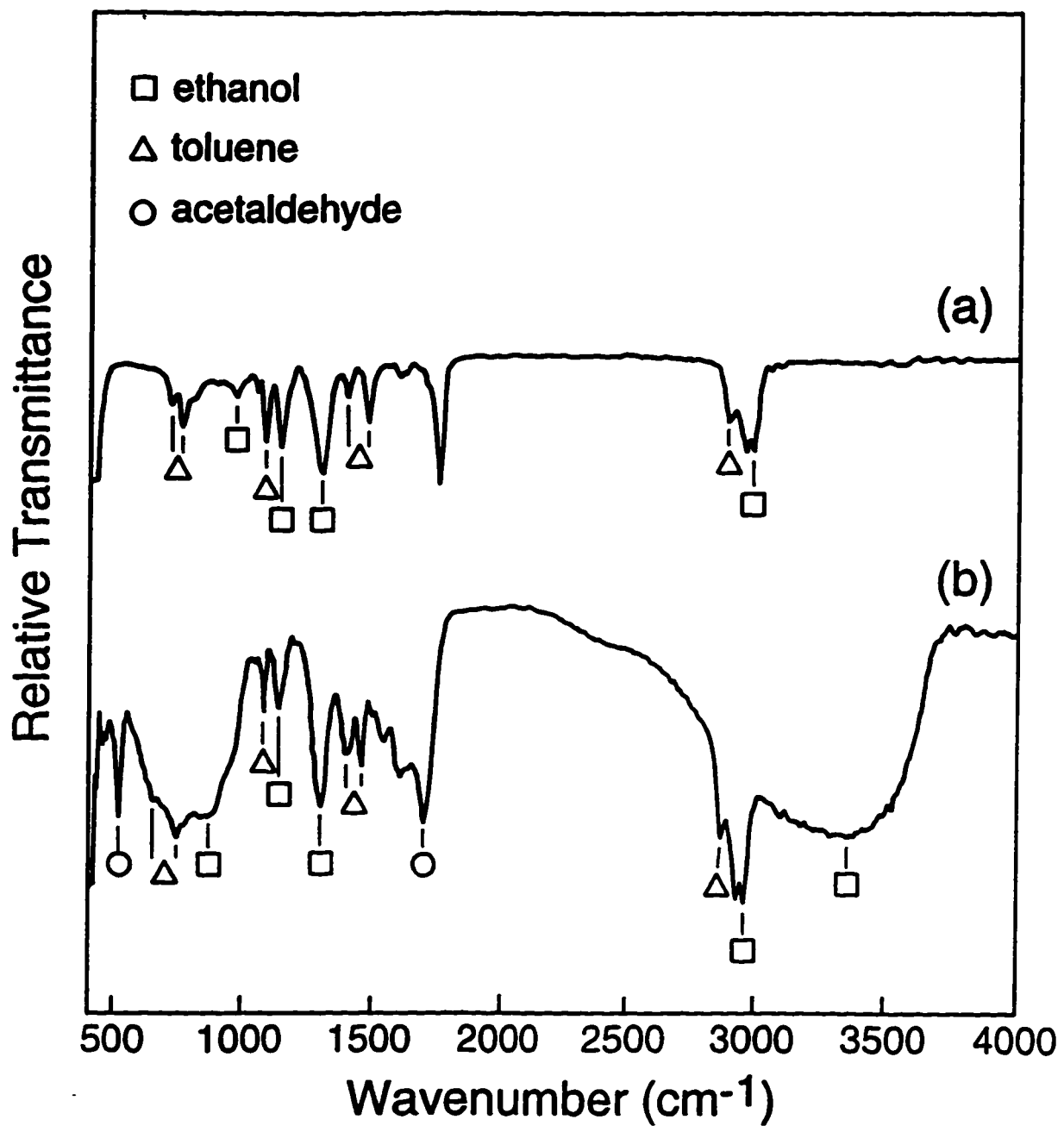


Fig. 3.4.6 IR spectrum collected in the range from 400-4000 cm⁻¹ of: a) tungsten sulfide gel; b) tungsten sulfide powder.

The strong absorption peak at $\approx 525 \text{ cm}^{-1}$ could be assigned to acetaldehyde [96]. The infrared spectrum of Product 2 in the range from 200-600 cm^{-1} is shown in Fig. 3.4.7. Along with the sharp peak at $\approx 525 \text{ cm}^{-1}$ previously assigned to acetaldehyde, a broad peak at $\approx 320 \text{ cm}^{-1}$ appeared due to W-S-W asymmetric stretching [97]. Energy dispersive spectrometry shows that Products 1 and 2 have apparent W/S atomic ratios of 1:2.7 and 1:1.4, respectively.

The BET analysis of Product 2 yielded a specific surface area of 3.49 m^2/g . The isotherm is type III of BDDT classification [98]. The hysteresis loop in the isotherm belongs to type A which is usually associated with cylindrical pores [89]. The calculated volume of mesopores ($1 < r < 25 \text{ nm}$) is 42% and for the micropores 9.3%. The average pore radius is 8 nm.

The viscosity of Product 1 was measured. However, the gel liquified when it was under load. It regained its high viscosity appearance after unloading. This kind of behaviour indicates that Product 1 undergoes thixotropic alteration[91].

3.5. CHARACTERIZATION OF THIN FILMS

The XRD patterns of the metal sulfide thin films indicate that they are amorphous. The micrographs of the GeS_2 (TF1) and ZnS (TF5) thin films are shown in Fig. 3.5.1. They indicate that the films consist of colloidal particles. Film TF1 was

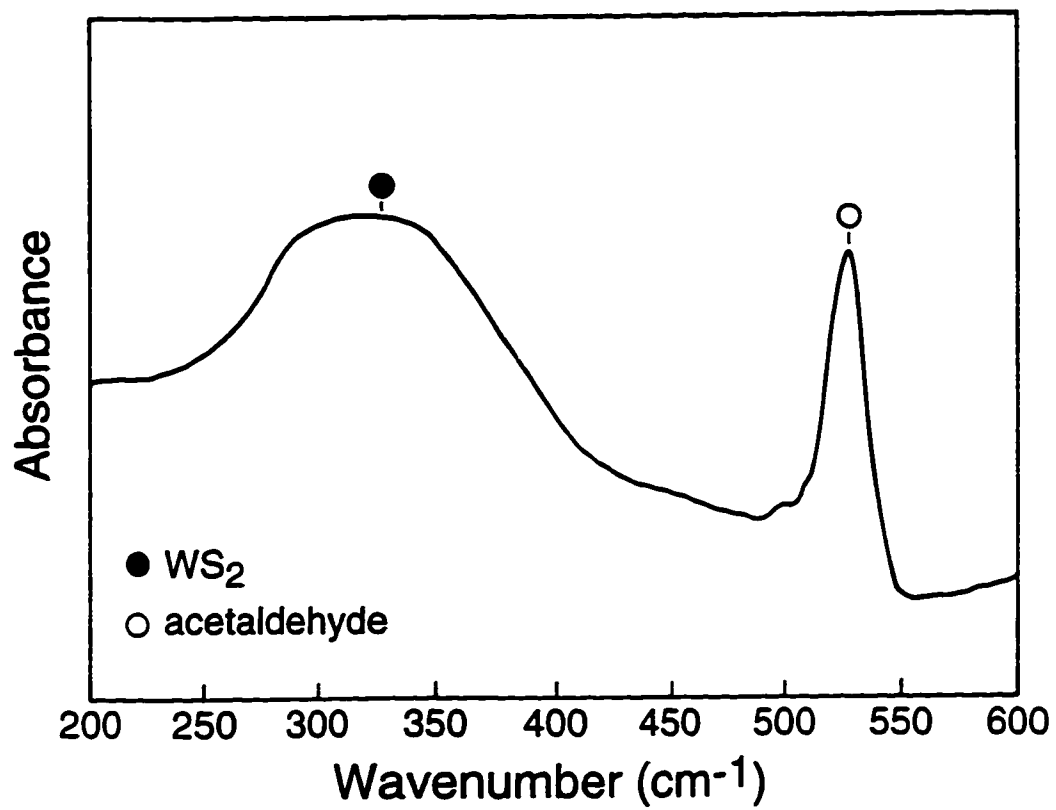


Fig. 3.4.7 IR spectrum of tungsten sulfide powder collected in the range from 200-600 cm⁻¹.

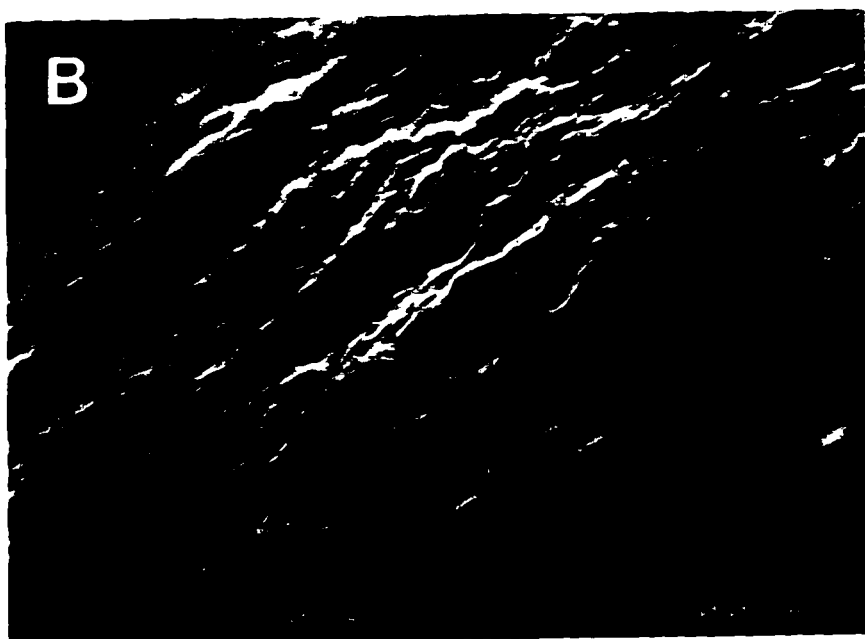
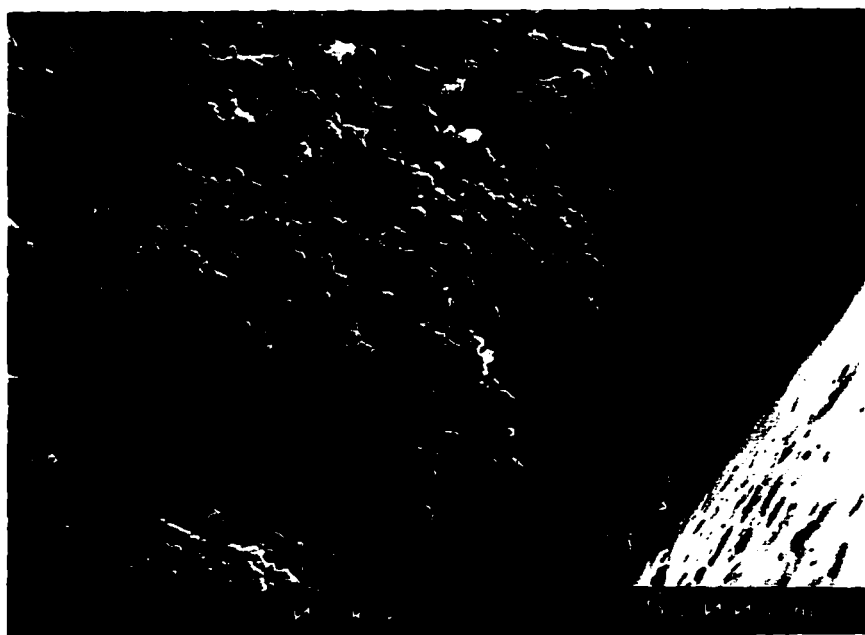


Fig. 3.5.1 Scanning electron micrographs of the thin films: a) TF1, prepared from $\text{Ge}(\text{OEt})_4$, solution 5; b) TF5, prepared from $\text{Zn}(\text{OBu})_2$.

formed by one immersion of the glass slide into solution 5 just before the gel point. The thickness of the film estimated from the micrograph (Fig. 3.5.1a) is $\approx 5 \mu\text{m}$. Film TF5 prepared by one dip of the slide into the colloidal dispersion of ZnS covered the substrate uniformly. The thickness of this film is $\approx 0.5 \mu\text{m}$. Both films TF1 and TF5 demonstrated good adhesion to the slide when tested by scotch tape.

The size of the particles is different for different films. For instance, it is less than $0.1 \mu\text{m}$ for the GeS_2 film (TF2), prepared by one dipping of the slide into the solution 6. The size of the particles increased ($\sim 3x$) after the second immersion of the slide into the same solution. Film TF3 consists of particles size $\sim 1 \mu\text{m}$ which irregularly covered the slide. The tungsten sulfide film (TF4) containing spherical colloidal particles size $\sim 1 \mu\text{m}$ inconsistently adhered to the substrate.

3.6. POTENTIOMETRIC TITRATION

3.6.1. Accuracy

The accuracy of the applied method was tested by performing potentiometric titration of two equal volume aliquots of the H_2S /toluene solution by HgCl_2 and AgNO_3 . The resulting potentiometric curves are shown in Fig. 3.6.1. The inflection point on the curve, if HgCl_2 is a titrant, is at 1.75 mL, while on the curve of AgNO_3 titrant, it is at 3.5 mL. From a previous equation [99],

$$V_1N_1 = V_2N_2 \quad (3.6.1)$$

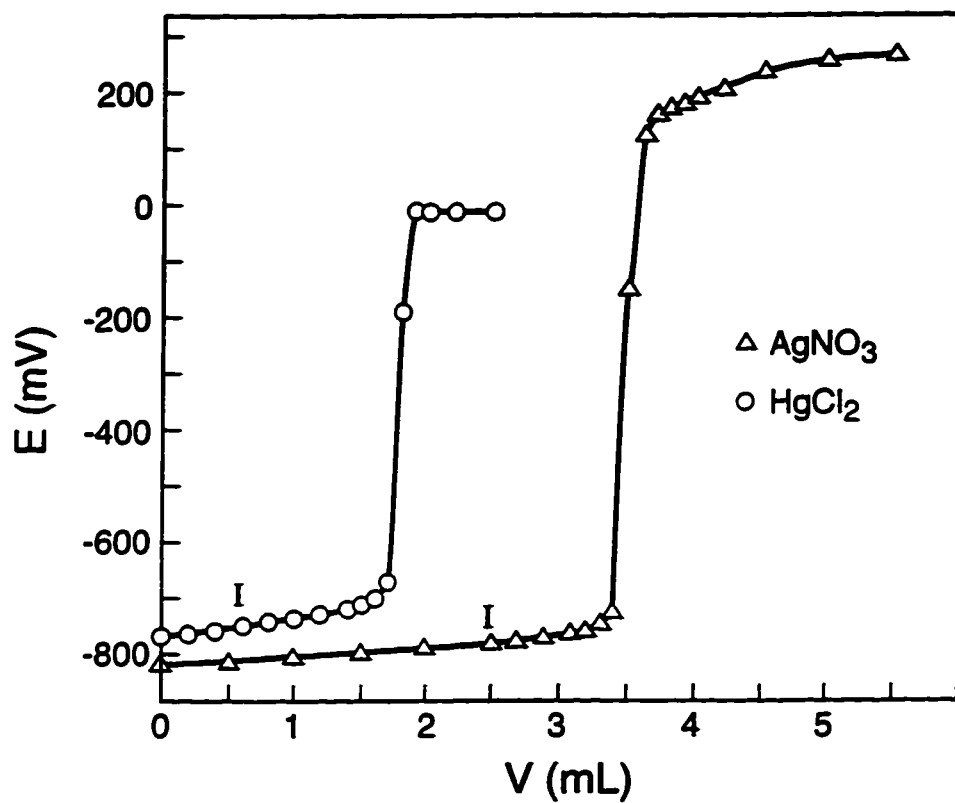


Fig. 3.6.1 Potentiometric titration curves of the same samples of H_2S in toluene, titrated with: (O) 1×10^{-2} M HgCl_2 ; (Δ) 1×10^{-2} M AgNO_3 .

the concentrations in the H₂S samples were calculated for both titrants. The same result, 1.75X10⁻² M, was obtained. In eq.(3.6.1) V₁ and N₁ are the volume and normality of the H₂S solution, V₂ is the volume of the titrant corresponding to the equivalence point and N₂ is the titrant normality. The concentrations of HgCl₂ and AgNO₃ were 1x10⁻² M, which correspond to 1x10⁻² N HgCl₂ and 5x10⁻³ N AgNO₃ in regard to S²⁻.

3.6.2. Reproducibility

The reproducibility of the method was tested by titrating five separate 0.1 mL aliquots of the H₂S/toluene solution with 1x10⁻² M AgNO₃. The volume of titrant at the equivalence point was 8.4 mL for all five titrations.

Fig. 3.6.2 represents potentiometric curves of two samples taken from the sol-gel reaction mixture at the same time (3.5 h from the start). The curve in Fig. 3.6.2a was obtained by titrating a 0.1 mL sample containing H₂S, germanium sulfide and germanium mercaptide with 1x10⁻² M AgNO₃; however, the curve in Fig. 3.6.2b is the result of the titration of a 1 mL sample with the same titrant after H₂S removal by purging. The difference between the titrant volumes at the first (5.2 mL) and the second (5.6 mL) equivalence points in Fig. 3.6.2a was 0.4 mL, while in Fig. 3.6.2b it was 4.1 mL. If it is assumed that the first equivalence point represents the precipitation of Ag₂S (sulfide S²⁻ from H₂S and GeS₂) and the second the precipitation of GeSAg (GeS⁻ mercaptide from GeSH), the volume difference between equivalence points on the curves (Fig. 3.6.2) recalculated for the same sample volumes is equal and indicates the concentration of the mercaptide. Thus, the total mercaptide (SH) concentration is C_{SH} = 4.1x10⁻² M,

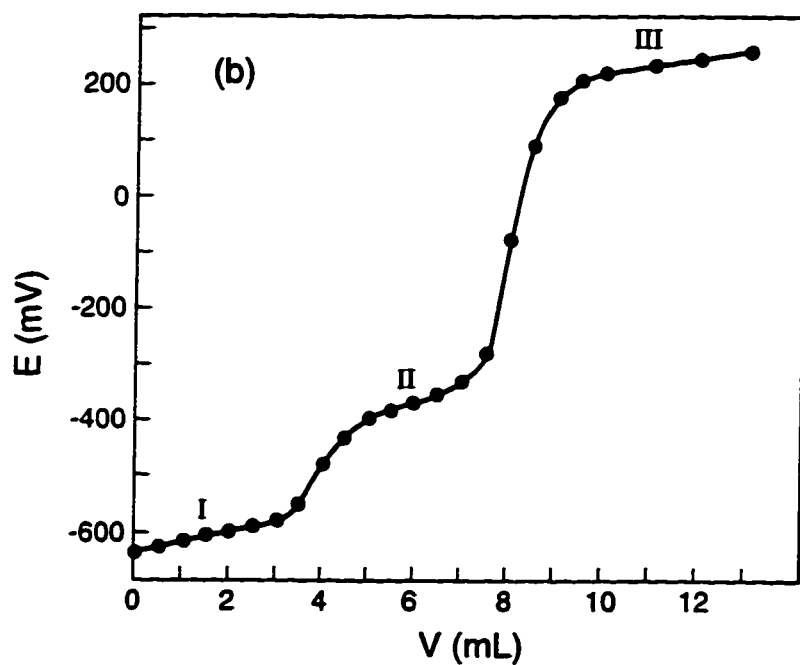
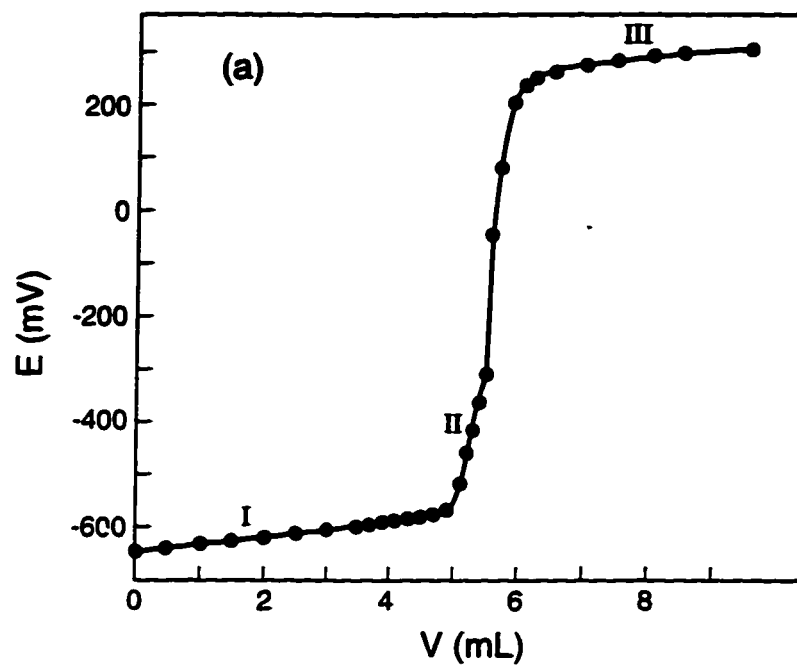


Fig. 3.6.2 Potentiometric titration curves of the sample taken from the sol-gel reaction mixture after 3.5 h: a) 0.1 mL of the sample titrated with 1×10^{-2} M AgNO_3 ; b) 1 mL of the sample titrated with 1×10^{-2} M AgNO_3 after removal of H_2S .

making that of germanium mercaptide $\text{Ge}(\text{SH})_4$ four times lower, 1.025×10^{-2} M. Further, the concentration of total sulfide (S) from the Fig. 3.6.2b is $C_s = 2.05 \times 10^{-2}$ M indicating the concentration of GeS_2 is 1.025×10^{-2} M. From the first equivalence point in Fig. 3.6.2a the calculated total sulfur concentration is 26×10^{-2} M. The difference of total sulfide concentrations determined from Fig. 3.6.2a and 2b gives the H_2S concentration before purging.

3.6.3. Selectivity

The Ag/AgS_2 electrode potential dependence on the concentration of free ions is defined by the Nernst equation. In the case of free Ag^+ in the test solution, the potential equation is

$$E_{\text{Ag}^+/\text{Ag}} = E^{\circ}_{\text{Ag}^+/\text{Ag}} + \frac{2.3RT}{F} \log C_{\text{Ag}^+} \quad (3.6.2)$$

where $2.3RT/F$ is 58.1 mV at 20°C and C_{Ag^+} is the silver ion concentration. The number of electrons n involved in eq.(3.6.2) is 1. The apparent standard electrode potential E° includes the standard electrode potential $E^{\circ}_{\text{Ag}^+/\text{Ag}}$, liquid junction potential, reference electrode potential (saturated calomel) and activity coefficient of silver ion, $\log \gamma_{\pm}$. However, if there are sulfide ions in the solution, then the Nernst equation is expected to be

$$E = E^{\circ}_{\text{Ag}^+/\text{Ag}} + \frac{2.3RT}{2F} \log K_{\text{Ag}_2\text{S}} + \frac{2.3RT}{2F} \log C_s \quad (3.6.3)$$

where K_{Ag_2S} is the solubility product of silver sulfide formed during precipitation and number of electrons $n=2$ involved in the reaction. Similarly, the Nernst equation for the electrode potential depending on mercaptide concentration is

$$E = E^{\circ}_{Ag+/Ag} + \frac{2.3RT}{F} \log K_{GeSAg} - \frac{2.3RT}{F} \log C_{SH} \quad (3.6.4)$$

where K_{GeSAg} is the solubility product of germanium silver mercaptide GeSAg formed during titration and $n=1$.

In order to check the agreement of the experimental results with the Nernst equation, measured electrode potentials E , used for plotting curves as those in Fig. 3.6.1 and 3.6.2, were also plotted as $E = f(\log C_i)$. Representative curves are shown in Fig. 3.6.3. The concentrations C_i of free, potential determining species S^{2-} from H_2S or GeS_2 , GeS^- from $GeSH$, and Ag^+ from excess $AgNO_3$ were calculated in the following way

$$C_S = (V_{eq1} - V)M/2 \text{ mole/L} \quad (3.6.5)$$

$$C_{SH} = (V_{eq2} - V)M \text{ mole/L} \quad (3.6.6)$$

$$C_{Ag^+} = (V - V_{eq2})M \text{ mole/L} \quad (3.6.7)$$

where V_{eq1} and V_{eq2} are the first and second equivalence points, V is the volume of added titrant and M is the titrant molarity.

Results of evaluation of these linear plots are shown in Table 3.6.1. The slopes of the graphs, $p(2.3RT/F) = p58 \text{ mV}$, indicate the stoichiometry of the electrochemical reactions involving S^{2-} , GeS^- or Ag^+ at the electrode. The stoichiometric coefficient p

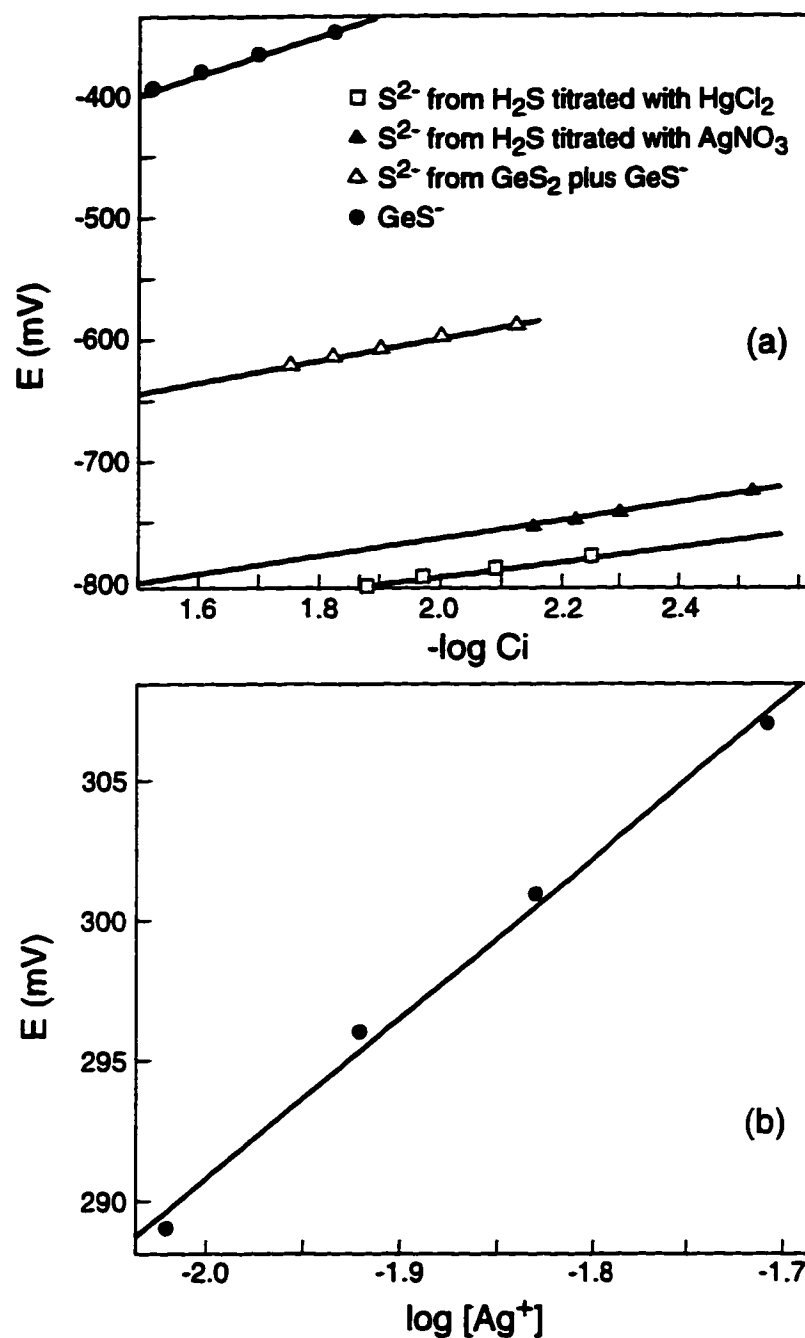


Fig. 3.6.3 Electrode response to different ions plotted as $E=f(\log C_i)$. Graphs were obtained from data for: a) Fig. 3.6.1, part I, S^{2-} from H_2S titrated with $HgCl_2$ (\square); Fig. 3.6.1, part I, S^{2-} from H_2S titrated with $AgNO_3$ (\blacktriangle); Fig. 3.6.2, part I, S^{2-} from GeS_2 and GeS^- were present in the solution (\triangle); Fig. 3.6.2, part II, only GeS^- was in the solution (\bullet); b) Fig. 3.6.2a, part III, Ag^+ from the excess $AgNO_3$ in the solution.

is defined as $1/n$. If the Nernst equation were applicable to eq.(3.6.2), (3.6.3) and (3.6.4), then the stoichiometric coefficients p would be 1, 1/2 and 1 mV, respectively. Apparently, the slopes for reactions involving S^{2-} and GeS^- are greater than expected (Table 3.6.1). They indicate complex formation. Nevertheless, the slope of the linear graph for electrode response to Ag^+ is 58 mV as expected.

Table 3.6.1 Results of the electrode response to different ions obtained from the linear graphs in Fig. 3.6.3.

Electrode response to	Slope (mV)	Intercept (mV)	p	$-\log K_{sp}$	Detection limit $-\log C_i$
S^{2-} from H_2S ($AgNO_3$ titr)	69	-932	1.2	23.0	13.1
S^{2-} from H_2S ($HgCl_2$ titr)	78	-921	1.3	22.8	11.8
S^{2-} from GeS_2	89	-770	1.5	20.3	9.0
GeS^-	155	-630	2.7	17.9	4.0
Ag^+	58	+406	1.0	-	7.0

The linear graphs $E=f(\log C_i)$, where C_i is either of S^{2-} , SH^- or Ag^+ , were extrapolated to limiting cases when C_S , C_{SH} and $C_{Ag^+} = 1$ M. The obtained intercepts E_i are listed in Table 3.6.1. The intercept of the plot $E=f(\log C_{Ag^+})$ is actually the standard silver-silver ion electrode potential, $E^{\circ}_{Ag^+/Ag}$, and experimental value is +406 mV for the present conditions. Since the equations of the intercepts for the graphs of S^{2-}

and GeS^- are

$$E_i = E^{\circ}_{\text{Ag}^+/\text{Ag}} + q58 \log K_s \quad (3.6.8)$$

$$E_i = E^{\circ}_{\text{Ag}^+/\text{Ag}} + p58 \log K_{\text{SH}} \quad (3.6.9)$$

the experimental intercepts were used to calculate apparent solubility constants for the silver-sulfide complex K_s and silver mercaptide complex K_{SH} formed at the electrode. The results are shown as $-\log K_p$ in Table 3.6.1. The coefficients q and p , equal $1/n$, define the stoichiometry of the corresponding electrochemical reactions.

Further, the graphs $E=f(\log C_i)$ were extrapolated to $E=0$. The obtained values $-\log C_i$ represent the intrinsic detection limits for the particular ions[100]. Thus,

$$\log C_i = (E^{\circ}_{\text{Ag}^+/\text{Ag}} + p58 \log K_{\text{Ci}}) / p58 \quad (3.6.10)$$

is the equation which defines the detection limit. The results experimentally obtained from the extrapolations are shown in Table 3.6.1.

In Table 3.6.2 results of the study of the electrode response to GeSH are shown. The test solutions were prepared from samples taken at early stages of the sol-gel reaction when only GeSH was formed (1-3) or after sulfide precipitation (4,5). The column Time(h) in Table 3.6.2 represents elapsed time from the beginning of the sol-gel reaction. From the results in Table 3.6.2 it is evident that silver-mercaptide complexes were formed. The complexity of formed compounds increased with time as seen from the stoichiometric coefficient p . Detection limits are almost constant, ≈ 4.2 ,

corresponding to a mercaptide (SH) concentration of 6.0×10^{-5} M.

Table 3.6.2 Electrode response to GeS^- ions.

N°	Time (h)	Slope (mV)	Intercept (mV)	p	$\log K_{sp}$	Detection limit $-\log C_{SH}$
1	1	77	-315	1.3	12.4	4.1
2	4	120	-547	2.1	16.4	4.6
3	5	184	-771	3.2	20.3	4.2
4	11	202	-875	3.5	22.0	4.3
5	12	257	-994	4.4	24.0	3.9

The electrode potential for the mixture of S^{2-} and GeS^- should be defined with the following equation[101]

$$E = E^{\circ}_{\text{Ag}^+/\text{Ag}} + \frac{2.3RT}{F} \log K_{SH} - \frac{2.3RT}{F} \log (C_{SH} + k_{SH,S}^{\text{Pot}} C_S^{1/2}) \quad (3.6.11)$$

where $k_{SH,S}^{\text{Pot}}$ is a selectivity coefficient given by the ratio of the corresponding solubility products of the compounds formed

$$k_{SH,S}^{\text{Pot}} = \frac{K_{SH}}{K_S} \quad (3.6.12)$$

The selectivity coefficient was determined experimentally by a method for mixed solutions[101]. In order to realize better agreement with experimental results eq.(3.6.11) was modified to

$$E = E^{\circ}_{Ag^+/Ag} + \frac{2.3RT}{F} \log K_{SH} - \frac{2.3RT}{F} \log(C_{SH}^p + k_{SH,S}^{Pot} C_S^q) \quad (3.6.13)$$

Based on

$$E = E^{\circ}_{Ag^+/Ag} + \frac{2.3RT}{F} \log K_{SH} + \frac{2.3RT}{F} \log C_{SH}^p \quad (3.6.14)$$

electrode potential E determined by concentration C_{SH} in a solution of pure GeS^- , and

$$E' = E^{\circ}_{Ag^+/Ag} + \frac{2.3RT}{F} \log K_{SH} + \frac{2.3RT}{F} \log(C'_{SH}{}^{p'} + k_{SH,S}^{Pot} C'_S{}^{q'}) \quad (3.6.15)$$

electrode potential E' defined by concentrations C'_{SH} and C'_S in the mixed solution of GeS^- and S^{2-} , the following equation was derived from E-E'

$$(e^{(E-E')/RT} C_{SH}^p) - C'_{SH}{}^{p'} = k_{SH,S}^{Pot} C'_S{}^{q'} \quad (3.6.16)$$

used for experimentally determined selectivity coefficient. Parameters p, p' and q' are the corresponding stoichiometric coefficients. Results for the selectivity coefficients at different concentrations are shown in Table 3.6.3. The coefficients are of the same order, 10^3 , although the ranges of the primary GeS^- and the interfering S^{2-} ions were sufficiently wide.

Table 3.6.3 Selectivity coefficients obtained experimentally for different concentrations of pure primary GeS^- ion (C_{SH}) and mixtures of the primary (C'_{SH}) and interfering S^{2-} ion (C'_s).

Mixture	C_{SH} (10^{-3} M)	C'_{SH} (10^{-3} M)	C'_s (10^{-3} M)	$k_{\text{SH,S}}^{\text{Pot}}$
1	0.5	1.1-160	0.1-50	1.4×10^3
2	1.1	2.4-12	1.8-20	4.7×10^3
3	2.0	3.7-23	1.0-15	0.9×10^3

The selectivity coefficients were also determined directly from the plots $E=f(\log C_i)$. This can be explained from data used in mixture 2, Table 3.6.3. From a potentiometric curve $E=f(V_{\text{add. titr.}})$, the concentrations of S^{2-} and GeS^- ions in the mixed solution determined from equivalence points were $C'_s = 20 \times 10^{-3}$ M and $C'_{\text{SH}} = 8 \times 10^{-3}$ M. Then, the plot $E=f(\log C_i)$ was made. From the parts of the plots $E=f(\log C_i)$ before equivalence points 1 and 2, the intercepts E_i for $\log C_s=0$ and $\log C_{\text{SH}}=0$ were obtained, -828 mV and -637 mV, respectively. Taking the experimentally determined $E^{\circ}_{\text{Ag}^+/\text{Ag}} = +406$ mV, the solubility products were calculated from equations

$$E_i = E^{\circ}_{\text{Ag}^+/\text{Ag}} + (2.3RT/F) \log K_{\text{SH}} \quad (3.6.17)$$

$$E_i = E^{\circ}_{\text{Ag}^+/\text{Ag}} + (2.3RT/F) \log K_s \quad (3.6.18)$$

Hence, $K_{\text{SH}} = 10^{-18}$ and $K_s = 10^{-21.3}$; when substituted in eq.(3.6.15), $k_{\text{SH,S}}^{\text{Pot}} = 2.0 \times 10^3$.

3.7. CHEMICAL KINETICS

3.7.1. Kinetic data

Typical potentiometric curves $E=f(V_{\text{add.titr.}})$ are shown in Fig. 3.7.1. They were obtained by potentiometric titration of samples taken from the reaction mixture at different times after purging the unreacted H_2S . From the equivalence points of the curves, the concentrations of S^{2-} (M) and $\text{SH}(\text{C})$ evolved during the reaction were determined. They are listed in Table A2, A3 and A4 (Appendix I) for the reaction mixtures containing $[\text{H}_2\text{S}]/[\text{Ge}(\text{OEt})_4]$ in molar ratios 9:1 and 1:1.2 and for mixture $[\text{Ge}(\text{OPr}^i)_4]$ and $[\text{H}_2\text{S}]$, respectively.

3.7.2. Reaction mixture containing $[\text{H}_2\text{S}]_0/[\text{Ge}(\text{OEt})_4]_0$ in ratio 9:1

The sol-gel reaction of germanium ethoxide and hydrogen sulfide in a molar concentration ratio 1:9 was performed at four different temperatures 30, 40, 45 and 50°C. The Tyndall effect appeared after ~9.5 h, while all samples gelled within 12-14 h from the beginning of the reaction.

Typical concentration-time data for reactant ethoxide (A), intermediate mercaptide (C) and product sulfide (M) are plotted in Fig. 3.7.2. There is a concentration-time delay, induction period, before sulfide (M) appeared in significant concentrations, as seen on the curve $[\text{M}] = f(t)$. The extent of the induction period varies with temperature. It was the shortest at 50°C, 5 h, increased to 6 h at 45 and 40°C and even to 9 h at 30°C. The concentration of germanium mercaptide [C] measured at the end of the induction periods was $\approx 1.29 \times 10^{-3}$ M at all temperatures.

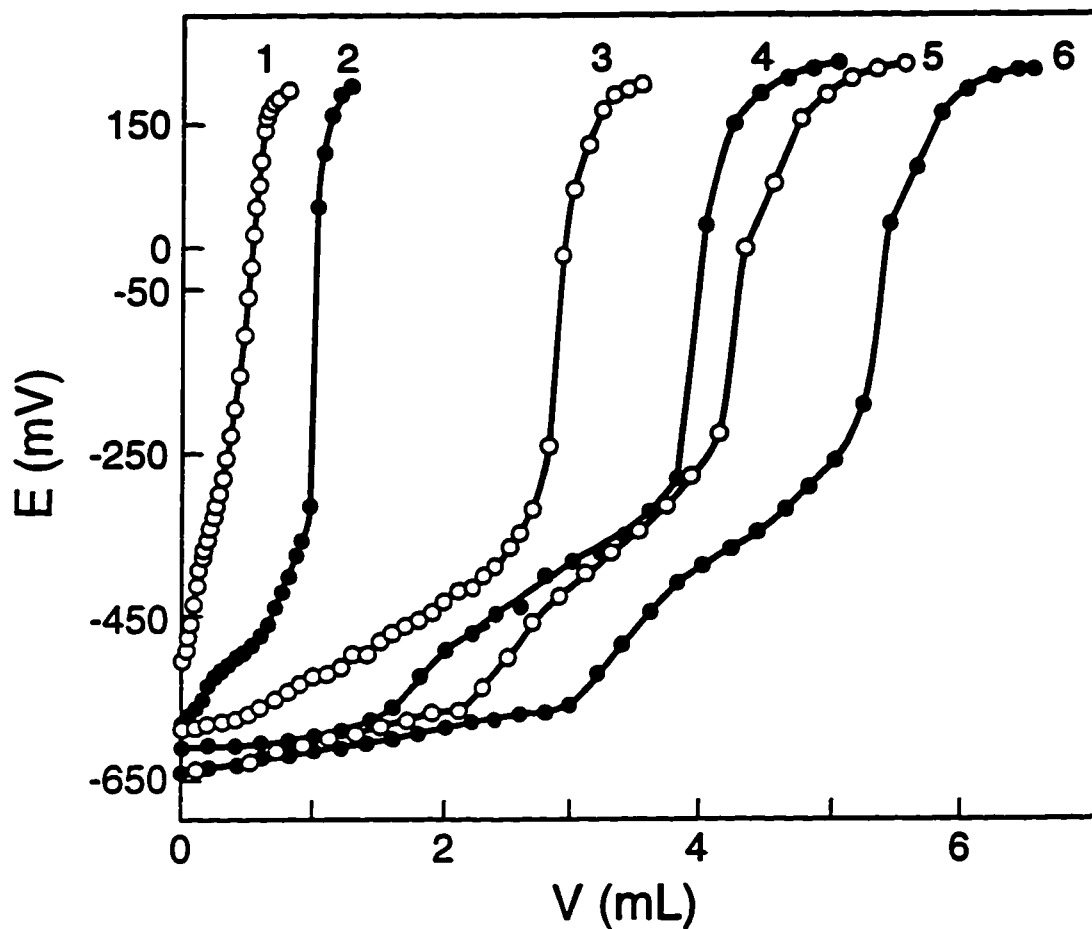


Fig. 3.7.1 Potentiometric titration curves of samples undergoing the sol-gel reaction performed at 30°C with $\text{Ge}(\text{OPr})_4$, titrated with AgNO_3 . The samples were taken : 1) 0.5h; 2) 1.5h; 3) 2.5h; 4) 3.5h; 5) 4.5h; 6) 5.5h, from the beginning of the reaction.

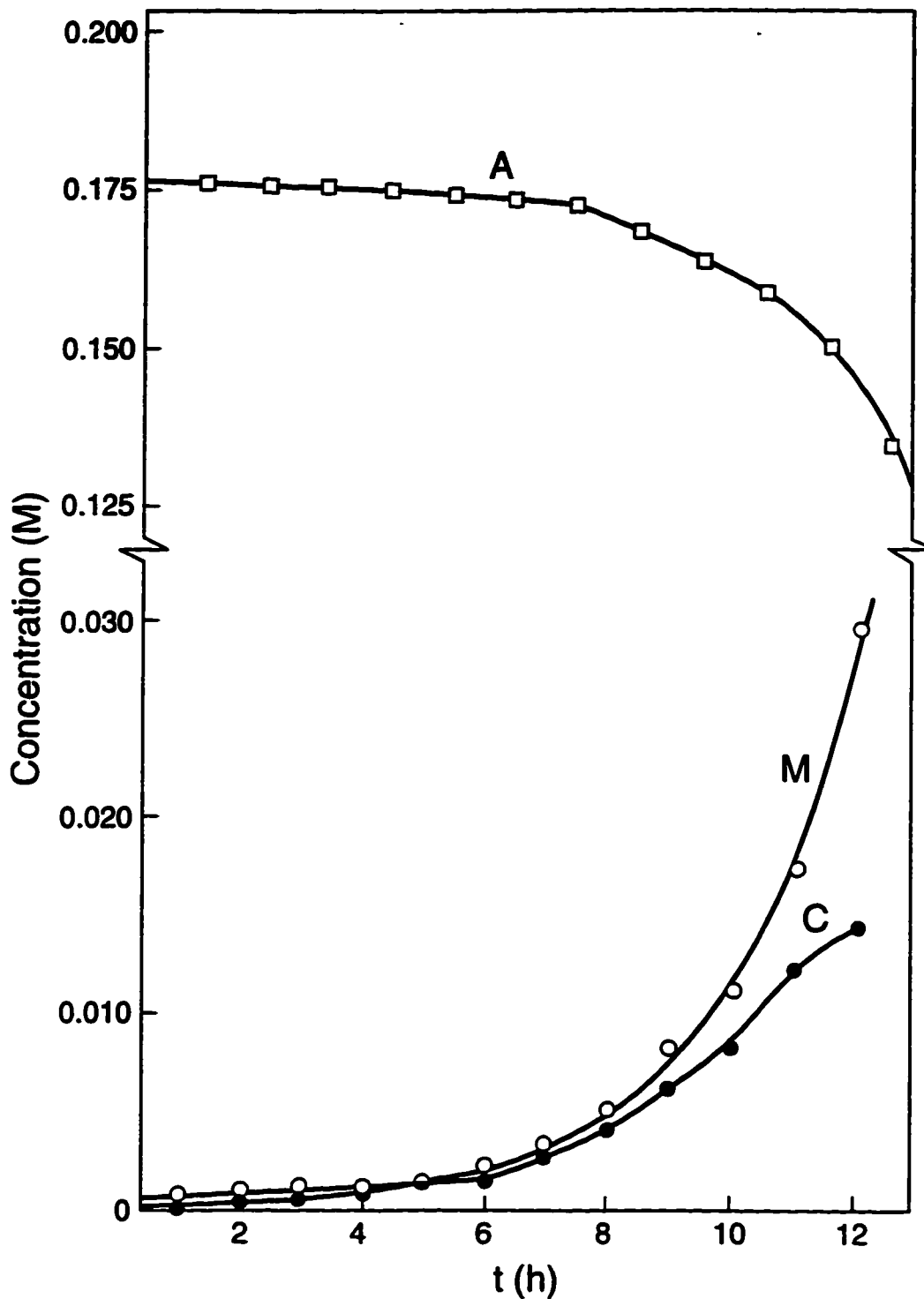


Fig. 3.7.2 Concentration as a function of time for: M - sulfide ($\equiv\text{GeSGe}\equiv$); C - mercaptide ($\equiv\text{GeSH}$); A - ethoxy group ($\equiv\text{GeOEt}$), for the sol-gel reaction if $[\text{H}_2\text{S}]_0/[\text{Ge}(\text{OEt})_4]_0$ is 9:1. The reaction was performed at 50°C .

There are two distinguishable linear parts on plots of $-\ln([A]/[A]_0)$ versus time. In Fig. 3.7.3 the first linear parts of these curves for various temperatures are shown. The length of this linear part overlaps with the induction period. Its linearity indicates that thiolysis is of first order with respect to the concentration of ethoxide groups [A] in this reaction period. It was assumed that thiolysis was a pseudo-first order reaction in regard to [A]. The slopes of the straight lines $-\ln([A]/[A]_0) = f(t)$ are assigned to the apparent thiolysis rate constants $k_{app}' = k_1 B_0$. The apparent constants k_{app}' and calculated k_1 constants are listed in Table 3.7.1.

In order to determine the condensation rate constants, plots of $\Delta M/\Delta t$ as ordinate against [C] as abscissa were made for various temperatures (Fig. 3.7.4). The reaction rate of sulfide appearance, $\Delta M/\Delta t$, was calculated for sulfide concentrations in the reaction period which coincides with the second linear part of the graph $-\ln([A]/[A]_0) = f(t)$. The slope of this plot is assigned to the apparent alcohol forming condensation rate constant $k_{app}''' = k_3 [A]_0$. The apparent constants k_{app}''' and calculated values of k_3 are shown in Table 3.7.1. Values of the same order were obtained for k_3 when the concentration-time integral method was used.

In order to determine the functional relationship for the reaction rates k_1 and k_3 with temperature, Arrhenius plots, $\ln k$ vs. $1/T$, and transition-state theory plots, $\ln(k/T)$ vs. $1/T$, were made. They are shown in Fig. 3.7.5a and b, respectively. From the slopes of the lines in Fig. 3.7.5a, the activation energies of thiolysis and condensation are calculated and from the intercepts the frequency factors. The enthalpies ΔH^\ddagger of thiolysis and condensation reactions were calculated from the slopes of the graphs in Fig. 3.7.5b.

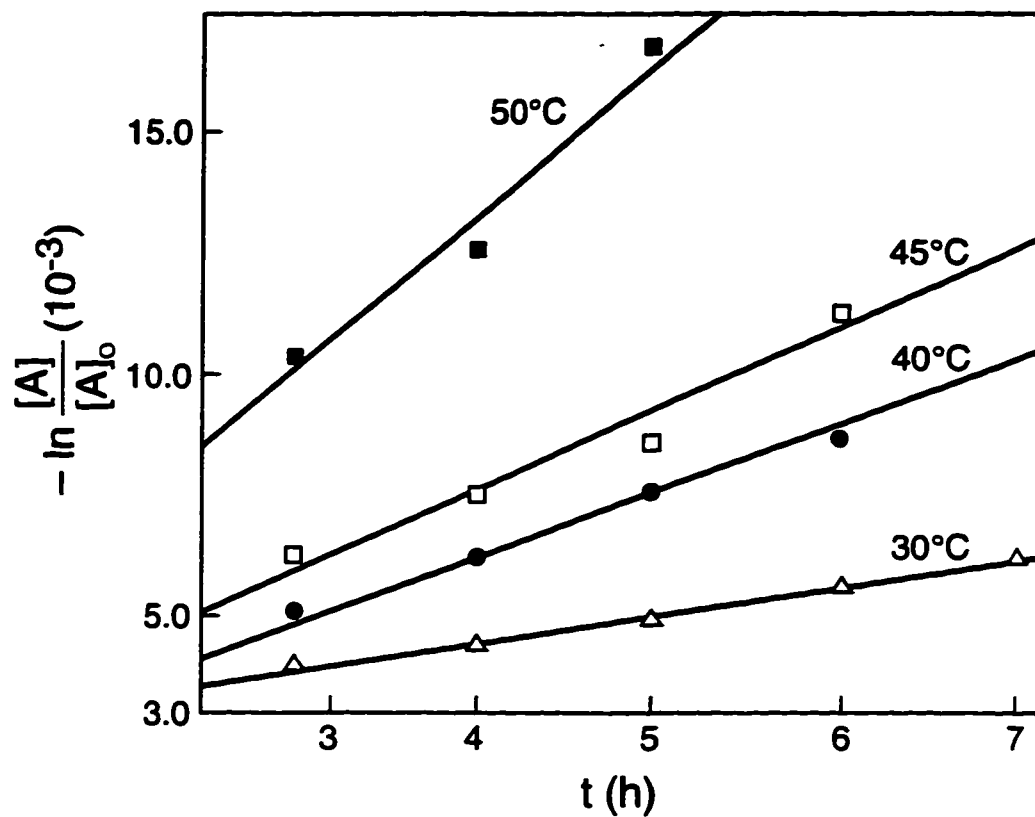


Fig. 3.7.3 Plots of $-\ln([A]/[A]_0)$ as a function of time for various temperatures when $[H_2S]_0/[Ge(OEt)_4]_0$ is 9:1

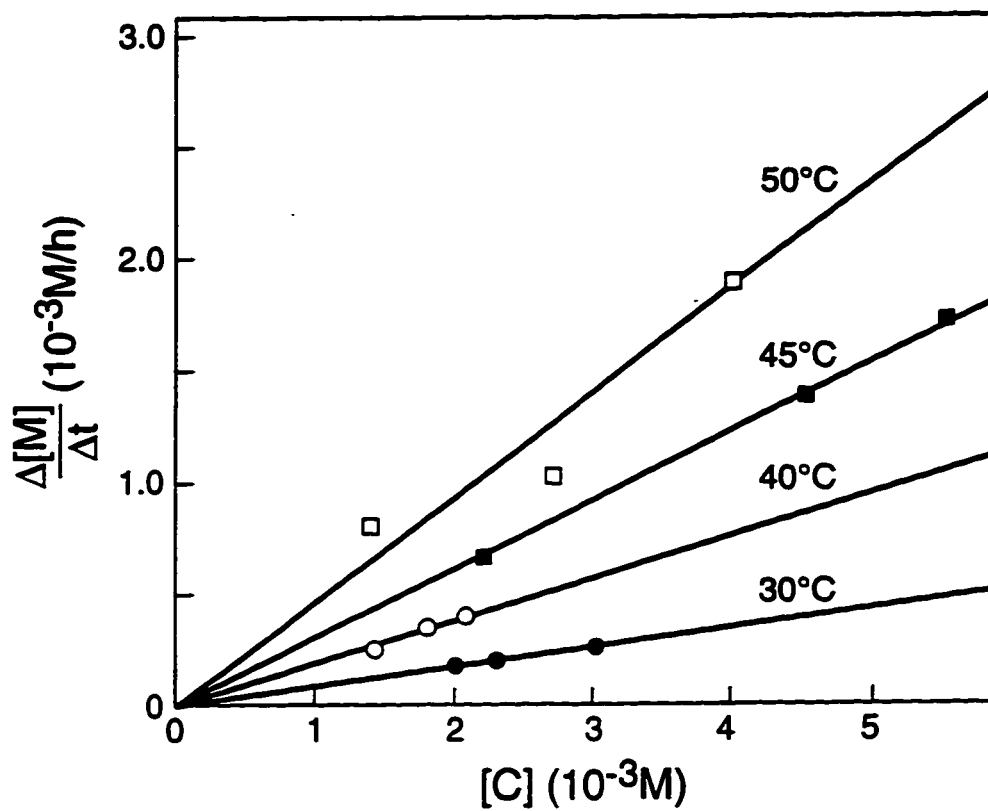


Fig. 3.7.4 Plots of reaction rate of sulfide formation $\Delta[M]/\Delta t$ as a function of mercaptide concentration $[C]$ at various temperatures for the sol-gel process when $[H_2S]_0/[Ge(OEt)_4]_0$ is 9:1.

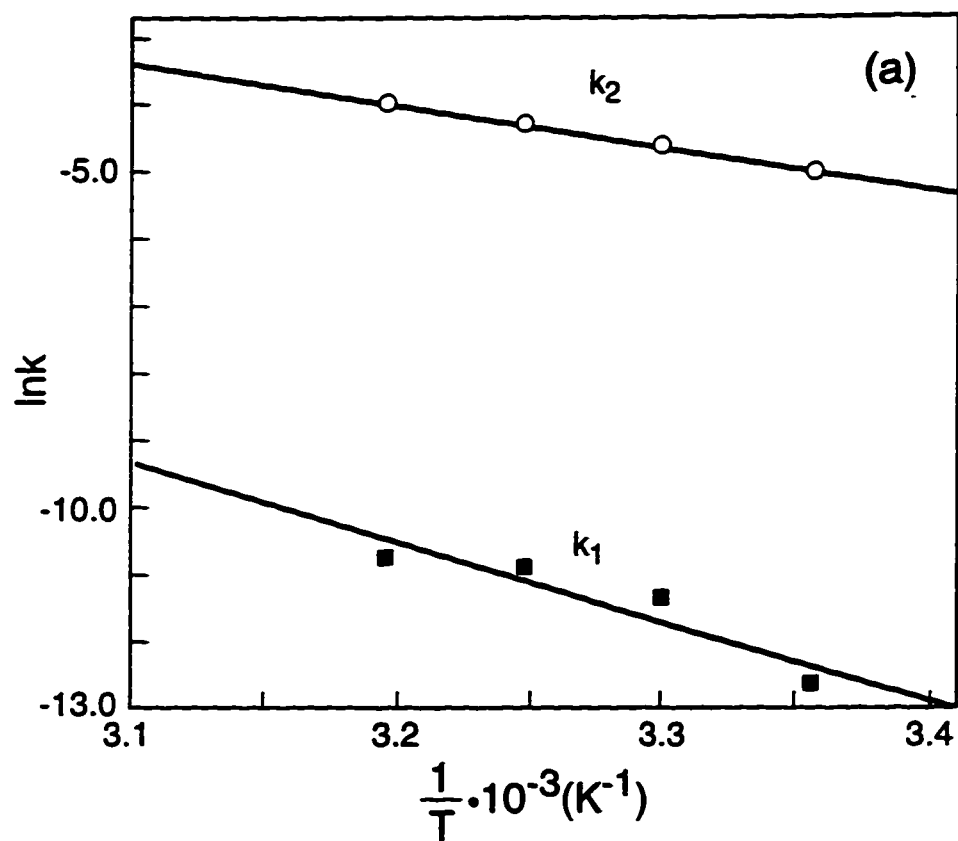


Fig. 3.7.5 Influence of the reaction temperature on the thiolysis (k_1) and the condensation (k_2) rate constants: a) Arrhenius plot, $\ln k$ vs. ($1/T$);

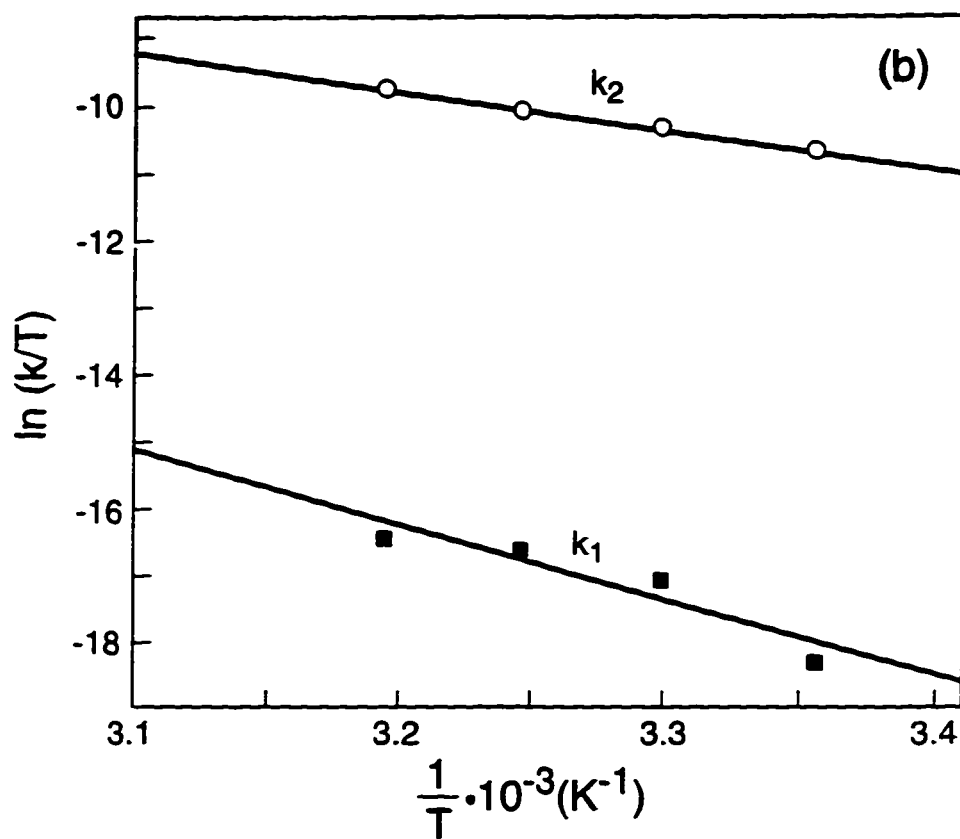


Fig. 3.7.5 b) transition-state theory plot, $\ln(k/T)$ vs. $(1/T)$, for the sol-gel process if $[\text{H}_2\text{S}]_0/[\text{Ge}(\text{OEt})_4]_0$ is 9:1.

Table 3.7.1 The thiolysis (k_1) and the condensation (k_3) rate constants obtained from apparent values k_{app}' and k_{app}''' respectively at different temperatures for the sol-gel process if $[H_2S]_0/[Ge(OEt)_4]_0$ is 9:1. The values are shown along with standard deviations ($\pm\sigma$).

Temperature (°C)	k_{app}' $10^{-7}(s^{-1})$	k_1 $10^{-7}(M \cdot s)^{-1}$	k_{app}''' $10^{-4}(M \cdot s)^{-1}$	k_3 $10^{-4}(M \cdot s)^{-1}$
30	1.54 ± 0.07	3.9 ± 0.2	0.22 ± 0.007	1.28 ± 0.04
40	3.9 ± 0.2	9.8 ± 0.4	0.51 ± 0.02	2.9 ± 0.1
45	5.6 ± 0.7	14 ± 2	0.84 ± 0.02	4.7 ± 0.1
50	7.9 ± 0.5	20 ± 1	1.3 ± 0.1	7.4 ± 0.6

The intercepts were used to calculate the entropies of activations ΔS^\ddagger of both reactions. From these activation parameters the free energies of activation for the transition state of thiolysis (TS1) and condensation (TS2), were obtained from the Gibbs-Helmholtz equation[102]

$$\Delta G^\ddagger = \Delta H^\ddagger - T\Delta S^\ddagger \quad (3.7.1)$$

where T represents the middle of the studied temperature range, $T = 314.25$ K. The activation energies E_a , frequency factors A and activation parameters are listed in Table 3.7.2.

The sol-gel reaction enthalpy ΔH was calculated from the enthalpies of activations for thiolysis ΔH^\ddagger_t and condensation ΔH^\ddagger_c

$$\Delta H = \Delta H^\ddagger_c - \Delta H^\ddagger_t = 4 \text{ kJ/mole} \quad (3.7.2)$$

Table 3.7.2 Activation energies, frequency factors, activation parameters and corresponding standard deviations ($\pm\sigma$), of the sol-gel reaction if $[\text{H}_2\text{S}]_0/[\text{Ge}(\text{OEt})_4]_0$ is 9:1.

Reaction	E_a (kJ/mole)	A ($\text{M}\cdot\text{s}^{-1}$)	ΔS^\ddagger (J/moleK)	ΔH^\ddagger (kJ/mole)	ΔG^\ddagger (kJ/mole)
Thiolysis (k_1)	67 ± 1	1.3×10^5	-160 ± 16	64 ± 1	114 ± 5
Condensation (k_3)	71 ± 3	2.0×10^8	-94 ± 10	68 ± 3	98 ± 6

3.7.3. Reaction mixtures containing $[\text{H}_2\text{S}]_0/[\text{Ge}(\text{OEt})_4]_0$ in ratio 1:1.2

Sol-gel processing of germanium sulfide from germanium ethoxide and hydrogen sulfide in an initial molar ratio of 1.2:1 was performed at various temperatures: 30, 40, 45 and 50°C. The Tyndall effect appearing after ~ 10 h from the reaction start was succeeded by gelation within the next two hours.

The material balance graph shown in Fig. 3.7.6 is typical for all reactions followed at different temperatures. The curve representing the sulfide concentration as a function of time, $[\text{M}] = f(t)$, exhibits an induction period as demonstrated in Fig. 3.7.6. The induction periods ended after 2.5 h at 50°C and after 3.5 h at the lower temperatures 45, 40 and 30°C. The concentrations of the intermediate mercaptide were different at these points: 2.20×10^{-3} M at 30°C, 2.63×10^{-3} M at 40°C, 8.1×10^{-3} M at 45°C and 8.69×10^{-3} M at 50°C (Table A3, Appendix I).

In Fig. 3.7.7, plots of $-\ln([\text{A}]/[\text{A}]_0)$ and $-\ln([\text{B}]/[\text{B}]_0)$ versus time are represented. There is a linear part on each curve whose extent coincides with the

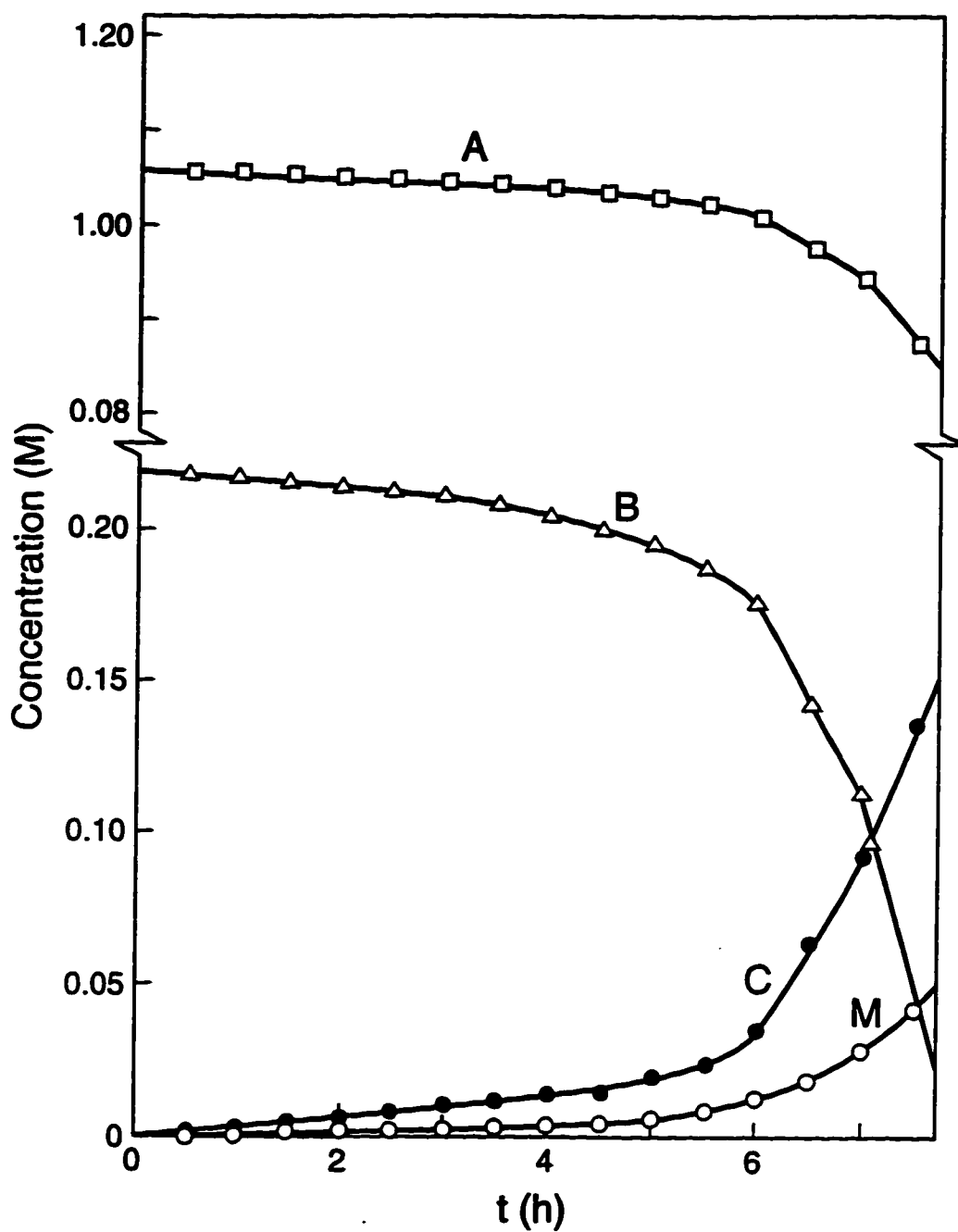


Fig. 3.7.6 Mass balance as a function of time for the sol-gel process if $\text{H}_2\text{S}/[\text{Ge}(\text{OEt})_4]_0$ is 1:1.2. The concentrations of sulfide M and mercaptide C were determined experimentally, while the concentrations of ethoxy group A and hydrogen sulfide B were calculated. The reaction was performed at 50°C .

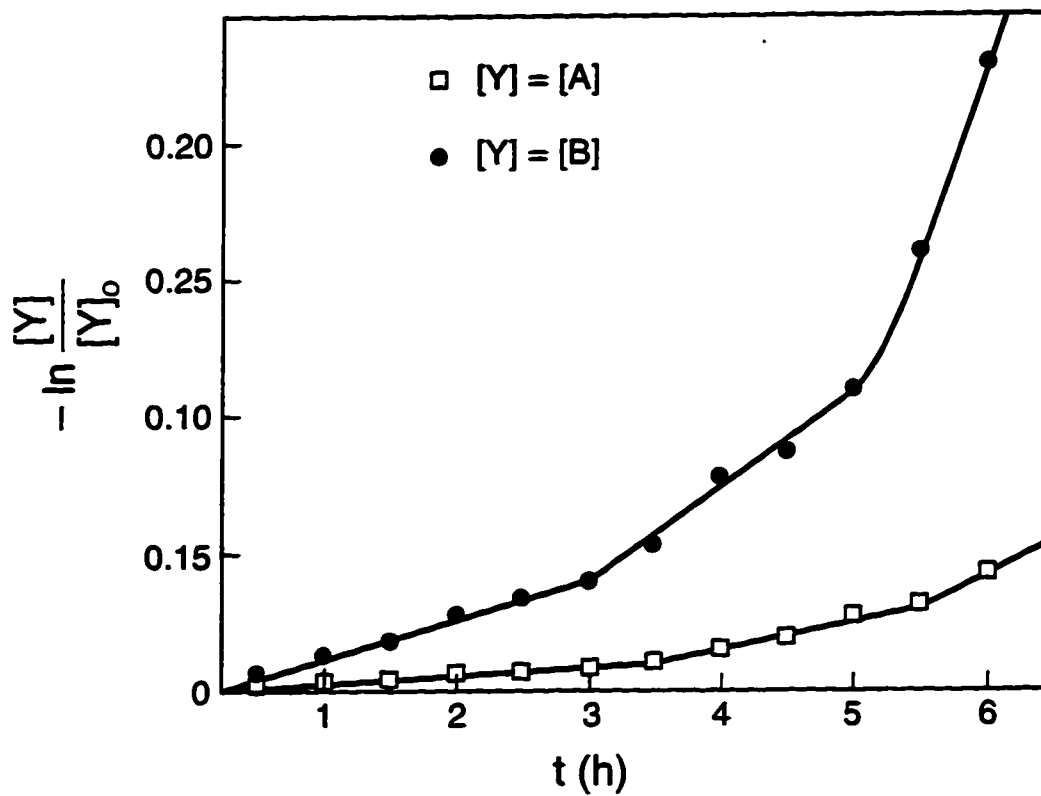


Fig. 3.7.7 Plot of $-\ln([Y]/[Y]_0)$ as a function of time if Y is: ethoxide group concentration [A]; hydrogen sulfide concentration [B]. The reaction was performed at 50°C with the $[H_2S]/[Ge(OEt)_4]$ ratio 1:1.2.

performed at different temperatures are shown in Fig. 3.7.8. The slopes of these graphs are assigned to the thiolysis rate constants, listed in Table 3.7.3.

Table 3.7.3 Thiolysis rate constants obtained at various temperatures for the sol-gel processing if $[\text{H}_2\text{S}_x]/[\text{Ge}(\text{OEt})_4]_0$ is 1:1.2. The values are presented with standard deviations ($\pm\sigma$).

Temperature ($^{\circ}\text{C}$)	$k_1 \times 10^{-6} (\text{M} \cdot \text{s})^{-1}$
30	0.94 ± 0.04
40	1.31 ± 0.06
45	3.2 ± 0.2
50	3.94 ± 0.04

In order to determine the influence of temperature on the thiolysis rate constant, an Arrhenius plot, $\ln k$ vs. $1/T$ (Fig. 3.7.9a), and a transition-state theory plot, $\ln(k/T)$ vs. $1/T$ (Fig. 3.7.9b), were made. From the slope of the line in Fig. 3.7.9a an activation energy $E_a = (61 \pm 2)$ kJ/mole was calculated. The intercept of the graph $\ln A = 10.3$ (Fig. 3.7.9a) was used to calculate the frequency factor $A = 3 \times 10^4$. Activation parameters obtained from the plot in Fig. 3.7.9b are: $\Delta H^\ddagger = (58 \pm 2)$ kJ/mole, $\Delta S^\ddagger = (-170 \pm 10)$ J/moleK and $\Delta G^\ddagger = (111 \pm 5)$ kJ/mole, for the middle of the temperature interval, $T = 314.25$ K.

3.7.4. Reaction mixtures containing $[\text{H}_2\text{S}]_0/[\text{Ge}(\text{OPr}^i)_4]_0$ in ratio 2.25:1

The sol-gel preparation of germanium sulfide from germanium isopropoxide and hydrogen sulfide at a concentration ratio 1:2.25 was performed at four different temperatures: 25, 30, 35 and 40°C . The Tyndall effect appeared after ~ 2 h from the

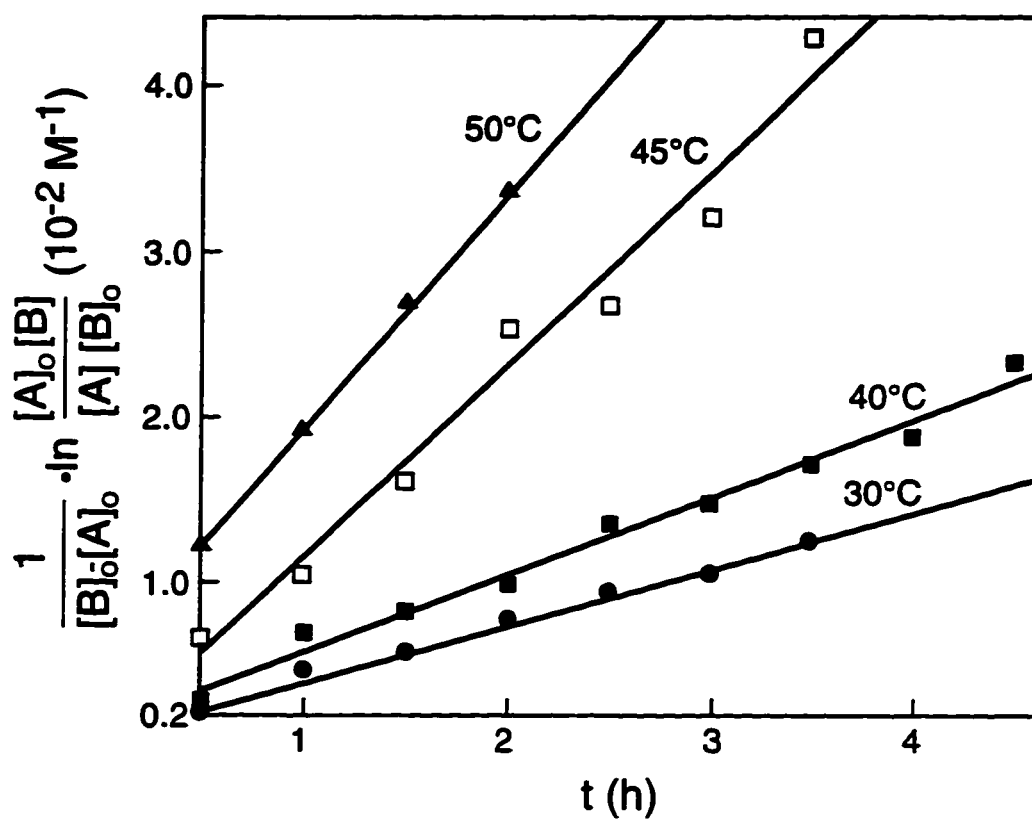


Fig. 3.7.8 Plots of $\frac{1}{[B]_0[A]_0} \ln \frac{[A]_0[B]}{[A][B]_0}$ as functions of time made for the induction period at different reaction temperatures and a $[H_2S]_0/[Ge(OEt)_4]_0$ ratio 1:1.2.

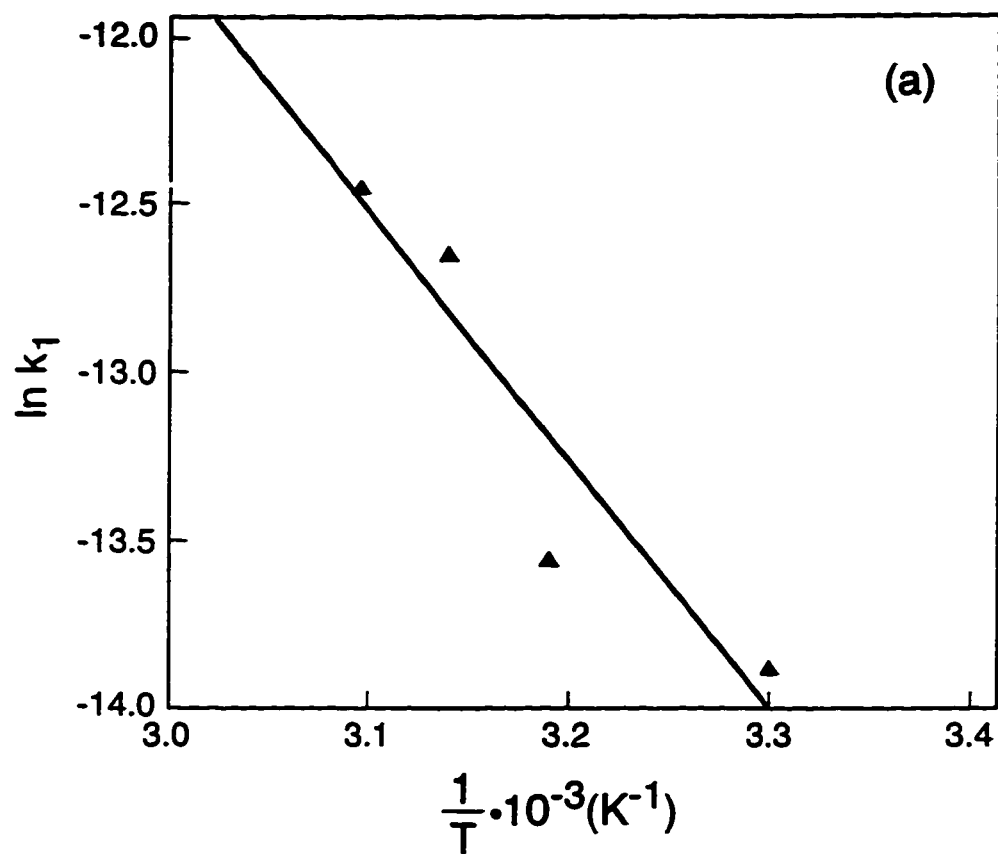


Fig. 3.7.9 Functional relationship of the thiolysis constant (k_1) with temperature:
a) Arhenius plot, $\ln k$ vs. $(1/T)$;

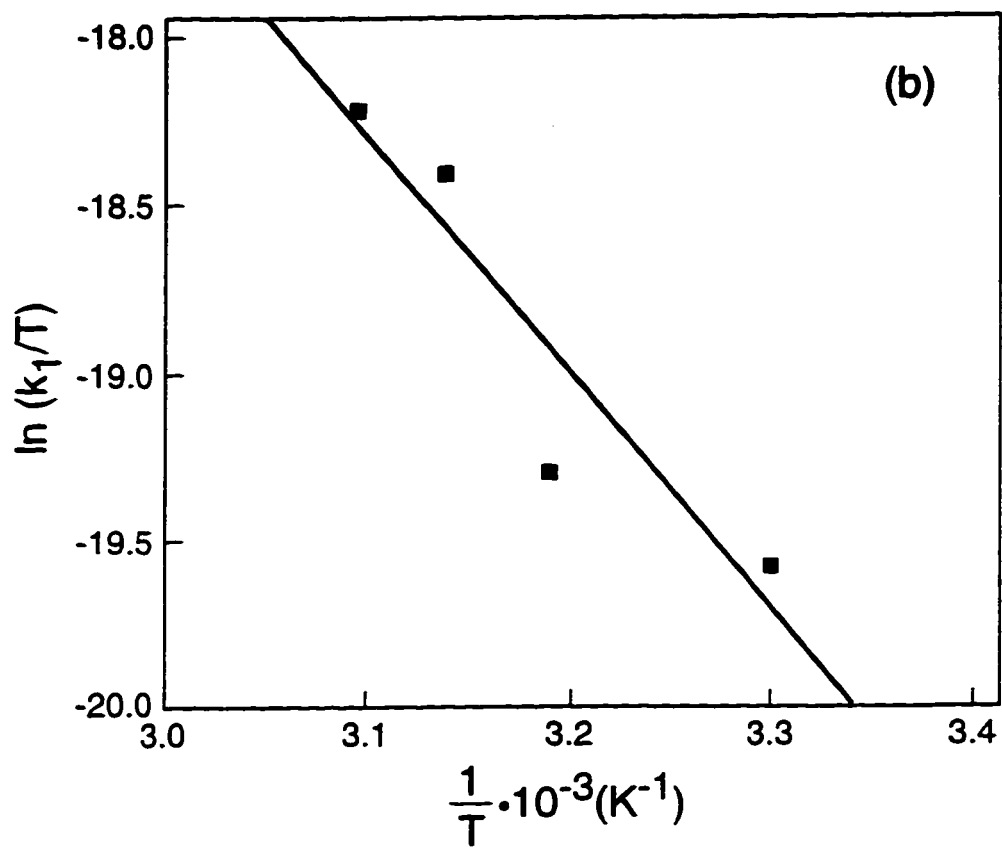


Fig. 3.7.9 b) transition-state theory plot, $\ln(k/T)$ vs. $(1/T)$, for the sol-gel process with $[\text{H}_2\text{S}]_0/[\text{Ge}(\text{OEt})_4]_0$ ratio 1:1.2.

beginning of the reaction. Gelation started after ~ 12 h.

A typical graph of concentration plotted against reaction time for reactants and products is shown in Fig. 3.7.10 for the sample prepared at 40°C. The intermediate mercaptide (C), approaches almost a constant concentration of 3.9×10^{-3} M after 3.5 h. Similar behaviour of intermediate (C) was observed for all the other samples prepared at different temperatures. Nonetheless, the limiting concentration and the time when it was achieved was affected by temperature. Thus, the concentrations were 3.2×10^{-3} , 2.7×10^{-3} and 2×10^{-3} M and corresponding time 4, 4.5 and 5.5 h for samples prepared at 35, 30 and 25°C, respectively.

The plotted graphs $\ln([A]/[A]_0)$ and $\ln([B]/[B]_0)$ vs. time yielded straight lines for reactions performed at all temperatures, indicating that the reactions were first order with the respect to the concentrations of reactants A and B. Typical plots are shown in Fig. 3.7.11.

In Fig. 3.7.12, graphs $\{1/([B]_0 - [A]_0)\} \cdot \ln([A]_0[B]/[A][B]_0)$ vs. time plotted for various temperatures are presented. The plots are linear, indicating that reactions are second order with the respect to both the concentrations of the isopropoxide group and hydrogen sulfide. The slopes of these lines are assigned to the thiolysis rate constant k_1 . The values for k_1 are recorded in Table 3.7.4.

When $[M]$ was plotted against $\int [C]^2 dt$ for various temperatures, linear graphs were obtained as shown in Fig. 3.7.13. The slopes of these straight lines were assigned to the H_2S forming condensation rate constant k_2 . The k_2 values are listed in Table 3.7.4.

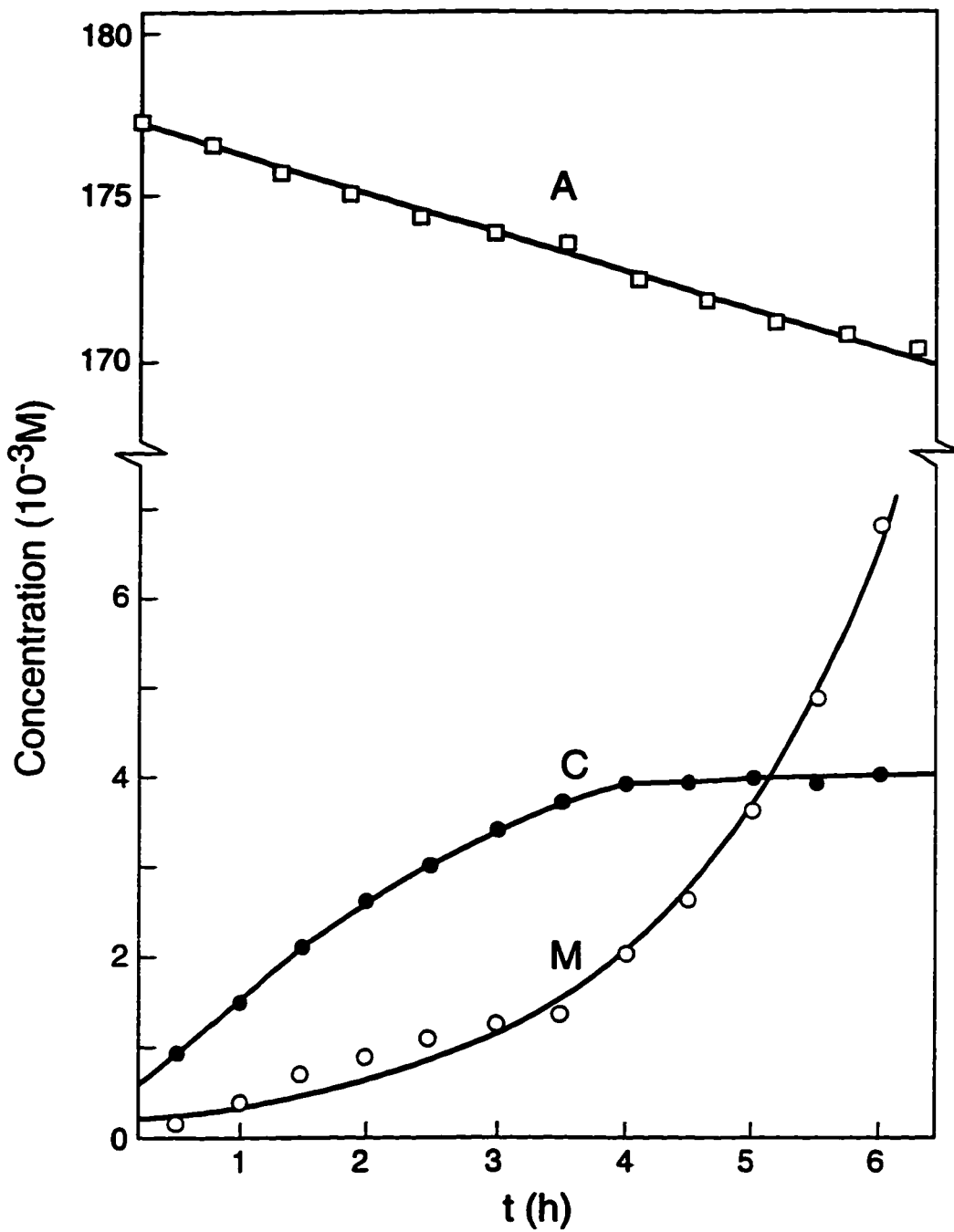


Fig. 3.7.10 Mass balance of the components present in the sol-gel process reaction mixture containing $[H_2S]_0/[Ge(OPr^i)_4]_0$ in ratio 2.25:1 : M- sulfide; C-mercaptide; A-isopropoxide group concentrations. The reaction was performed at 40°C.

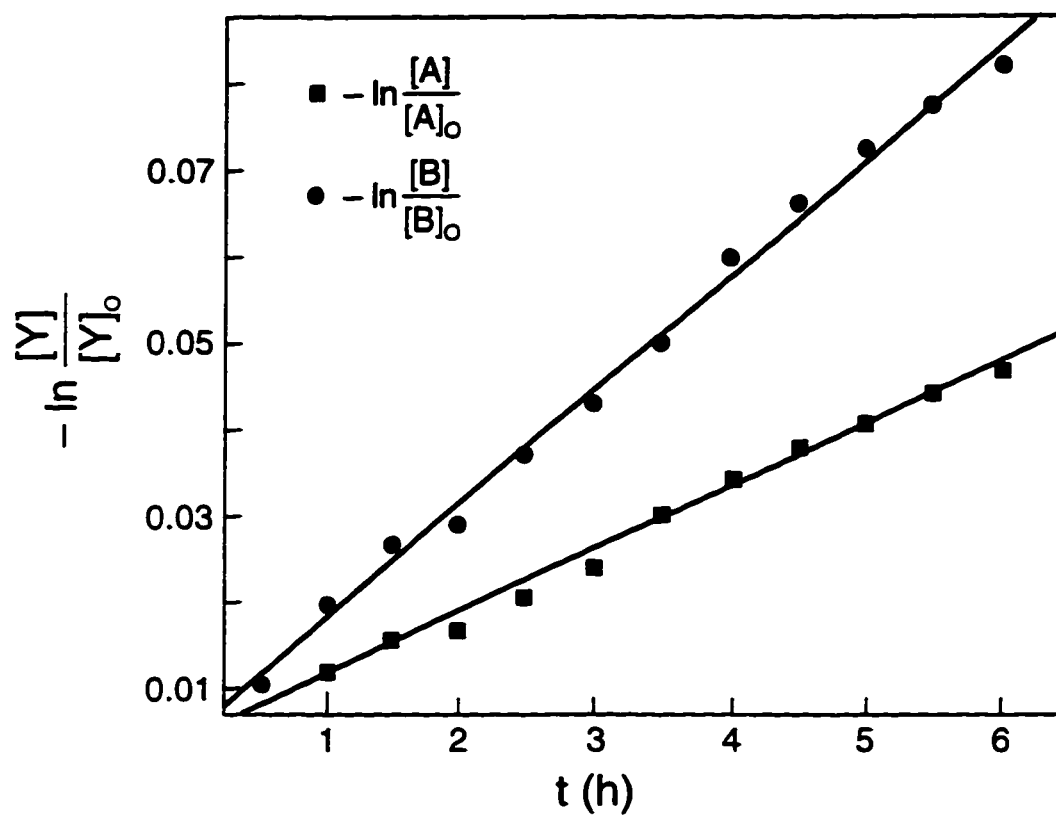


Fig. 3.7.11 Determination of the reaction order of the sol-gel process with $[\text{H}_2\text{S}]_0/[\text{Ge}(\text{OPr}^i)_4]_0$ ratio 2.25:1, performed at 25°C. Plots $-\ln([Y]/[Y]_0)=f(t)$ for : ethoxide group (A); hydrogen sulfide (B).

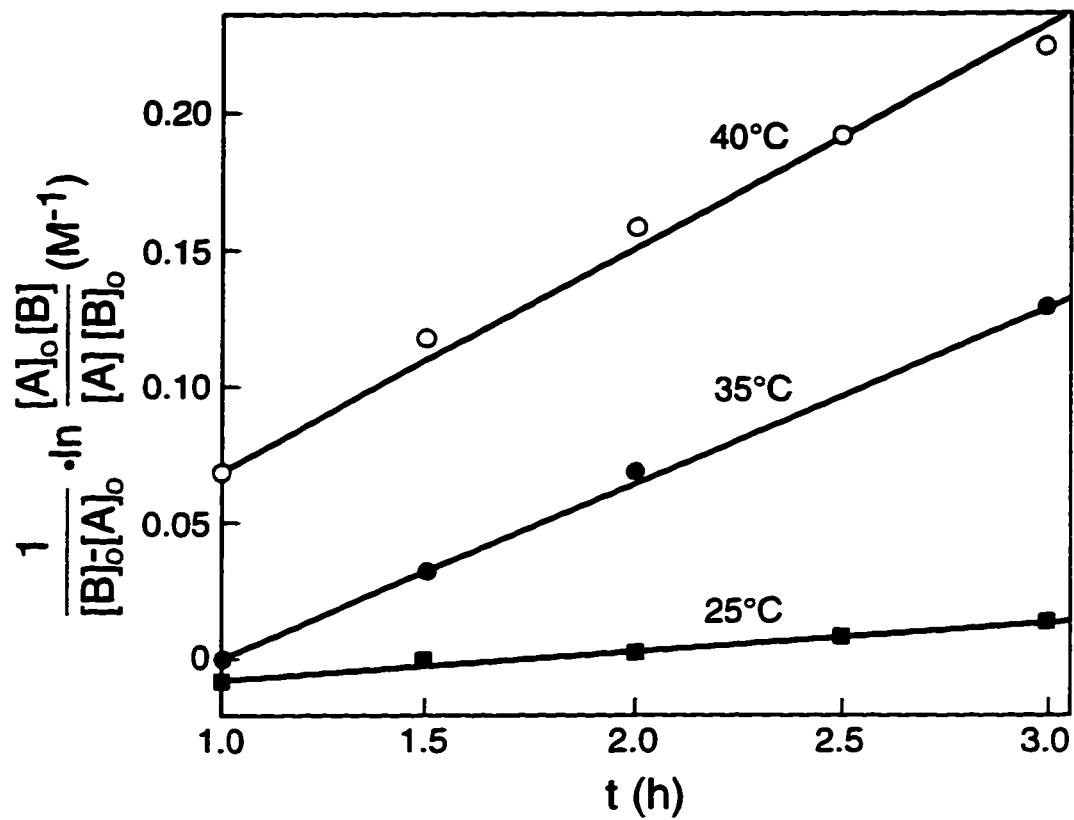


Fig. 3.7.12 Plots of $\frac{1}{[B]_0 - [A]_0} \ln \frac{[A]_0[B]}{[A][B]_0}$ as a function of time for various reaction temperatures. The slopes of the plots are assigned to k_1 .

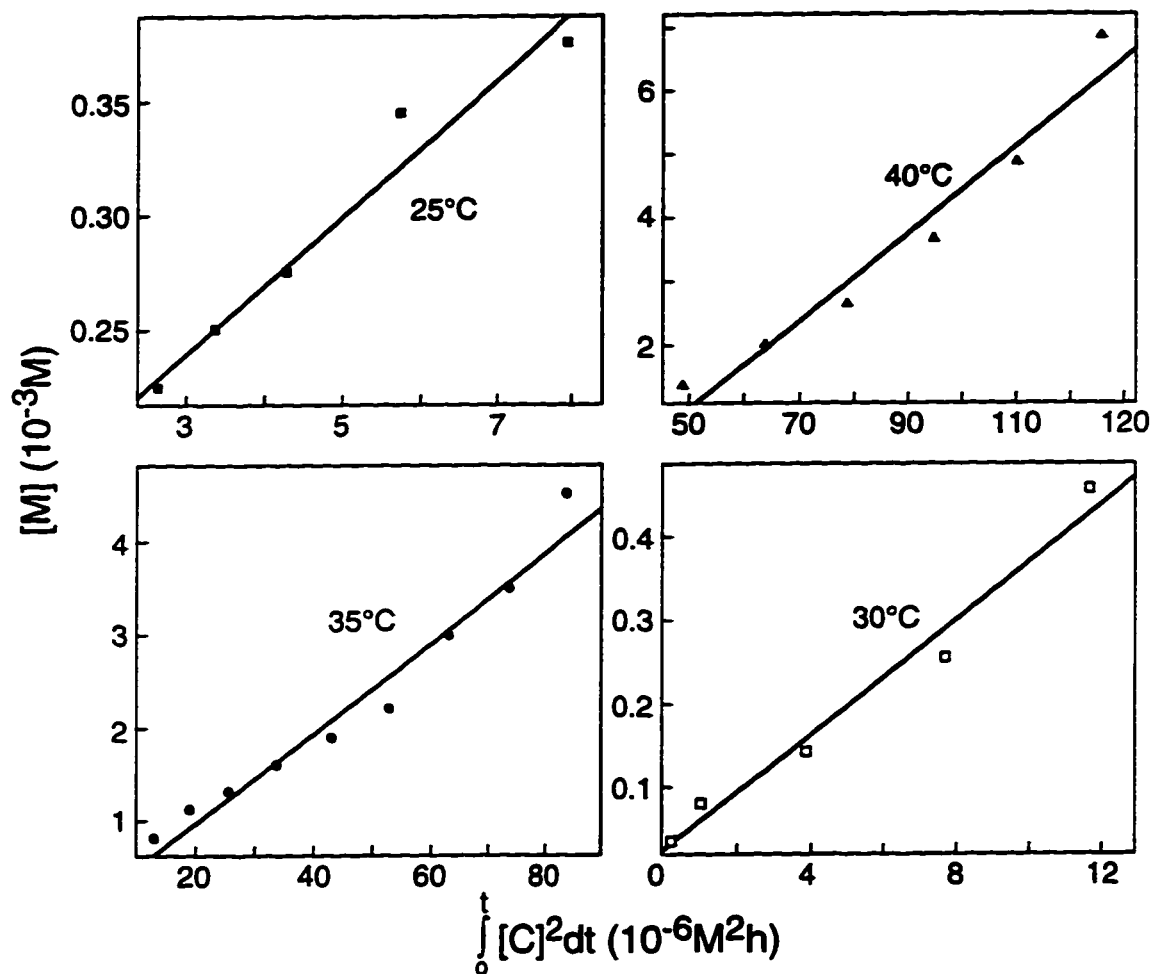


Fig. 3.7.13 Plots of concentration of sulfide $[M]$ as a function of the mercaptide concentration-time integral, $\int_0^t [C]^2 dt$, for various temperatures. The slopes of these lines are assigned to the constant k_2 .

Table 3.7.4 The thiolytic (k_1) and the condensation (k_2) rate constants of the sol-gel process with $[\text{H}_2\text{S}]/[\text{Ge}(\text{OPr}^i)_4]$ ratio 2.25:1 at various temperatures. The constants are shown along with standard deviations ($\pm\sigma$).

Constant ($\text{M}\cdot\text{s}^{-1}$)	Reaction temperature ($^{\circ}\text{C}$)			
	25	30	35	40
$(k_1 \pm \sigma) \times 10^{-6}$	3.3 ± 0.2	11.9 ± 0.1	19 ± 2	22.4 ± 0.9
$(k_2 \pm \sigma) \times 10^{-3}$	6.8 ± 0.1	9.9 ± 0.1	13 ± 1	18.8 ± 0.7

Activation energies were determined from Arrhenius plots (Fig. 3.7.14a) and the activation parameters from the transition-state theory equation (Fig. 3.7.14b) for both rate constants k_1 and k_2 . The results are presented in Table 3.7.5.

Table 3.7.5 Activation energy, frequency factor, activation parameters and standard deviations ($\pm\sigma$) of thiolytic and condensation when $\text{Ge}(\text{OPr}^i)_4$ is a precursor.

Reactions	E_a (kJ/mole)	A ($\text{M}\cdot\text{s}^{-1}$)	ΔS^\ddagger (J/moleK)	ΔH^\ddagger (kJ/mole)	ΔG^\ddagger (kJ/mole)
Thiolytic (k_1)	98 ± 2	6.7×10^{11}	-28.9 ± 0.9	95 ± 2	104 ± 2
Condensation (k_2)	51.8 ± 0.9	8.4×10^6	-121 ± 4	49.3 ± 0.8	86 ± 2

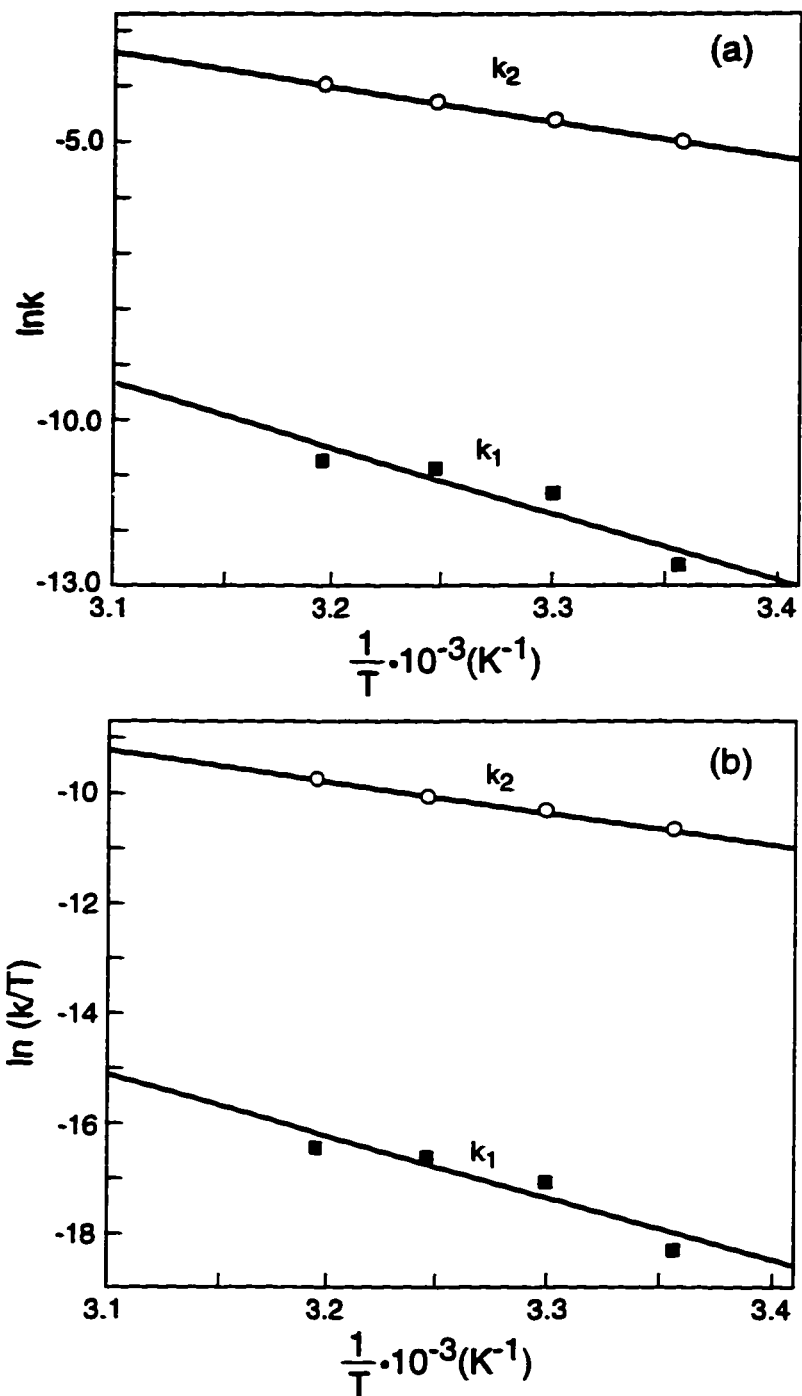


Fig. 3.7.14 Influence of reaction temperature on the thiolysis (k_1) and condensation (k_2) rate constants: a) Arrhenius plot, $\ln k$ vs. $(1/T)$; b) transition-state theory plot, $\ln(k/T)$ vs. $(1/T)$.

From the activation enthalpies of thiolysis ΔH^\ddagger_t and condensation ΔH^\ddagger_c listed in Table 3.7.5, the sol-gel reaction enthalpy is calculated

$$\Delta H = \Delta H^\ddagger_c - \Delta H^\ddagger_t = -45.7 \text{ kJ/mole} \quad (3.7.3)$$

CHAPTER 4

DISCUSSION

4.1. PREPARATION OF GeS₂ WITH LOW OXYGEN CONTENT

4.1.1. Dried gels

Gels 1A and 1B were produced using undried H₂S, while gels 2 and 3 were processed from H₂S dried with anhydrous CaSO₄. There was an air leak into the reaction mixture when gel 3 was synthesized.

Infrared spectra of dried gels 1A, 1B and 3 from 400-4000 cm⁻¹ indicate that the solid network consist of GeO₂ and GeS₂, while the liquid medium within it is a mixture of toluene and ethanol. The IR spectrum of gel 1A has well defined absorption peaks, typical for hexagonal GeO₂, while gels 1B and 3 have only broad bands. Gel 2 does not show any absorption in the IR region 400-1000cm⁻¹ which indicates no GeO₂.

The XRD pattern of gel 1A also indicates the presence of hexagonal GeO₂.

Although the XRD peaks of gel 1B are broad, they also confirm the presence of hexagonal GeO_2 . The XRD patterns of gels 2 and 3 show that they are amorphous products with no indication of crystalline GeO_2 . Comparing the IR and XRD results of gels 1A, 1B and 3 with those reported by Melling[11] and Seddon[12], similarities between them are obvious. The XRD pattern of gel 1B matches that of product A obtained by Seddon[12]. Also, the IR spectra of gels 1B and 3 are similar to the IR spectrum reported for product A[12]. They have the broad bands at 570 and 880 cm^{-1} , assigned by Mukerjee and Sharma[86] to gel derived GeO_2 . The IR spectrum of gel 1A in the range 400-1000 cm^{-1} matches the spectrum of Seddon's product synthesized from germanium ethoxide exposed to ambient atmosphere before reaction with H_2S [12]. The difference between these two spectra is the presence of toluene peaks in the 1A gel spectrum. This study's gel 1A and the gel synthesized by Melling[11] have XRD patterns which are almost identical and are representative of GeO_2 .

Among IR and XRD results previously reported for gel derived GeS_2 , those obtained for gel 2, are unique. Thus, the IR spectra of vitreous GeS_2 , produced from the melt by Seddon[12] and Kawamamoto and Kawashima[87], are comparable to that of gel 2. Results of IR and XRD analyses show the presence of hexagonal GeO_2 , which is indicative of a water impurity involved in the sol-gel reaction. Drying of the H_2S gas decreased contamination of the reaction mixture by water, thus reducing or eliminating GeO_2 formation. Gel 1A has well defined IR absorption peaks and XRD lines due to GeO_2 , which broadened in gels 1B and 3, and did not appear in gel 2.

The fact that drying the H_2S reduced the amount of water in the reaction

was confirmed by the quantitative chemical analysis of gels 1B and 2. Gel 1B contains ten times more oxygen than gel 2.

The results of chemical analysis of gels 5 and 6 indicate that the synthesis method is reproducibly.

The IR spectrum of gel 2 indicates the presence of an absorption peak at 2516 cm^{-1} , assigned to GeS-H. It also shows appearance of ethanol (peaks at $\approx 1124, 1280, 1713, 1939, 2860, 3330\text{ cm}^{-1}$). This evidences that the sol-gel synthesis of GeS_2 from $\text{Ge}(\text{OC}_2\text{H}_5)_4$ and H_2S follows the reaction mechanism proposed by Melling[11].

The GeS-H vibration absorption peak, seen for gel 2, does not exist in the IR spectra of gels 1A, 1B and 3. Since there is IR evidence (shoulder peaks at 405 and 438cm^{-1}) that these gels contain GeS_2 , it seems that the condensation reaction was completed. There are the two possible reactions to explain the results:

a) In gels 1A, 1B and 3, H_2S liberated per reaction (1), was removed from the reaction mixture by the H_2S gas flow, causing the Ge-SH to react completely:



b) Since gels 1A, 1B and 3 contain both GeO_2 and GeS_2 , sol-gel processing of both compounds occurred simultaneously. Heterogeneous condensation is also possible and the following reactions could be proposed:





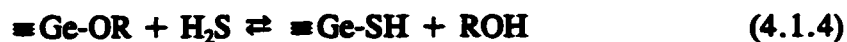
The reaction (4.1.3) is favoured thermodynamically due to formation of stronger bonds (Ge-O). Calculated ($\Delta G^\circ_{(2)} - \Delta G^\circ_{(3)}$) is 163.1kJ/mole.

Continued condensation of monomers $\equiv\text{Ge-S-Ge}\equiv$ with functionality $f > 2$ caused their crosslinking into three dimensional structures which formed the nuclei of colloidal particles. Scanning electron micrographs of the gels reveal that they consist of linked, essentially monodispersed spheres (size $\approx 0.1\mu\text{m}$). These particles are connected by necks to form a porous 3-dimensional network. Due to similarities between Ge and Si ethoxide chemistry, it is likely that the growth mechanism of GeS_2 and SiO_2 colloidal particles in a sol-gel process would be similar. For a neutral pH solution condition, Keefer[103] simulated a reaction-limited monomer-cluster growth of SiO_2 by the Eden model. This growth model assumed fast condensation with slow hydrolysis being the rate limiting reaction. Primary particles formed assuming this model is valid should be compact, smooth structures.

The BET analysis of gels 1A, 1B and 2 confirm this proposed aggregation growth model. For instance, amorphous gel 2 has a particle size $\approx 0.1\mu\text{m}$ estimated from the SEM micrographs. The surface area determined by BET is $227\text{ m}^2/\text{g}$, which is consistent with a particle radius of 4.5 nm calculated from the GeS_2 density, $2.94\text{ g}/\text{cm}^3$. Therefore, the 4.5 nm particles could be considered to be the primary particles whose aggregation resulted in formation of the secondary $0.1\mu\text{m}$ particles. Gels 1A and 1B have the same structure, with primary particles of 12 and 15 nm, respectively.

Comparing the volume of micropores within the secondary particles to the pore volume between them (mesopore volume), it is evident that the primary particles are highly packed, whereas the gels are formed by packing the secondary particles into open structures. The surface areas of gels 1A, 1B and 2 differ radically, although the micrographs show similar sizes for the secondary particles. This apparent inconsistency is probably due to differences in the primary particle size. Gel 2 has the highest surface area, hence this gel consists of the smallest primary particles. Since interparticle connection or fusion can diminish the surface area, this could be the reason for the difference in the surface areas of gel 1A and 1B, obtained from the same reaction solution. The type A BET isotherms of gels 1A, 1B and 2 indicate that particles were connected by necks, leading to cylindrical porosity.

It has been shown that slow hydrolysis of tetraethoxysilane (TEOS) in neutral solutions promotes formation of colloidal particles[104]. The analogy between SiO₂ and GeO₂ solution chemistry, renders it likely that slow thiolysis occurred in the neutral toluene solution of Ge(OC₂H₅)₄. From equation (4.1.4) it is apparent that the concentration of precursors, their concentration ratio and the reaction temperature are important



reaction parameters. Even though the concentration of Ge(OEt)₄ was ten times lower for the synthesis of gel 2, it has a particulate structure similar to gels 1A and 1B. However,

the primary particle size of gel 2 is smaller due to the $\text{Ge}(\text{OEt})_4$ concentration change.

4.1.2. Heat treated gels

Infrared spectra of the heat treated gels 1A and 1B reflect changes in the physical, chemical and structural properties which occurred during isothermal heating at 630°C . Toluene and ethanol were desorbed, condensation reactions were completed, and the GeO_2 and GeS_2 phases separated, transformed and densified.

At this temperature, amorphous GeS_2 densified by viscous sintering. Hexagonal GeO_2 was transformed to the tetragonal allotropic form. XRD and SEM investigations show that the tetragonal GeO_2 forms large grains. Differences in the peaks observed and the intensity of the same XRD peaks of tetragonal GeO_2 in 1A and 1B are indicative of a preferred crystal orientation caused by the XRD sample preparation. SEM observations of the crystal cross section show that the structure of GeO_2 coarsened (Fig. 3.1.6c,d), and that isolated pores were formed. Further densification of the crystals was arrested by these pores. Upon further heating, the shape of the pores in product 1B will cause shrinkage, while in product 1A the pores will grow.

Heat treatment of gel 2 also resulted in desorption of toluene and ethanol, condensation of non-reacted $\text{Ge}(\text{SH})_n(\text{OC}_2\text{H}_5)_{4-n}$ and sintering. The IR and XRD analyses of the heat treated gel 2 indicate that the product is solely monoclinic GeS_2 . Thus, during the heating, the gel 2 densification and phase transformation occurred. The micrograph of the heat treated gel 2 (Fig. 3.1.6g) reveals a vermicular structure of monoclinic GeS_2 , which probably formed by homogeneous nucleation. Amorphous GeS_2

behaved differently on heating in gels 1A and 1B than in gel 2. In gels 1A and 1B the GeS₂ phase densified, while in gel 2 it crystallized. To understand this phenomenon, the explanation given by Zarzycki[105] for silica gel can be employed. He pointed out that both processes, crystallization and viscous sintering, are determined by viscosity according to the following equation, derived by Uhlmann[106]

$$V \propto (t/\eta)^4 T^3 \exp(-W^* /kT) \quad (4.1.5)$$

where η is the viscosity of the gel at temperature T, t is the time of crystal volume fraction V formation, and W^* is the energetic barrier for spherical nucleus formation. Anything that changes viscosity, such as the content of OH or O, will influence the crystal volume fraction.

Since heat treatment parameters were the same for gels 1A, 1B and 2, the only significant factor which influenced the behaviour of the GeS₂ was the presence of OH and O in gels 1A and 1B, which increased viscosity in the gels. The consequence of the increased viscosity was a decreased crystal volume fraction V. In gel 2, homogeneous nucleation was able to proceed. The temperature was obviously high enough to allow for the formation of crystal nuclei and to allow diffusion sintering to proceed.

Results indicate that when water content decreased in the reaction mixture, the Ge/S atomic percent ratio decreased. In the gels, the Ge/S ratio is higher than stoichiometric, which could be explained by the presence of non-condensed species, or by the formation of germanium oxide. After heat treatment, the Ge/S ratio changed in all products. The

big crystals of GeO₂ in 1A and 1B have a very low sulphur content, which actually originates from the GeS₂ phase. The Ge/S ratio in amorphous GeS₂ in products 1A and 1B has decreased radically from 1:0.3 and 1:0.7 to \approx 1:1.7, indicating that during heat treatment, the homogeneous gel mixture of GeS₂ and GeO₂ separated into two immiscible phases. After heat treatment the Ge/S ratio in sample 2 also decreased, from 1:1.8 to 1:2.3, indicating that the condensation was completed.

4.2. PREPARATION OF GeS₂ FROM THE MIXTURE OF GeS₂-GeO₂ GEL AND SULFUR

The IR spectrum of the gel has well defined absorption peaks, typical for hexagonal GeO₂ whose presence is also confirmed by the sharp peaks in the XRD pattern of the gel. Although the XRD pattern of the gel does not indicate amorphous GeS₂, its presence was confirmed by IR spectroscopy. However, both the IR spectrum and XRD pattern of the gel confirmed the presence of crystalline orthorhombic sulfur.

The overall reaction for H₂S oxidation could be proposed as



The sulfur formed per reaction (4.2.1) was carried into the reaction mixture by the H₂S gas flow and it crystallized into the stable orthorhombic structure within the gel.

Influence of the acid on the H₂S oxidation can be explained by the following electrochemical reactions



If the reaction (4.2.1b) is the slow step then the presence of the concentrated acid helps the oxidation of H₂S to occur. The oxygen involved in this reaction (4.2.1b) probably comes from air trapped above sulfuric acid in the erlenmeyer.

Since the gel contains both GeO₂ and GeS₂, the sol-gel processing of these compounds occurred simultaneously. The following reactions could describe the formation of GeO₂



In the IR spectrum of the gel, the GeO-H bond was identified providing evidence for this reaction mechanism for the sol-gel processing of GeO₂. Water involved in the reaction was formed according to reaction (4.2.1) and also present in H₂S. It was introduced into the mixture by the H₂S gas flow.

The reaction mechanism for the sol-gel processing of GeS₂, proposed by Melling[11], consists of the following reaction steps



In reaction (4.2.7), formation of $\equiv\text{Ge-S-Ge}\equiv$ is favoured since the H₂S gas is easily removed from the reaction system.

Characterization results of the gel after heat treatment indicate that the product is monoclinic GeS₂. From Table 3.2.1 it is evident that the agreement of d-spacing and 2θ of heat treated product and standard is excellent showing that the product is primarily GeS₂. Its structure consists of large crystals with no porosity present at the grain boundaries. The IR spectrum of the heat treatment product indicates that, besides consolidation in the gel during heating, reduction of GeO₂ by elemental sulfur occurred via the following reaction



Calculated ΔG° is -46.3 kJ/mole for this reaction. In the IR spectrum of the gel an absorption peak which appeared at 473 cm⁻¹ was assigned to the S-S bond in elemental sulfur. This peak has shifted to a higher wave number 483 cm⁻¹, indicating the presence

of S-S bridging in the heat treated product. Therefore, it can be concluded that, besides conversion, curing of GeS_2 molecules due to sulfur excess occurred which produced Ge-S-S-Ge type of connections.

The result of semiquantitative analysis of the heat treated gel shows that the obtained product is homogeneous, with a Ge/S atomic percent ratio 1:2.9. This result also indicates an excess of sulfur introduced into the gel during synthesis.

4.3. PREPARATION AND CHARACTERIZATION OF OTHER METAL SULFIDES

4.3.1. Zinc sulfide gel

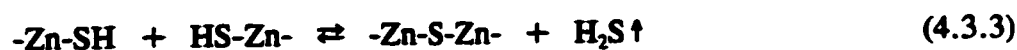
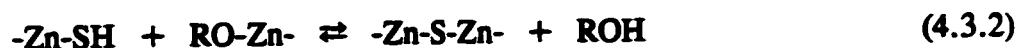
Reaction of $\text{Zn}(\text{O}i\text{Bu})_2$ and H_2S in toluene yielded a yellow, semi-transparent gel which dried into transparent reddish-orange solid. A similar product was obtained from zinc ethyl (Et_2Zn) and an excess of dibenzyl trisulfide, $(\text{BzS})_2\text{S}$ in toluene[21].

The average crystallite size calculated from x-ray line widths[95] is ≈ 10 nm. The zinc powder obtained by Johnson et al.[25] from zinc methyl, Me_2Zn , and H_2S in toluene has a primary particle size also ≈ 10 nm. Its XRD pattern is very similar to that shown in Fig. 3.4.1. The x-ray line broadening indicates that the spherical particles observed by the SEM (Fig. 3.4.2) are agglomerates of the primary particles. Since the $0.1 \mu\text{m}$ particles barely agglomerated, the prepared gel is semi-transparent. The scanning electron micrograph of ZnS gel reveals that the gel is colloidal. Formation of colloidal gels

requires an excess of formed monomers (-Zn-SH). Therefore, it could be assumed that this condition was achieved by bubbling the H₂S through the solution.

Both IR spectra and the XRD pattern confirmed that the product is a ZnS gel.

The following reaction mechanism can be proposed for the formation of ZnS



where R is the (C₄H₉)^o- group. Although the butanol was detected by IR, this can not be used as proof of the proposed mechanism since it was introduced into the solution with Zn(OBu^o)₂. There is no evidence of ZnS-H absorption band (~ 2500cm⁻¹) in the IR spectrum. The absence of the band was caused either by weak intensity of S-H stretching[107] or by completion of condensation reactions (4.3.2) and (4.3.3). Energy dispersive spectrometry (EDS) shows that the dried gel has Zn/S atomic ratio ≈ 1:1. This result may indeed indicate that the condensation reactions have been completed.

4.3.2. Colloidal tungsten sulfides

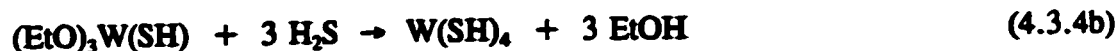
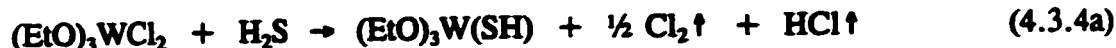
Infrared spectra of the tungsten sulfide gel and the powder in the range from 400-4000 cm⁻¹ are similar and they indicate the presence of toluene and ethanol which remained in both products after drying. Since the spectra were collected under the same conditions, the difference in the amount of absorbed ethanol is obvious: the powder

retained much more than the gel. The intensity of the ethanol absorption peaks did not diminish after additional drying of the powder in a vacuum oven at 110°C. The type of BET isotherm confirms that atomic interaction forces are stronger between nitrogen atoms than they are between nitrogen and the tungsten sulfide powder. The particle radius calculated from the BET data and the density of WS₂, 7.73 g/cm³, is 0.1 μm. However, these particles are not observed as a constituent of the bigger ones in the powder micrograph (Fig. 3.4.4b). This discrepancy indicates that the primary particles are probably much smaller than calculated and that the small specific surface area was obtained due to powder poisoning by retained ethanol and toluene.

The IR spectrum of Product 2 in the range 400-4000 cm⁻¹ has an adsorption band at ≈ 525 cm⁻¹ which is indicative of acetaldehyde. The peak at ≈ 1700 cm⁻¹ could be also indicative for acetaldehyde. However, it can also represent adsorbed water. The formation of acetaldehyde in the powder can be explained by the following overall reactions:



For reaction (4.3.4) it can be assumed that it is a complex reaction mechanism which consists of the several steps, described schematically as



or



It is suspected that reaction (4.3.4) initiates at chlorine atoms since Cl is a weaker base than (OEt) and it occurs as per the E_N2 mechanism. One chlorine atom is eliminated with hydrogen from the H_2S molecule, while the other atom leaves the ethoxide giving up an electron and oxidizing tungsten from the 5+ to 4+ valence state. In reaction (4.3.4a) the monomer $(\text{RO})_3\text{W}(\text{SH})$ is formed. It could be assumed that further reactions, thiolysis (4.3.4b) and condensations (4.3.4c), occur as per the S_N2 mechanism analogous to the previously suggested reaction of germanium ethoxide and H_2S [11]. Similarly, reactions (4.3.4b) and (4.3.4c) can be proposed for the reaction of $\text{W}(\text{OEt})_6$ and H_2S .

Microanalysis of the sol-gel products reveals that the powder and gel are nonstoichiometric WS_x compounds with W/S atomic percent ratios 1:1.4 and 1:2.7, respectively. These results indicate that powder should be WS_2 and gel WS_3 if thiolysis and condensation reactions were completed. Even though there is no WS-H absorption band in the IR spectra of Products 1 and 2, it may not have been identified due to low absorption intensity.

Products 1 and 2 consist of colloidal particles. However, they are connected in different patterns forming products with different morphologies. In Product 1 they are

smaller, connected into a 3-D gel network, while in Product 2 they agglomerated into larger particles. There are two possible reasons which caused such a difference: The higher concentration of $WCl_2(OEt)_3$ and the presence of Cl in the molecule of this alkoxide. Both, higher concentration and Cl, apparently increased the $WCl_2(OEt)_3$ thiolysis rate when an excess of monomers ($\equiv W-SH$) was produced, a condition necessary for monodispersed sols to be formed [108].

The gel was formed by the connection of colloidal particles into asymmetrical aggregates. From the micrograph in Fig. 3.4.4a, it is apparent that particle densification also occurred which caused the formation of macropores. Thixotropy of the gel indicates that it consists of asymmetrical particles connected with weak van der Waals bonds which break if the gel is exposed to a low shear stress.

4.4. PREPARATION OF THE THIN METAL SULFIDES FILMS

The thin films prepared from GeS_2 and ZnS colloidal suspensions were smooth and transparent. They demonstrated good adhesion to the glass slides when tested with the scotch tape. The micrographs of GeS_2 (Fig. 3.5.1a) and the ZnS (Fig. 3.5.1b) thin films also indicate their good adhesion to the substrate. There is no observed fusion line between the substrate and the films. The connection of glass slides and the films is probably not only physical, van der Waals attraction. The terminal groups SH and OR possibly reacted by condensation reaction with OH groups from the silica glass.

The microstructure of the prepared thin films is similar to that of the corresponding bulk gels. This indicates that the adhesion of the colloidal particles already formed in the solution occurred on the glass slide. This observation is also supported by the thickness of the films TF1 and TF2. The thickness of the film TF1 estimated from the scanning electron micrograph (Fig. 3.5.1a) is $\sim 5 \mu\text{m}$. In addition, it has a porous structure. However, the ZnS sulfide film is $\sim 0.5 \mu\text{m}$ thick and has a more compact structure. These differences of the GeS_2 and ZnS thin films can be attributed to the extent of the sol-gel reaction when the slides were dipped into the solutions. The results show that the more aggregated colloidal GeS_2 gel particles adhered to the slide making a thicker and more porous film than the ZnS particles.

4.5. DETERMINATION OF SULFUR PRODUCTS IN THE SOL-GEL PROCESSING OF GeS_2 BY POTENTIOMETRIC TITRATION

4.5.1. The method accuracy

The calculated concentrations from the data shown in Fig. 3.6.1 and 3.6.2 indicate that potentiometric titration with the ion selective $\text{Ag}/\text{Ag}_2\text{S}$ electrode is a very accurate method for quantitative determination of H_2S , germanium sulfide and mercaptide. Besides, the method's reproducibility is excellent as demonstrated with the repeatable titration of the same aliquots of the H_2S /toluene solution. The accuracy of the concentration determination can be assessed using relative deviation[99]. From

eq.(4.5.1), the average relative concentration deviation ($\Delta C/C$) in terms of the deviations of the quantities from which it is derived is given by:

$$\frac{\Delta C_i}{C_i} = \sqrt{\left(\frac{\Delta V_1}{V_1}\right)^2 + \left(\frac{\Delta V_{eq,p}}{V_{eq,p}}\right)^2} \quad (4.5.1)$$

where $V_1=1$ mL is the sample volume measured by 1 mL syringe divided in 0.01 mL increments, $\Delta V_1=0.005$ mL is the absolute deviation of a single sample volume measurement. A relative equivalence point volume deviation ($\Delta V_{eq,p}/V_{eq,p}$)=0.1% represents the precision of the titrant volume measurement, calculated for a 50 mL burette. Thus, the experimental concentration error is $\approx \pm 0.6$ %. However, a method error, representing the difference between equivalence point and theoretical end point [109], is negligible due to the high solubility of precipitates Ag_2S and $GeSAg$ [110]. Although the calculated error is higher than the ultimate of 0.1% [110], for such analysis this is still acceptable accuracy for quantitative analysis.

In the Nernst equation the ion concentrations were used instead of ion activities, $a_i=c_i\gamma_i$. This approximation is valid for any ion concentration c_i if activity coefficient $\gamma_i \approx 1$. To show that the approximation was satisfied, the activity coefficients are calculated.

Toluene and 2-propanol are low dielectric constant solvents. Ion formation is quite different from that in water. In toluene, which is an aprotic solvent, the ions are formed by solvent solute association[111]. Free ions can be neglected since they are present as

molecular aggregates. However, in 2-propanol, free ions exist since this solvent is a protic one. Dissociation of solutes occurs by an ion-pairing mechanism[111]. This mechanism is responsible for low molecular dissociation. In order to demonstrate this, the dissociation constant of NaCH₃COO in 2-propanol was calculated. The measured pH = 8.6 is equal to the concentration of ions Na⁺ and CH₃COO⁻ that are present. Hence, the solubility of the electrolyte is

$$[\text{Na}^+] = [\text{CH}_3\text{COO}^-] = 2.5 \times 10^{-9} \text{ M} \quad (4.5.2)$$

The dissociation constant calculated from this solubility of Na⁺ and CH₃COO⁻ and the concentration of dissolved NaCH₃COO of 5x10⁻³ M is 1.26x10⁻¹⁵, which is 10⁹ less than that in water (K_d^w = 3.0x10⁻⁵ M).

Possibly, ion-pairs such as 2(PrH⁺)S²⁻, 2(PrGe⁺)S²⁻ and PrH⁺GeS⁻ were formed from H₂S, GeS₂ and GeSH with 2-propanol(Pr), respectively. They further dissociate into appropriate ions. However, toluene solvates solutes by π electron donation so that an association reaction occurs. The associates presented in the simplest form could be TH₂S, TGeS₂ and THSGe formed from H₂S, GeS₂ and GeSH with toluene(T), respectively. Dissociation of these associates can be completely neglected. Therefore, the influence of other ionic species except those originating from the electrolyte on the ionic strength of the solution is absolutely negligible.

Titration of H₂S was performed in the NaCH₃COO 2-propanol solution. The dielectric constant of 2-propanol is ε_r = 18. It could be considered that the ionic strength

of the solution is only determined by the NaCH_3COO electrolyte. The influence of dissolved H_2S is neglected due to its expected low dissociation ($K_{\text{dis}} = 6.84 \times 10^{-23}$ [112] in water). From the concentrations of Na^+ and CH_3COO^- , the ionic strength of the solution is

$$I = \frac{1}{2} \sum c_i z_i^2 = 2.5 \times 10^{-9} \text{ M} \quad (4.5.3)$$

for $z_+ = z_- = 1$. Substituting this value into the Debye-Hückel equation [111] for the mean activity coefficient γ_{\pm} of H^+ and S^{2-}

$$-\log \gamma_{\pm} = \frac{A |z_+ z_-| I^{1/2}}{1 + B a I^{1/2}} \quad (4.5.4)$$

gives $\gamma_{\pm} = 0.998$. In eq.(4.5.4) $z_+ = 1$ and $z_- = 2$ are the H^+ and S^{2-} charges, respectively and a is the ionic radius of the sulfide ion, arbitrarily taken $\approx 5 \text{ \AA}$. Constants A and B were determined for $T = 293 \text{ K}$ and $\epsilon_r = 18$,

$$A = \frac{1.825 \times 10^6}{(T \epsilon_r)^{3/2}} = 4.6 \text{ mole}^{-1/2} \quad (4.5.4a)$$

$$B = \frac{50.29 \times 10^8}{(T \epsilon_r)^{1/2}} = 6.9 \times 10^7 \text{ mole}^{-1/2} \text{ cm}^{-1} \quad (4.5.4b)$$

Therefore, the approximation that $a_i \approx c_i$ is permissible. Similar calculations can be performed for the S^{2-} ion from GeS_2 and for GeS^- from GeSH titrated in the 50:50 vol %

mixture of the electrolyte and toluene. In this case, the mean activity coefficients for sulfide ion and mercaptide were 0.999 and 0.997, respectively

The thermodynamically derived Nernst equation should be independent of the type of solvents. Accordingly, if the measured Ag/Ag₂S electrode potential is plotted against logC_{Ag+} (Fig. 3.6.3b), then the slope of the electrode response $2.3RT/F$ should be equal in any solvent. The result shown in Table 3.6.1, 58 mV, representing the electrode response in the AgNO₃-2-propanol solution is in an excellent agreement with the slope obtained in a AgNO₃-water solution at 20°C[114]. The constant $E^{\circ}_{Ag+/Ag}$ in eq.(3.6.2) experimentally determined is +406 mV (Table 3.6.1). It includes the standard electrode potential $E^{\circ}_{Ag+/Ag}$, liquid-junction potential, reference electrode potential (saturated calomel) and activity coefficient of the silver ion $\log\gamma_{\pm}$. The expected theoretical value for $E^{\circ}_{Ag+/Ag}$ in 2-propanol is 680 mV and for the saturated calomel electrode 275 mV[113]. The difference between experimental and calculated values for $E^{\circ}_{Ag+/Ag}$ can be assigned to the liquid junction potential since $\gamma_{\pm} \approx 1$.

4.5.2. The Ag/Ag₂S electrode response to the S₂ and GeS₂ ions

Fig. 3.6.3 confirms Nernstian electrode response to any of the titrating species. The slopes of these plots were different than expected for S²⁻ and GeS₂⁻ (Table 3.6.1 and 3.6.2). They indicate formation of silver complexes with different stoichiometry whose general formulas can be defined as [Ag(S)_p]^{1-2p} and [Ag(GeS)_p]^{1-p}. Comparing results obtained from H₂S titration with AgNO₃ and HgCl₂ (Table 3.6.1), the similarities between them are obvious. They produced complexes of the same stoichiometry (≈ 1)

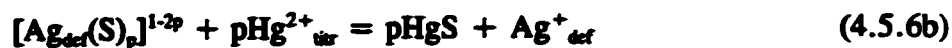
and similar solubility products, 1×10^{-23} and 1.6×10^{-23} , respectively. These results indicate that the same reaction occurred at the electrode. Moreover, results in Table 3.6.2 confirm formation of silver mercaptide complexes. The stoichiometric term p increased with the mercaptide concentration, as did the apparent solubility product of the complexes.

However, the potentiometric titration products were the stoichiometric compounds Ag_2S , HgS and GeSAg , as confirmed by calculations from the equivalence points. Consequently, the following reactions are proposed in order to explain this discrepancy:



Obviously, free S^{2-} ions react with Ag^+_{def} defects present in the Ag_2S electrode membrane forming complex (4.5.5a). When the AgNO_3 titrant is added, it reacts with the complex producing barely soluble Ag_2S (4.5.5b). Combination of (4.5.5a) and (4.5.5b) determines the net ion equation (4.5.5). Therefore, the Nernst equation only explains reaction (4.5.5a) since only free S^{2-} ions determine the electrode potential.

Similarly, the titration with HgCl_2 can be described



and the reaction of the germanium mercaptide and silver nitrate:



Hence, the equivalence point corresponds to the stoichiometry of the net ion reaction (4.5.5, 4.5.6 or 4.5.7).

4.5.3. Detection limits

The intrinsic detection limit is assigned either to the concentration of the Ag^+ defects at the solid membrane surface or to its solubility [100]. Results for detection limits are presented in Tables 3.6.1 and 3.6.2. There is a consistency in the determined detection limits of mercaptide, mean value $\approx 6.3 \times 10^{-5}$ M, comparable to those obtained for thiols with the same type of electrode [78]. Therefore, this result can be assigned to the Ag^+ defects in the membrane. Furthermore, a value $\log C_{\text{Ag}^+} = -7$ was obtained as a detection limit for the electrode response of Ag^+ in an excess of AgNO_3 . It is similar to that previously reported [100] and can also be assigned to the Ag^+ defects in the membrane. However, the detection limits of S^{2-} (Table 3.6.1) indicate solubility of the

Ag₂S membrane.

4.5.4. The interference of the S²⁻ and GeS⁻ ions

Results of the S²⁻ and GeS⁻ ion interference in the Ag/Ag₂S electrode response are shown in Table 3.6.3. The agreement among determined separation coefficients is apparent. Also, the alternative method suggested for the determination of the separation coefficients gave a result in excellent agreement with a mean value obtained by a method for mixed solutions[101]. The mean value $k_{SH,S}^{pot} = 2.3 \times 10^3$, calculated from $k_{SH,S}^{pot}$ in Table 3.6.3, is sufficiently high and indicates that there is no interference between GeS⁻ and S²⁻ ions. Consequently, the precipitation of GeS⁻ will not begin until the concentration of sulfide is not less than $5.2 \times 10^{-4} C_{SH}$. Moreover, a high separation coefficient explains why the graph plotted per the Nernst equation is linear although both ions are present in the solution (Fig. 3.6.3a). Hence, the modified Nernst equation (3.6.1) representing the Ag/Ag₂S electrode potential dependence on the S²⁻ and GeS⁻ ions in the 2-propanol or the mixed 2-propanol and toluene is in good agreement with experimental results,

$$E = E^{o'}_{Ag+/Ag} + \frac{2.3RT}{F} \log K_{SH} - \frac{2.3RT}{F} \log [C_{SH}^p + k_{SH,S}^{pot} C_S^q] \quad (4.5.8)$$

Two limiting cases can be approximated:

a) since $k_{SH,S}^{pot} C_S^q \gg C_{SH}^p$, then the electrode potential is determined only by S²⁻ ions present in solution,

$$E = E^{\circ}_{\text{Ag}^+/\text{Ag}} + \frac{2.3RT}{F} \log K_s - \frac{2.3RT}{F} \log C_s^4 \quad (4.5.9)$$

b) if $C_s < 5.2 \times 10^{-4} C_{\text{SH}}$, then equation (4.5.8) reduces to,

$$E = E^{\circ}_{\text{Ag}^+/\text{Ag}} + \frac{2.3RT}{F} \log K_{\text{SH}} - \frac{2.3RT}{F} \log C_{\text{SH}}^4 \quad (4.5.10)$$

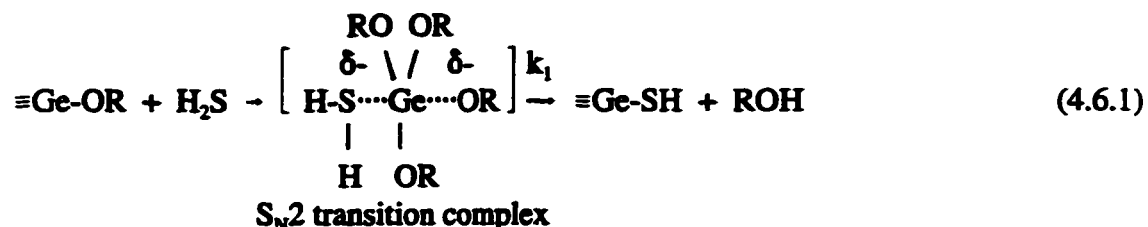
A similar expression for thiols was obtained earlier[78,100]. Equations (4.5.9) and (4.5.10) appear to describe quite well the results obtained for the Ag/Ag₂S electrode response to S²⁻ and GeS⁻.

4.6. CHEMICAL KINETICS STUDY OF THE SOL-GEL PROCESSING OF GeS₂

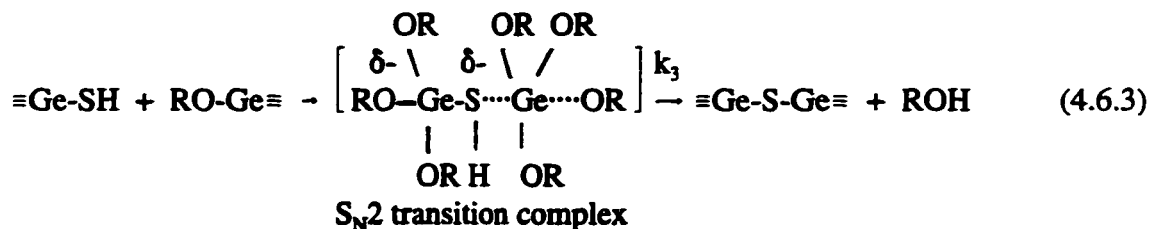
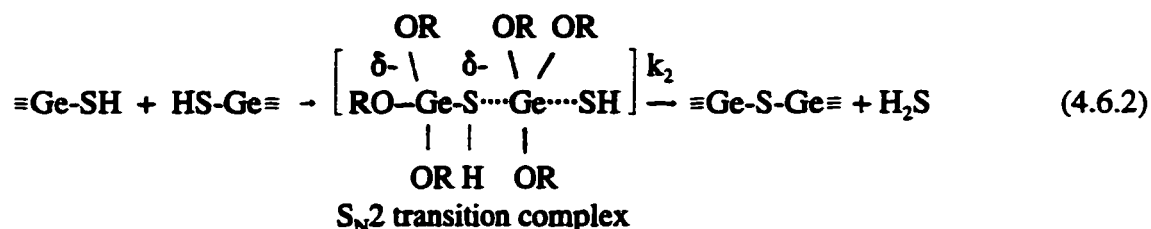
4.6.1. Theoretical consideration

Melling[11] proposed the mechanism of Ge(OEt)₄ and H₂S reaction analogous, to that of Si(OEt)₄ and H₂O, involving two steps per S_N2 (bimolecular nucleophilic substitution):

I step: thiolysis



II step: condensations



where R is the ethyl or isopropyl group, k_1 is the thiolysis rate constant, k_2 is the hydrogen sulfide forming condensation rate constant and k_3 is the alcohol forming condensation rate constant. This is a simplified scheme of a very complex reaction mechanism consisting of a series of consecutive, parallel and reverse reactions whose intermediate products can have structures as complicated as $\text{GeS}_x(\text{SH})_y(\text{OR})_{4-z}$, where $x+y+z=4$. The overall reaction from eq.(4.6.1-4.6.3) is



Therefore, germanium alkoxide, germanium mercaptide, germanium sulfide and the corresponding alcohol are present at equilibrium. All these compounds were identified in the dried gels by infrared spectroscopy (Fig. 3.1.3c).

Assuming that reaction rate constants are independent of the number of substituted functional groups per Ge atom during thiolysis (-OR) and condensations (-SH), the reaction rate equations can be expressed from eq.(4.6.1-4.6.3):

$$-\frac{d[\text{A}]}{dt} = k_1[\text{A}][\text{B}] + k_3[\text{A}][\text{C}] \quad (4.6.5)$$

$$-\frac{d[\text{B}]}{dt} = k_1[\text{A}][\text{B}] - k_2[\text{C}]^2 \quad (4.6.6)$$

$$\frac{d[\text{C}]}{dt} = k_1[\text{A}][\text{B}] - k_2[\text{C}]^2 - k_3[\text{A}][\text{C}] \quad (4.6.7)$$

$$\frac{d[\text{M}]}{dt} = k_2[\text{C}]^2 + k_3[\text{A}][\text{C}] \quad (4.6.8)$$

$$\frac{d[\text{D}]}{dt} = k_1[\text{A}][\text{B}] + k_3[\text{A}][\text{C}] \quad (4.6.9)$$

where $[\text{A}] = [\equiv\text{GeOR}]$, $[\text{B}] = [\text{H}_2\text{S}]$,

$$[C] = [≡\text{GeSH}], [D] = [\text{ROH}],$$

$$[M] = [≡\text{Ge-S-Ge}≡],$$

are the reactant and product concentrations in mole/L (M) present in the reaction mixture at time t.

From the reaction stoichiometry and mass conservation, the relationship among concentrations of reactants and products can be given:

$$[A]_0 = 4[\text{Ge(OR)}_4]$$

is the initial concentration of alkoxy groups from which the concentration of substituted alkoxy groups, $[X]_A$, is

$$[X]_A = [A]_0 - [A]$$

and reacted hydrogen sulfide, $[X]_B$, is

$$[X]_B = [B]_0 - [B].$$

From the mass conservation law,

$$[X]_A = [C] + 2[M]$$

$$[X]_B = [C] + [M]$$

the concentrations of the reacted alkoxy groups, $[X]_A$, or hydrogen sulfide, $[X]_B$, are equal to the sum of concentrations of mercaptide [C], and sulfide [M]. In early stages of thiolysis, it could be assumed that the reaction occurs with no interference of the condensation reactions. Therefore,

$$[X]_A \approx [X]_B = [X]$$

and

$$[X] = [C] + [M]$$

$$[A]_0 - [A] = [B]_0 - [B]$$

$$[A] = [A]_0 - [B]_0 + [B],$$

represents the concentration of unreacted alkoxy groups. In addition, the concentration of the formed alcohol is

$$[D] = [X] = [A]_0 - [A]$$

Hence, by measuring the concentrations of evolved mercaptide and sulfide it is possible to monitor how the concentrations of all other products and reactants change with time.

It is speculated that the proposed reaction mechanism (eq. 4.6.1-4.6.3) can also involve the reverse reaction steps. Therefore, the agreement of the experimentally determined rate law and the proposed mechanism will evidence the actual reaction mechanism.

In the suggested reaction scheme, germanium mercaptide is an intermediate product. It reacts further by two competitive parallel reactions, eq.(4.6.2) and (4.6.3). The kinetics of this complex reaction system can conveniently be approximated, provided the intermediate $\equiv\text{GeSH}$ is either equilibrated or transient[115]. According to approximation competition for an equilibrated intermediate (CEI)[115], the concentration of the intermediate ($\equiv\text{GeSH}$) will equilibrate under the assumption that thiolysis is a fast and reversible reaction and thus,

$$[C] = \frac{k_1}{k_{-1}} \cdot \frac{[A][B]}{[D]} \quad (4.6.10)$$

This approximation is only valid if substitution in the kinetic eq.(4.6.5-4.6.9) gives

agreement with the experimental results.

However, the approximation competition for the transient intermediate (CTI)[115] is applicable if the rate constants for the competition condensation reactions, k_2 and k_3 , are much greater than the thiolysis rate constant. In such a case, the concentration of the intermediate $[C]$ is much less than $[A]$. Therefore, from the approximation

$$\frac{d[C]}{dt} \approx 0 \quad (4.6.11)$$

and eq.(4.6.7) the concentration of the intermediate, $[C]$, can be calculated. If thiolysis is a reversible reaction, then

$$k_1[D] \gg k_2[C] + k_3[A] \quad (4.6.12)$$

meaning the intermediate germanium mercaptide is equilibrated as well as transient and then both approximations are applicable. However, if

$$k_1[D] \ll k_2[C] + k_3[A] \quad (4.6.13)$$

thiolysis is virtually irreversible.

The experiments will confirm the reaction scheme and give solutions as to which of the conditions lead to certain approximations and simplify interpretation of the kinetic data. Even after these approximations, CTI or CEI, the multiple term differential

eq.(4.6.5-4.6.9) are difficult mathematical problems to obtain exact solutions of the rate constants. One of the methods which enables simplification of the mathematical expressions for computation of the reaction rate constants is the method of concentration-time integrals[116]. For example, if the reaction occurs only per two steps described by eq.(4.6.1) and (4.6.3), then the differential rate eq.(4.6.5) is

$$-\frac{d[A]}{dt} = k_1[A][B] + k_3[A][C] \quad (4.6.14)$$

After rearrangement and integration it becomes

$$\ln \frac{[A]_0}{[A]} = k_1 \int_0^t [B] dt + k_3 \int_0^t [C] dt \quad (4.6.15)$$

or

$$\frac{\ln \frac{[A]_0}{[A]}}{\int_0^t [B] dt} = k_1 + k_3 \frac{\int_0^t [C] dt}{\int_0^t [B] dt} \quad (4.6.16)$$

From experimental data of [C] and [M], the concentrations [A] and [B] can be calculated as functions of time and then used for obtaining the concentration integrals. Equation (4.6.16) suggests a linear plot whose intercept is k_1 and slope is k_3 .

However, if condensation occurs only by the H₂S forming condensation reaction, eq.(4.6.2), then the differential rate equation for sulfide formation is

$$\frac{d[M]}{dt} = k_2[C]^2 \quad (4.6.17)$$

After concentration-time integration it becomes,

$$\int_0^t d[M] = k_2 \int_0^t [C]^2 dt \quad (4.6.18)$$

$$[M] = k_2 \int_0^t [C]^2 dt \quad (4.6.19)$$

since $[M] = 0$ at $t = 0$. If the proposed mechanism is correct, then a plot of eq.(4.6.19) is linear with slope equal k_2 .

The other mathematical method which permits calculation of the rate constants is a differential method[117]. The procedure considers a single run where the measured reaction rate at different reaction times corresponds to the reactant (or product) concentration. For example, if it is assumed that condensation occurs only per the alcohol forming condensation reaction, eq.(4.6.3), then the reaction rate of sulfide formation is

$$\frac{d[M]}{dt} = k_3[A][C] \quad (4.6.20)$$

If the reaction rate is measured in the early stages of the reaction, the

following assumption can be made:

$$[A] \gg [C] + [M],$$

and therefore,

$$[A] = [A]_0.$$

Thus, a plot of eq.(4.6.20) is linear with slope equal $k_3[A]_0$ from which the reaction rate constant can be calculated.

If it is possible to make a supposition that only thiolysis (4.6.1) occurs with no condensation reaction interference, as the second order reaction, then the differential rate eq.(4.6.5) becomes

$$-\frac{d[A]}{dt} = k_1[A][B] \quad (4.6.21)$$

and after integration it is,

$$\frac{1}{[B]_0 - [A]_0} \ln \frac{[A]_0[B]}{[B]_0[A]} = k_1 t \quad (4.6.22)$$

Experimental data will give a linear plot of eq. (4.6.22) if the assumption is correct. Additional simplification in the integration of eq. (4.6.21) is possible to make if one of the reactants, for instance (B), is in a great excess, considered as constant in the observed reaction interval. This assumption provides pseudo-first order kinetics[116]. Hence, the

integrated form of eq. (4.6.21) will be

$$\ln \frac{[A]}{[A]_0} = k_{app}' t \quad (4.6.23)$$

The constant $k_{app}' = k_1[B]_0$ can be determined from the slope of the linear graph, if the experimental results coincide with the pseudo-first order assumption.

The temperature dependence of the rate constants of thiolysis and condensations reactions were studied using two different equations. One of them was the Arrhenius relation[102] in which the two parameters are A, the pre-exponential factor (or frequency factor), and E_a , the activation energy:

$$k = A \exp\left(-\frac{E_a}{RT}\right)$$

The frequency factor A is taken as independent of temperature. The other one is the absolute reaction rate theory relation (or the transition-state theory)[102]

$$k = \frac{RT}{Nh} \exp\left(\frac{\Delta S^\ddagger}{R}\right) \exp\left(-\frac{\Delta H^\ddagger}{RT}\right)$$

The pre-exponential parameter shows a first power temperature dependence. In this case ΔS^\ddagger is the activation entropy and ΔH^\ddagger is the activation enthalpy. Parameters R, N_a and h are the well known gas constant, Avogadro's number and Planck's constant, respectively.

4.6.2. Reaction mixtures containing $[H_2S]$, and $[Ge(OEt)_4]$, in ratio 9:1

The induction period, exhibited in Fig. 3.7.2, indicates that reaction occurs slowly. During this time there was a build-up towards a small but critical concentration of the intermediate, germanium mercaptide. This critical concentration was found to be -1.29×10^{-3} M, regardless of the reaction temperatures. However, the temperature influenced the length of the induction period. Once the critical concentration was achieved, the reaction rate suddenly increased indicating that another much faster reaction began. From this result it was assumed that the reaction rate of the ethoxy group depletion, eq.(4.6.5), could be simplified during the induction period, to:

$$-\frac{d[A]}{dt} = k_1[A][B] \quad (4.6.24)$$

This assumption is a consequence of a very low concentration of intermediate C in comparison to the reactant concentrations. Thus, the expression in eq. (4.6.5) containing [C] can be neglected. Therefore, it could be concluded that, during the induction period, thiolysis occurs with no interference from the condensation reactions.

The linearity of graphs $-\ln([A]/[A]_0)$ vs. time during the induction period indicates that the reaction was first order in regard to the concentration of the ethoxy group. Moreover, since the concentration of hydrogen sulfide was in excess and almost constant during the induction period, it was suspected that the reaction occurred as a pseudo-first order. Consequently, the integrated form of eq. (4.6.24) is

$$\ln \frac{[A]}{[A]_0} = k_{app}' t \quad (4.6.25)$$

where

$$k_{app}' = k_1[B]_0 \quad (4.6.26)$$

is the apparent first order rate constant obtained from the slope of the plot $-\ln[A]/[A]_0$ vs. time. From the experimentally determined rate constant and initial concentration of hydrogen sulfide $[B]_0$, the thiolysis rate constant was calculated. As a second order rate constant, it indicates that thiolysis is a bimolecular reaction.

After the induction period, the reaction became complicated. It is possible that two condensation reactions started to proceed more extensively. The experimental results for $[M]$ and $[C]$, when plotted as $\Delta[M]/\Delta t$ vs. $[C]$ (Fig. 3.7.4), indicate that the dominant condensation reaction is the alcohol forming condensation (k_3). The linearity of these plots unambiguously confirms that eq. (4.6.8) is valid in the simplified form

$$\frac{d[M]}{dt} = k_3[A][C] \quad (4.6.27)$$

and that

$$k_3[A] \approx k_3[A]_0 \approx \text{const.} \quad (4.6.28)$$

The approximation in eq.(4.6.28) is reasonable for this initial period of the condensation

reaction when the concentration of intermediate C is still very low, that is $[C] \ll [A]$. Therefore, the reaction rate of sulfide formation defined by eq.(4.6.27) represents the initial rate of the condensation reaction k_3 .

The absence of the hydrogen sulfide forming condensation in this early reaction stage can be explained by the very low $[C]$, if the condensation rate constants k_2 and k_3 are of the same order. When this small value is squared it becomes negligible. Accordingly, there is a critical mercaptide concentration which triggers the hydrogen sulfide forming condensation probably later on during the sol-gel process. However, it is also possible that $k_2 \ll k_3$ and that germanium sulfide is mainly a product of the alcohol forming condensation regardless of the concentration of intermediate C.

From these experimental results, a simplified reaction scheme can be proposed for the reaction conditions imposed:



Hence, the rate law which defines the proposed reaction mechanism is

$$-\frac{d[A]}{dt} = k_1[A][B] + k_3[A][C] \quad (4.6.31)$$

$$\frac{d[C]}{dt} = k_1[A][B] - k_3[A][C] \quad (4.6.32)$$

$$\frac{d[M]}{dt} = k_3[A][C] \quad (4.6.33)$$

The experimentally determined thiolysis and condensation rate constants at different temperatures exhibit good agreement with the Arrhenius equation as demonstrated in Fig. 3.7.5a. The activation energies of thiolysis and condensation (Table 3.7.2) determined from the slopes of these graphs have values typical for a bimolecular nuclear substitution[118]. Therefore, the functional relationship of the rate constants and temperature is represented as follows:

$$\ln[k_1(\text{M} \cdot \text{s})^{-1}] = -(8845 \text{ K})/T + 11.8 \quad (4.6.34)$$

$$\ln[k_3(\text{M} \cdot \text{s})^{-1}] = -(8525 \text{ K})/T + 19.2 \quad (4.6.35)$$

For bimolecular reactions involving relatively simple molecules, the frequency factor A generally has values of order 10^9 to $10^{11} (\text{M} \cdot \text{s})^{-1}$ [119]. However, for the thiolysis reaction it was 1.3×10^5 and condensation 2×10^8 , indicating reactions between complex molecules[119]. Understanding of such values of A can be gained if transition-state theory is employed. The activation entropy ΔS^\ddagger is a measure of disorder in the activated complex. The decrease in entropy reflects the decrease in the activated complex disorder caused by loss of motional mode of molecules in the transition state. For a bimolecular reaction, such as S_N2 , two reactant particles are converted to a single activation complex

in a transition state. The loss of the molecular rotational and translational degrees of freedom in the transition state causes a decrease of corresponding entropies. The resulting total entropy changes ΔS^\ddagger during thiolysis and condensation are negative, typical for an associative mechanism of ligand substitution by S_N2 [119].

From the results in Table 3.7.2, it is obvious that the activation complex formed during thiolysis is a more ordered structure than that formed during condensation. This difference in entropy could be explained by a steric effect. Increased steric crowding during condensation increased the entropy of TS2. However, steric crowding increases the activation energy of Ge-S-Ge formation as seen from ΔH^\ddagger and E_a (Table 3.7.2).

Using data from Table 3.7.2 for the activation free energies ΔG^\ddagger for the transition state of thiolysis (TS1) and condensation (TS2), the free energy vs. reaction coordinate diagram was sketched in Fig. 4.6.1. The transition states correspond to the maxima in the diagram. There is a free energy local minimum between them assigned to the intermediate germanium mercaptide. The first maximum is obviously higher than the second one. From this result and from the reaction rate constants k_1 and k_3 , it is evident that the rate-limiting step for this sol-gel reaction is thiolysis.

The positive enthalpy of the sol-gel reaction evidences that it is endothermic. Since the reaction occurs spontaneously, probably the high entropy, 61 J/moleK, defined as $(\Delta S_c^\ddagger - \Delta S^\ddagger)$, exerts a greater influence on the chemical change than the reaction enthalpy.

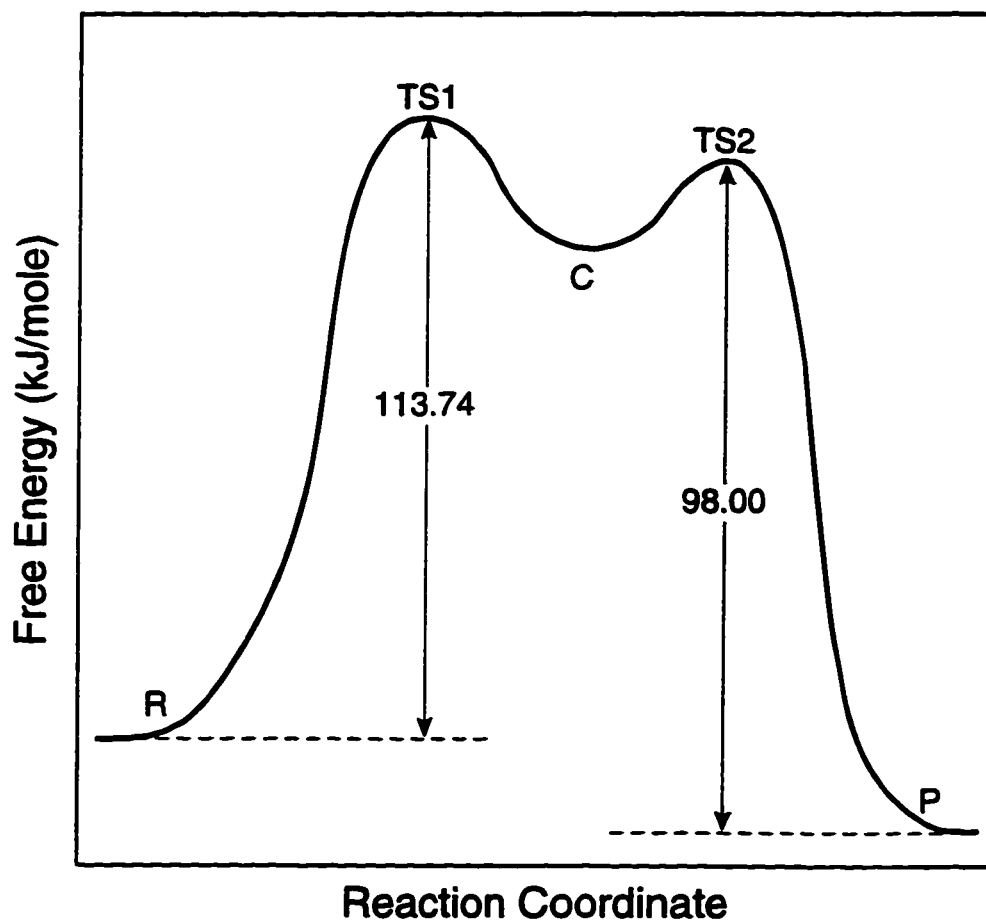


Fig. 4.6.1 Free energy-reaction coordinate diagram for the sol-gel processing of GeS_2 when $[\text{H}_2\text{S}]/[\text{Ge}(\text{OEt})_4]$ is 9:1.

4.6.3. Reaction mixtures containing $[H_2S]_0$ and $[Ge(OEt)_4]_0$ in ratio 1:1.2

Initial mixtures for the chemical kinetics investigation were prepared with H_2S in a substoichiometric amount (< 2). The concentration-time plots indicate the presence of an induction period, as shown in Fig 3.7.6, curve (M). During this period the reaction was second order as demonstrated with the plots in Fig 3.7.8. According to this, it was assumed that, during the induction period, thiolysis occurred with no condensation interference.

Moreover, the concentration-time curves (Fig. 3.7.6) are similar to those obtained for the pseudo-first order reaction (Fig. 3.7.2). That is, after the induction period, a much faster reaction started when the intermediate mercaptide reached the critical concentration. Further, none of the applied mathematical methods for the condensation rate constant calculations gave a reasonable match with the experimental results. Therefore, it is suspected that both hydrogen sulfide and alcohol forming condensations simultaneously started after the induction period. Consequently, the proposed complex reaction mechanism, given by eq. (4.6.1-4.6.3), is applicable for the sol-gel reaction with low H_2S content. For these conditions, the proposed rate law is

$$-\frac{d[A]}{dt} = k_1[A][B] + k_3[A][C] \quad (4.6.36)$$

$$\frac{d[C]}{dt} = k_1[A][B] - k_2[C]^2 - k_3[A][C] \quad (4.6.37)$$

$$\frac{d[M]}{dt} = k_2[C]^2 + k_3[A][C] \quad (4.6.38)$$

The best fit straight line for the thiolysis rate constant dependence on temperature is represented by

$$\ln k_1(\text{M} \cdot \text{s})^{-1} = -(7360 \text{ K})/T + 10.3 \quad (4.6.39)$$

The activation energy E_a and the activation enthalpy ΔH^\ddagger of thiolysis obtained for these reaction conditions are very similar to those for the reaction with H_2S in excess (Table 3.7.2). This result is reasonable since, in both reactions the same reactants, $\equiv\text{GeOEt}$ and H_2S , and same products, $\equiv\text{GeSH}$ and EtOH , are involved. Although the reaction conditions were different, the same bonds are broken and formed during thiolysis. Moreover, the activation entropy ΔS^\ddagger was negative, indicating that thiolysis occurs by an associative mechanism of two molecules ($\text{S}_{\text{N}}2$). The numerical value of ΔS^\ddagger was lower than that for the pseudo-first order reaction (Table 3.7.2), increasing the thiolysis rate constant ~ 2 times.

Therefore, it could be suggested that low H_2S concentration influenced only the simultaneous occurrence of both condensation reactions due to a significant increase in the intermediate mercaptide concentration. However, it did not change the reaction type. All of them followed the $\text{S}_{\text{N}}2$ mechanism. The increase in the thiolysis rate constant could be assigned to the $\text{Ge}(\text{OEt})_4$ concentration change. From the similarities of the concentration-time curves obtained for low and high H_2S concentrations, it seems that

both sol-gel processes occurred by slow thiolysis and fast condensations.

4.6.4. Reaction mixtures containing $[\text{Ge}(\text{OPr}^i)_4]$ and $[\text{H}_2\text{S}]$

The mass balance graph shown in Fig. 3.7.10 is indicative of consecutive reaction occurrence. It means that the intermediate compound mercaptide (C) undergoes subsequent chemical reaction to form a product, in this case sulfide (M). According to the analysis of the reaction order (Fig. 3.7.11), it was found that the consecutive reaction is of second order with respect to both reactants, germanium isopropoxide and hydrogen sulfide. Hence, the rate law can be defined as:

$$-\frac{d[\text{A}]}{dt} = -\frac{d[\text{B}]}{dt} = k_1[\text{A}][\text{B}] \quad (4.6.40)$$

or in integrated form:

$$\frac{1}{[\text{B}]_0 - [\text{A}]_0} \ln \frac{[\text{A}]_0[\text{B}]}{[\text{B}]_0[\text{A}]} = k_1 t \quad (4.6.41)$$

It is obvious that the complicated rate laws (eq. 4.6.5-4.6.9) reduced to a simple one by deduction from experimental results. Apparently, reaction conditions, concentration, temperature and particularly the use of germanium isopropoxide, enforced some limiting conditions.

The intermediate concentration $[\text{C}]$ achieves a plateau (ranging from 2×10^{-3} to 3.4×10^{-3} M). Since $[\text{C}] \ll [\text{A}]$ in this stage of the sol-gel reaction, it is possible to apply

approximation competition for the transient intermediate (CTI). It follows that:

$$k_1[A][B] \ll k_2[C]^2 + k_3[A][C] \quad (4.6.42)$$

$$\frac{d[C]}{dt} = k_1[A][B] - k_1[C][D] - k_3[A][C] - k_2[C]^2 \quad (4.6.43)$$

If thiolysis is an irreversible process, the assumption

$$k_1[D] \ll k_2[C] + k_3[A] \quad (4.6.44)$$

leads to the simplified kinetic equations

$$-\frac{d[A]}{dt} = k_1[A][B] + k_3[A][C] \quad (4.6.45)$$

$$\frac{d[C]}{dt} = k_1[A][B] - k_2[C]^2 - k_3[A][C] \approx 0 \quad (4.6.46)$$

The concentration [C], calculated from eq. (4.6.46) is:

$$[C] = \frac{2k_1[B]}{k_3 \left(\sqrt{1 + \frac{4k_1k_2[B]}{k_3^2[A]} + 1} \right)} \quad (4.6.47)$$

If there is a limiting case:

$$\frac{4k_1k_2[B]}{k_3^2[A]} \ll 1 \quad (4.6.48)$$

then equation (4.6.48) for the transient [C] reduces to

$$[C] = \frac{k_1}{k_3} [B] \quad (4.6.49)$$

When this value for [C] is substituted in eq. (4.6.45), it becomes

$$-\frac{d[A]}{dt} = 2k_1[A][B] \quad (4.6.50)$$

Experimental data (Fig. 3.7.12) proved that thiolysis is a second order reaction with respect to reactants A and B. They could also show that the CTI approximation is valid.

However, another possible assumption is that the alcohol forming condensation (eq.4.6.3) is negligible in this reaction due to steric effects. This consideration allows simplification of the kinetic equations to

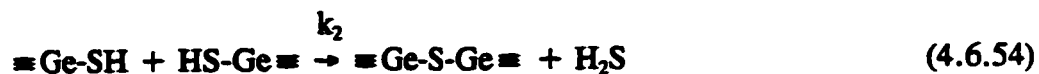
$$-\frac{d[A]}{dt} = k_1[A][B] \quad (4.6.51)$$

$$\frac{d[M]}{dt} = k_2[C]^2 \quad (4.6.52)$$

Therefore, both CTI and elimination of the alcohol forming condensation assumptions

lead to simple second order reaction. According to the CTI approximation $k_{app}' = 2k_1$, while it is $k_{app}' = k_1$ if the second assumption is also valid.

The graphs in Fig. 3.7.13 were obtained by concentration-time integration of eq.(4.6.52). They obviously show that the alcohol forming condensation is an insignificant reaction in this mechanism and its elimination is a correct assumption. Hence, the reaction mechanism for the sol-gel processing of germanium sulfide from $\text{Ge}(\text{OPr}^i)_4$ and H_2S can be reduced to



The corresponding rate laws are given by eq.(4.6.51) and (4.6.52).

The activation entropy ΔS^\ddagger of thiolysis (Table 3.7.5) indicates higher disorder in the transition state of $\text{Ge}(\text{OPr}^i)_4$ and H_2S than in the transition state of $\text{Ge}(\text{OEt})_4$ and H_2S . There are two possible reasons causing higher ΔS^\ddagger : bulkiness of isopropoxy groups and formation of isopropyl alcohol. This steric effect is likely the cause also of a higher thiolysis activation energy (Tables 3.7.2 and 3.7.5)

There is a slight decrease in the standard entropy of condensation in comparison to the condensation reaction k_3 of $\text{Ge}(\text{OEt})_4$. This could be also explained via a steric effect. In the condensation (k_2) transition state there are two molecules of $\equiv\text{GeSH}$ instead of $\equiv\text{GeSH}$ and bulkier $\equiv\text{GeOEt}$ in condensation k_3 . Moreover, the smaller

molecule H_2S was formed during condensation k_2 contrary to EtOH in k_3 . A bigger space requirement for formation of EtOH can disturb the rest of the structure within the activated complex, leading to a more disordered transition state and more positive activation entropy.

From the activation free energies (Table 3.7.5), the free energy-reaction coordinate diagram was sketched in Fig. 4.6.2 for the proposed reaction mechanism, eq.(4.6.53) and (4.6.54). From this diagram and the reaction rate constants (Table 3.7.4), it is apparent that, in this sol-gel process, thiolysis is the rate-determining step.

Calculated negative enthalpy evidences that the sol-gel reaction of $\text{Ge}(\text{OPr})_4$ and H_2S is an exothermic process. Since the entropy of the reaction is low, -92.09 J/moleK , the reaction enthalpy is a driving force which promotes spontaneous change.

4.6.5 Comparison of the $\text{Ge}(\text{OEt})_4$ and $\text{Ge}(\text{OPr})_4$ chemical kinetics

It has been demonstrated for many cases that steric crowding around electrophile centres affects the rates of $\text{S}_{\text{N}}2$ reactions[118]. When large groups are located in a small space, repulsion between reaction groups becomes severe increasing the activation energy of the reaction. Thus, the energy barrier of the transition state of long chain or branched molecules is higher than that of less sterically crowded molecules. Our results confirm this principle. The thiolysis activation energy increased when germanium ethoxide was replaced with germanium isopropoxide (Tables 3.7.2 and 3.7.5)

Furthermore, the inductive effect of substituting groups and substrate changes the reaction rate constants in $\text{S}_{\text{N}}2$ reactions[31]. Bimolecular nucleophilic substitution, $\text{S}_{\text{N}}2$,

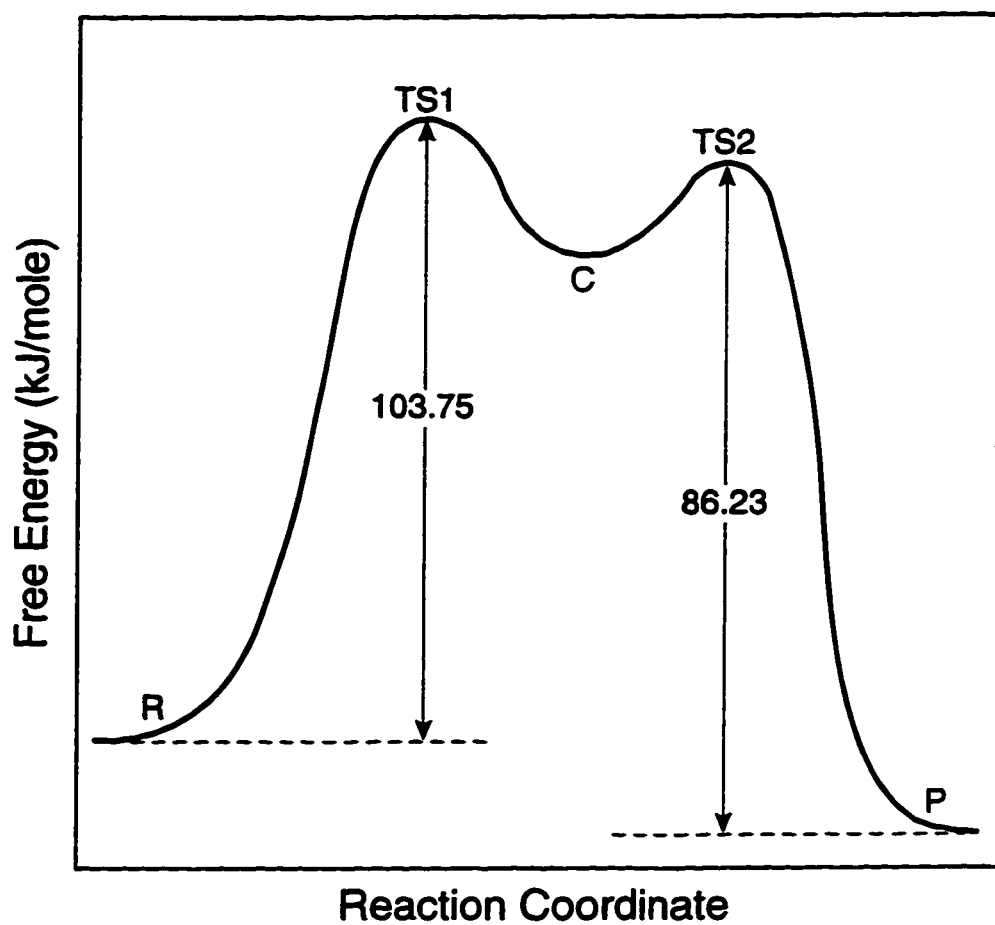
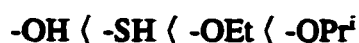


Fig. 4.6.2 Free energy-reaction coordinate diagram for the sol-gel process if $[\text{H}_2\text{S}]_0/[\text{Ge}(\text{OPr})_4]_0$ is 2.25:1.

occurs by exchange of ligands attached to the central metal atom. The bonds between metal atom and ligands are formed through electron acceptor-donor mechanism. For instance, the germanium atom has a $4s^2 4p^2$ outer shell electronic configuration. In a molecule, such as germanium alkoxide, its four electrons are placed in four sp^3 -hybrid orbitals. These orbitals are able to accept electrons from electron donors, alkoxy groups (-OR), making four σ -bonds.

Electron-donor characteristics of ligands depend on their ionization potential, proportional to z/r [120]. Thus, the increasing order of ligands in regard to their electron-donor ability is



Hence, the bigger the radius and the lower the electronegativity of the atomic group, the better the electron-donor properties of the ligand. Consequently, electrons are more loosely attached to them, causing an increase in the partial negative charge, δ^- , on the central metal atom and making the ligand more easily substituted. This provides an explanation for the increased thiolysis rate constants of $\text{Ge}(\text{OPr}^i)_4$. It is ~ 30 times higher at 30°C and ~ 20 times at 40°C than the thiolysis rate constants of $\text{Ge}(\text{OEt})_4$. Besides, the more electronegative -SH group is able to replace the more easily substituted alkoxy group. However, if there is also -OH present in solution, the alkoxide will rather be replaced with it than with -SH.

When the alkoxy group is substituted with the more electronegative -SH group, then

the partial positive charge, δ^+ , on Ge increases. Thus, during condensation, more polarizable molecules react. This is a possible cause of increased condensation rate constants in comparison to thiolysis in the sol-gel reaction with either germanium ethoxide or germanium isopropoxide. The condensation rate constants increased $\sim 10^3$ times for both precursors.

The condensation reactions of $\text{Ge}(\text{OEt})_4$ and $\text{Ge}(\text{OPr}^i)_4$ differ in two ways: in the type of reaction and the reaction rate constant. The steric effect is likely the reason for a different type of condensation reaction in the early stages of the sol-gel process. In the sol-gel process with $\text{Ge}(\text{OPr}^i)_4$, the small -SH groups attached to the Ge atom provide more accessible active sites for nucleophile attack on Ge during the H_2S forming condensation than it would be the case for the alcohol forming condensation. However, both steric and inductive effects probably have an equally important influence on the reaction rate constants. Decreased crowding in the transition state of the H_2S forming condensation and increased partial positive charge on the Ge atom, caused the condensation rate constant k_2 to be ~ 80 times higher at 30°C and ~ 60 times at 40°C than the condensation rate constant k_3 .

4.7. INFLUENCE OF REACTION PARAMETERS ON THE MICROSTRUCTURE OF THE GeS₂ GEL

4.7.1. Primary particle formation

The scanning electron micrographs reveal that all gels are colloidal xerogels regardless of the concentration of H₂S and Ge(OEt)₄, their ratio R and the reaction temperature. The smallest particles observed in the micrographs have a diameter ~0.1 μm. It is evident that the particles agglomerated.

From the specific surface areas apparent, mean particle radii were estimated from eq.(3.3.1). The particle radii range from 2 to 5.65 nm depending on the reaction conditions (Tables 3.3.1-3.3.3). There is a discrepancy among the size of particles estimated from SEM micrographs and calculated from BET surface area. It appears that 0.1 μm particles are complex particles, consisting of the smaller ones detected by BET analysis. The small particles are the primary particles and they are the building blocks for the GeS₂ gels.

The apparent radius varies with the reaction parameters, concentration, ratio and temperature. The results of the study of C and R influences on the GeS₂ gel particle size can be interpreted on the basis of La Mer's model of homogeneous nucleation of monodispersed spheres, established from classical thermodynamic theory of phase transformation, nucleation and growth[9]. According to the thermodynamic theory, the free energy barrier of nucleus formation is defined by the following equation[121]

$$\Delta G^{\circ} = \frac{16\pi\gamma_{SL}^3}{3(\Delta G_v)^2} \quad (4.7.1)$$

where γ_{SL} is the solid-liquid surface tension and ΔG_v is the volume free energy of spherical nucleus formation. The radius of the nucleus is defined by [121]

$$r^{\circ} = \frac{-2\gamma_{SL}}{\Delta G_v} \quad (4.7.2)$$

and

$$\Delta G_v = -\frac{kT}{V_m} \ln \frac{C_{min}^{nu}}{C_s} \quad (4.7.3)$$

In eq.(4.7.3) k is Boltzmann's constant, T is the temperature of nucleation and V_m is the molar volume of the nucleating species. The concentration of monomer C_{min}^{nu} is the minimum concentration required for nucleation to occur. The concentration C_s is the solubility of monomer. The ratio C_{min}^{nu}/C_s is the critical supersaturation. According to the LaMer's model, nucleation occurs when the concentration of the nucleating monomer C reaches C_{min}^{nu} . It stops when the concentration of the monomer C drops below C_{min}^{nu} . If the concentration of the monomer is within C_{min}^{nu} and C_s , the nuclei grow. When it falls below C_s , the growth of particles stops.

On the basis of La Mer's model, the formation of primary particles of GeS_2 gels

can be explained. In this case, the monomer which nucleates is $\equiv\text{GeSH}$, generated during thiolysis. It reacts by condensation reactions, forming complex molecules. If these molecules contain SH groups they are able to further react by a condensation reaction generating polymers. Once the polymers reach r^* , they become the nuclei of the GeS_2 gel primary particles. Therefore, the nuclei are formed by a condensation-polymerization reaction.

The observed induction period in the sol-gel reactions performed with ratio $R = 9$ and $R = 0.83$, can be assigned to the time lag required for the formation of $C_{\text{min}}^{\text{nu}}$ of the $\equiv\text{GeSH}$ monomer. The concentration of SH determined at the end of the induction period could be assumed to be $C_{\text{min}}^{\text{nu}}$. The nuclei grow by condensation reactions. Since thiolysis is a slower step in the sol-gel reaction and thus the rate determining, it will limit the growth of formed nuclei. Therefore, after the induction period when the critical nucleation concentration of $\equiv\text{GeSH}$ is formed, there is a continuous source of monomer. Its concentration is determined by the rate of formation $d[C]/dt$, eq.(4.6.32) and (4.6.37). The formation of $\equiv\text{GeSH}$ occurs until the reaction reaches equilibrium. When this happens, the concentration of monomer $C \leq C_s$, which stops further particle growth. Apparently, the size of the primary particles is determined by the initial concentrations of precursors. Results indicate that the particle size changed when the concentration of both H_2S and $\text{Ge}(\text{OEt})_4$ were varied and their ratio kept constant, $R = 2.5$ (Fig. 3.3.10b), as well as when the concentration of $\text{Ge}(\text{OEt})_4$ was constant and the concentration of H_2S was changed (Fig. 3.3.12b).

The influence of temperature on the primary particle size is complex. First of all,

the reaction rate constants of thiolysis and condensations are affected by temperature. Thus, if the temperature increases, the concentration of monomer $\equiv\text{GeSH}$ formed during thiolysis also increases. It is expected that the number of nuclei formed by condensation-polymerization reactions is raised due to increased condensation rate. However, the solubility C_s of monomers also increases at elevated temperature causing the supersaturation ratio $C_{\text{min}}^{\text{max}}/C_s$ to decrease and probably the nucleation rate to therefore stay approximately constant. Results of the primary particle radii of GeS_2 gels obtained at different temperatures indicate that solubility was more influenced by temperature than the nucleation rate was since larger particles were formed at higher temperatures.

Assume that the primary particles are formed of monoclinic GeS_2 unit cells packed with long range order. Since the volume of the monoclinic GeS_2 unit cell is 0.1235 (nm)^3 [85], then a spherical primary particle with 5 nm radius would contain 2×10^4 unit cells. Using the criterion that a substance has its characteristic XRD pattern with broadened lines if the crystal grains include more than 10^3 unit cells[95], it is apparent that the 5 nm primary particles of the GeS_2 gel would be crystalline. However, the XRD pattern of all GeS_2 gels were amorphous for all primary particle sizes. There are two possible reasons for the formation of amorphous structures. One is that they are formed of not completely thiolized species, such as $[\text{Ge}(\text{OEt})_{4-n}(\text{SH})_n]_m$, whose linking results in disordered structures. The other reason is that the monomer $\equiv\text{GeSH}$ reacts by condensation reactions so quickly that it has no time to align properly and make regular crystalline structures.

The formation of thermodynamically metastable primary particles can be explained

successfully using a kinetic approach to the nucleation and growth. For chemically limited nucleation and growth, as is the case of the GeS_2 gel primary particle due to slow thiolysis, the reaction limited monomer-cluster growth model can be considered[103]. This model was originally proposed by Eden[103] for the cell growth and then used for the first time in sol-gel processing by Keffer[103] for a growth model of silica colloids. This model enables one to predict the structure of the primary particles according to the reaction conditions.

The chemical kinetics results of GeS_2 synthesis by sol-gel processing performed with a concentration ratio $R = 9$ show that the alcohol producing condensation reaction is dominant. If the OEt groups are the terminal groups on the surface of the growing particle, they probably will not be prohibited sites for further particle growth. In this case, the primary particles of GeS_2 gel are homogeneous structures with a small surface roughness relative to their size (Eden model). This growth model is expected when H_2S is in excess and the fully thiolized monomers, $\text{Ge}(\text{SH})_4$, are formed (gels VIII and IX in Table 3.3.3).

Nonetheless, when the condensation reaction occurs per both alcohol and hydrogen sulfide forming reactions, such as in the reaction with $R = 0.83$, it is more likely that OEt terminal groups on the growing particles and OEt groups in partially thiolized monomers will prohibit further growth of the particles at some OEt sites by steric hindrance. As a result of prohibited growth, an inhomogeneous, rough surface on the GeS_2 gel primary particles is generated (poisoned Eden model). This growth model may occur when a shortage of H_2S generates partially thiolized monomers such as $\text{Ge}(\text{OEt})_4$.

Ge(SH)_n . Therefore, it is expected that homogeneous particles are formed if $R > 2$ and inhomogeneous if $R < 2$.

Besides growth by the monomer-cluster rate-determining mechanism, the primary GeS_2 gel particles also decrease their surface energy by aggregation. The results of aggregation are secondary particles with diameter $\sim 0.1 \mu\text{m}$ observed in SEM micrographs.

4.7.2. Aggregation-gelation

The results of SEM examination of the dried gels prepared at different concentrations of Ge(OEt)_4 and H_2S , ratios R and temperatures indicate that all gels are colloidal xerogels. The average radius of primary particles is 2-5 nm measured by BET nitrogen adsorption on the dried gels after aging of 24 h. In order to reduce the high surface energy these small particles grow and aggregate.

Since the sol-gel synthesis of GeS_2 gels was performed in toluene, an aprotic, low dielectric constant ($\epsilon_r = 2.23$) solvent, it is expected that the primary particles are neutral, forming an unstable sol. They undergo rapid aggregation as soon as they are generated due to lack of a charge. Consequently, growth and aggregation of the primary GeS_2 particles occur simultaneously, resulting in secondary particle formation. The particle radii estimated from the SEM micrographs are $\sim 50 \text{ nm}$.

The rapid aggregation is interpreted on the bases of Brownian and London-van der Waals forces[91]. The primary GeS_2 particles driven by Brownian motion diffuse and collide. When brought into close contact by collision, van der Waals attraction forces keep them

together. At their interface they probably attach via formation of $\equiv\text{Ge-S-Ge}\equiv$ bonds by condensation of terminal SH groups with either SH or OEt groups located on the particle surface. At the particle contact, a curvature with a negative radius is formed. Since thiolysis is slow, monomers are continuously formed during the sol-gel process. They first deposit at the contact point which is a high tension area[104] and react by the condensation reaction with terminal SH or OEt groups. Thus, once the primary particles are linked, their individual growth stops and the growth of necks continues. The primary particles connected in this way form a micropore network within the secondary particles.

The percentage of the gel micropore volume given in Table 3.3.1-3.3.3 indicates that the secondary particles are dense structures. For concentrations used and temperatures considered, the microporosity decreases if both parameters, C and T, increase. These results indicate neck formation whose growth may densify the secondary particles. Increased concentrations of precursors and reaction temperature raise the concentration of monomers resulting in faster growth rate of the necks. Moreover, growth of secondary particles by the monomer-cluster reaction-limited aggregation model can also produce dense structures. In this case, the primary particles are the monomers[31].

It can be expected that the secondary particles aggregate in the same way as the primary ones. Therefore, the proposed mechanism for the contact, linking and neck formation of the primary particles can be also proposed for the secondary ones. The secondary particles can be considered as microgel spheres since they consist of connected colloidal primary particles in a 3-dimensional solid network within the liquid. Since they

also have high surface energy and no charge, they rapidly aggregate forming the GeS₂ gel within toluene. Rapid aggregation probably caused open random packing of the secondary particles resulting in formation of highly porous gels. The results shown in Tables 3.3.1-3.3.3 evidence that the mesopores, formed by linking of secondary particles, are the main contributors to the gel porous structure. The pore distribution indicates that the secondary particles have a wide range of distribution and that they are irregularly packed.

According to Smoluchowski's equation[91], the reaction rate of uncharged particles, dN/dt , is proportional to their initial concentration, N_0 , that is

$$dN/dt = -k_r N_0^2 \quad (4.7.4)$$

where k_r is a second order rate constant for rapid aggregation. This equation is limited to the onset of aggregation where the only particles present are N_0 , uniform spheres.

The plot of gelation time vs. the Ge(OEt)₄ concentration shown in Fig. 3.3.4 is in agreement with this equation. From the graph it is obvious that, in dilute solution, gelation is slow although the particles are not charged. However, all samples with the same concentration gelled at similar times regardless of temperature.

During the sol-gel process the Tyndall effect appeared (Fig. 3.3.1a). This is indicative of aggregate formation, size ≤ 300 nm. As aggregation-gelation proceeded further, the solution developed a milky appearance indicating aggregate growth. Depending on the initial concentration of Ge(OEt)₄, these aggregates formed gels with

different appearance. For concentrations >0.044 M, aggregates connected into gel completely and included toluene within the network (Fig. 3.3.1c). However, when the concentration of $\text{Ge}(\text{OEt})_4$ was reduced to ≤ 0.044 M the aggregates first precipitated and then gelled. Moreover, for a low concentration ratio, $R = 0.7$, and low $\text{Ge}(\text{OEt})_4$ and H_2S concentrations, a semi-transparent gel was prepared as shown in Fig. 3.3.3a. In this case the aggregates also first precipitated and then gelled. Apparently, during rapid aggregation in more concentrated solutions, the aggregates made of secondary particles are more dense structures than those formed in dilute solutions. Results demonstrated that gels prepared from higher $\text{Ge}(\text{OEt})_4$ concentrations (gels obtained at different temperatures and gels IA, VII and IX) have similar macropore volume, indicating that they were formed by dense agglomerate linking. Therefore, there must be some critical concentration of aggregates causing gelation without precipitation. However, if their concentration is low, then the aggregates can be brought within a short distance by precipitation, where they are able to make links and thus to gel. Therefore, it can be suggested that gelation in this sol-gel system occurs per a reaction limited cluster-cluster aggregation mechanism.

4.7.3. Aging

The BET analysis results of gel IA, aged 24 h and 30 days at room temperature, are shown in Table 3.3.2. It is apparent that the surface area and pore volume decreased during aging. The average particle radius increased (from 2.88 to 17.00 nm) as well the pore radius (from 8.68 to 30.58 nm). Aging altered the pore volume distribution. Thus,

the macropore volume increased, whereas the meso and micropore volume decreased.

One of the possible explanations for these drastic changes in the microstructure of gel IA is continuation of the chemical reactions, thiolysis and condensation, during which the particles and contacts continue to grow. Since thiolysis is a very slow reaction, it is expected that chemical equilibrium is achieved slowly. The equilibrium is represented by the overall reaction



When equilibrium is reached, then probably Ostwald ripening begins. This process is the second possible reason causing changes in the microstructure of the GeS₂ gels during aging. This is a process in which small primary particles tend to decrease their surface area by dissolving and reprecipitating on the larger particles and their contacts. It is expected that, as a result of this dissolution-reprecipitation process, the number of initially present particles decreases and the average particle size increases. Consequently, the average pore size will also increase.

It could be suggested that dissolution-reprecipitation of the GeS₂ primary particles occurs by the equilibrium reaction represented in eq.(4.7.5). The results of the BET analysis of the aged gel IA confirm these expectations based on the Ostwald ripening (Table 3.3.2). Since growth of the necks occurred, this probably caused a decrease in the micro and mesopore volumes. The micrograph, Fig. 3.3.6e, demonstrates coarse, irregular, sintered globules. The XRD analysis showed that the gel was still amorphous

even after aging for 30 days.

Such change in the microstructure mostly caused by Ostwald ripening evidences that rapid agglomeration of the primary particles occurred resulting in a broad size distribution in comparison to the average calculated value. Therefore, Ostwald ripening is an important process controlling microstructure development in gels formed by rapid aggregation.

4.7.4. Drying

Drying of the prepared gels was carried out in a vacuum oven at room temperature. In cases when gel precipitated, the liquid above it was first poured off and then it was placed in the oven. During drying, enormous shrinkage was observed. For instance, from gel IA, whose initial volume was 50 mL (Fig. 3.3.1a), the dried pieces occupied only ~2 mL.

There are huge structural changes associated with gel shrinkage during drying, explained by capillary pressure that brings non-reacted terminal groups together and allows further condensation to proceed. As liquid evaporates from the gel surface, the gel network becomes exposed to the vapour. A solid-vapour interface appears at the place where a solid-liquid interface had been before. This raises the energy of the system, because $\gamma_{sv} > \gamma_{sl}$, so liquid tends to flow from the interior of the gel to cover the exposed solid. As it stretches toward the exterior, the liquid goes into tension. This has two consequences. One is that the liquid flows from the interior along the pressure gradient, while the other is that the tension is balanced by compressive stress in the

network that causes shrinkage. The rising capillary pressure forces the particles to rearrange into closer packing. It is initially easy due to the weak structure of the network. As shrinkage proceeds, the particles become too crowded to rearrange further and shrinkage stops. The tension in the liquid in the pores reaches a maximum when shrinkage stops and further evaporation of liquid drives the meniscus into the body. Cracking of the gels begins at that moment. If the pressure in the liquid was uniform, the network would be uniformly compressed and there would be no tendency to crack. However, the low permeability of the gel gives rise to a pressure gradient, meaning the tension in the liquid is greater near the drying surface. This produces differential strain leading to cracking.

All prepared GeS_2 gels cracked during drying regardless of reaction conditions C, T and R. This is a consequence of the wide pore size distribution in the gels. Fig 3.3.3a represents a gel monolith in equilibrium with the vapour, before cracking started. The capillary forces caused this gel to crack (Fig. 3.3.3b). Additional cracking of this gel is restrained by the contact of the gel with the flask walls. When drying was completed, yellowish pieces of the GeS_2 gel were obtained (Fig. 3.3.3c). Gels prepared from $\text{Ge}(\text{OEt})_4$ with concentrations ≤ 0.044 M and $R = 2.5$, had common drying characteristics. The gel pieces formed after drying had the appearance as shown in Fig. 3.3.5. This structure is a reminiscent of the crystal growth around a screw dislocation.

Since during drying particles rearrange and assemble to a structure with higher coordination number, it is expected that gels have even more open structures before drying[9,31].

CHAPTER 5

CONCLUSIONS

5.1. SUMMARY

It has been shown that metal alkoxides, germanium ethoxide, germanium propoxide, zinc tert-butoxide, tungsten ethoxide and tungsten dichloride ethoxide react spontaneously with hydrogen sulfide in toluene at room temperature. Tungsten ethoxides $W(OEt)_6$ and $WCl_2(OEt)_3$ yield products with different morphology and stoichiometry: a gel $WS_{2.7}$ and a powder $WS_{1.4}$. The prepared powder and gel have amorphous structures. The reaction of zinc tert-butoxide, $Zn(OBu^t)_2$ and H_2S in toluene exhibits solution/geleation behaviour. At the $Zn(OBu^t)_2$ concentration of 0.024 M, a semi-transparent yellow colloidal gel is formed. Energy dispersive spectrometry (EDS) shows that the dried gel has a Zn/S atomic ratio $\approx 1:1$. Germanium ethoxide and hydrogen sulfide produce GeS_x gels of different appearance: white coarse grain to semi-transparent white monolith. The appearance of the gels depends on the reactant concentrations. The semi-transparent GeS_x gel is prepared from 0.029 M of $Ge(OEt)_4$ and 0.019 M H_2S whereas the white smooth gel is synthesised from 0.220 M of $Ge(OEt)_4$ and 0.550 of H_2S .

The thin films prepared from GeS_2 and ZnS colloidal suspensions by dip process are smooth, transparent and well adhered to the substrate. The microstructure of the thin films is similar to that of the corresponding bulk gel.

The effective preparation of metal sulfide relies on preventing metal alkoxide hydrolysis by drying precursors and by maintaining a dry atmosphere during the reaction. Hence, germanium ethoxide and dried hydrogen sulfide yield GeS_2 with oxygen content <0.17 wt% if the GeS_x gel is heat treated. However, the sol-gel reaction of germanium ethoxide and non-dried hydrogen sulfide produces a mixture of GeO_x and GeS_x gels. The efficient preparation of GeS_2 from the resulting gel mixture is possible by conversion of produced GeO_2 with sulfur. Oxidation of H_2S by oxygen from the air in the presence of concentrated sulfuric acid ($\text{pH} \approx -2$) yields elemental sulfur and water. Both products are introduced into a toluene solution of germanium ethoxide by the H_2S gas and homogeneously distributed in it. The heat treatment product has two types of bonds Ge-S-Ge and Ge-S-S-Ge . Therefore the complete consolidation of GeS_x gel and reduction of GeO_x gel with sulfur occurs by heat treatment at 630°C .

Complete consolidation of GeS_x gel into GeS_2 occurs during heat treatment at 630°C . In the presence of OH and O groups, amorphous GeS_2 consolidates by viscous sintering. However, in their absence, it transforms into monoclinic GeS_2 by homogeneous nucleation and sinters via a diffusion mechanism.

The chemical kinetics study of the sol-gel processing of GeS_2 from either $\text{Ge}(\text{OEt})_4$ or $\text{Ge}(\text{OPr}^i)_4$ and H_2S in toluene solution confirms that the reaction occurs in three suggested steps: thiolysis, the hydrogen sulfide forming condensation and the alcohol forming

condensation. The intermediate germanium mercaptide formed during thiolysis is a stable product identified in the dry gel. The reaction conditions, concentration of reactants, their ratio and type of the alkoxide, enable the simplification of the proposed mechanism. The reaction occurs by three suggested steps when the molar ratio of H_2S and $\text{Ge}(\text{OEt})_4$ is 1:1.2. However, for the ratio 9:1 it simplifies to thiolysis and the alcohol forming condensation. Moreover, when germanium ethoxide is substituted with germanium isopropoxide, the sol-gel reaction occurs by thiolysis and the H_2S forming condensation.

Regardless the reaction conditions, thiolysis is a slow step and condensations are fast. If $\text{Ge}(\text{OEt})_4$ is a precursor, the thiolysis rate increases ~ 2 times when the concentration changes from 0.044 M to 0.264 M. The reaction rates of thiolysis and condensation drastically increase when germanium ethoxide is substituted with germanium isopropoxide.

The study of the temperature effect on the reaction rate constants shows that their behaviour is in good agreement with Arrhenius law and the transition-state theory in the observed temperature range ($25^\circ - 50^\circ\text{C}$). The thiolysis activation energies obtained for two different concentrations of $\text{Ge}(\text{OEt})_4$ are similar indicating rupture and formation of the same bonds. However, the higher activation energy of the $\text{Ge}(\text{OPr}^i)_4$ thiolysis indicates that more stable bonds are broken and formed.

The negative entropy, indicative of association of two molecules in the transition state, confirms that thiolysis and condensations occurs by $\text{S}_{\text{N}}2$ mechanism. Moreover, the second order reaction obtained for thiolysis and condensations regardless of the conditions is in agreement with this data.

Calculated standard activation free energies ΔG^\ddagger demonstrate that the rate-determining step is thiolysis in the sol-gel processing of GeS_2 from either alkoxide. The same conclusion is reached from the experimentally determined reaction rate constants.

Based on scanning electron microscopy and BET analysis results, it could be suggested that all GeS_2 dried gels are colloidal xerogels, having approximately the same hierarchical pore morphology made up of two sizes of particles, primary and secondary.

The primary particles are condensed structures. They nucleate and grow per the classical LaMer's model. The decrease in their surface areas occurs simultaneously by growth and aggregation. Since the particles are formed in a neutral solution, aggregation is rapid. As the result of rapid aggregation, secondary particles are formed. Concentration of $\text{Ge}(\text{OEt})_4$ and H_2S and reaction temperature influence the primary particle size. For formation of both primary and secondary particles, the monomer-cluster reaction-limited aggregation model can be invoked since they are compact structures as seen from low microporosity. The concentrations of precursors and their ratio affect the manner of packing of the primary and the secondary particles during aggregation. The secondary particles also decrease their surface areas by rapid aggregation. These aggregates are formed within domains and their connection into a solid 3-D network cause gelation. For $\text{Ge}(\text{OEt})_4$ concentrations > 0.044 M the gel includes the entire liquid within it. However, for the lower concentrations the gel is formed during aggregate precipitation. Therefore, for gelation, the cluster-cluster reaction-limited mechanism can be proposed. The gelation time is affected by the concentration of reactants. However it is not influenced by temperature in the examined range.

Potentiometric titration is a suitable method for the quantitative determination of germanium sulfide and germanium mercaptide formed during sol-gel processing of GeS_2 before gelation. It is accurate and reproducible. Although the accuracy is satisfactory, it could be improved only by choice of more precise equipment for measuring samples and adding the titrant. The error caused by interference of the ions during precipitation can be neglected due to the high selectivity coefficient.

Results obtained for the detection limits are in excellent agreement with the literature. When the electrode responds to the free GeS^- or Ag^+ ion, the detection limit is controlled by Ag^+ defects in the electrode membrane surface. However, if the electrode responds to the free S^{2-} ions, the detection limit is equivalent to the solubility of Ag_2S from the membrane. A corrected equation $E=f[\log(C_s, C_{SH})]$ is in a good agreement with the experimentally obtained results.

5.2. CONCLUSIONS

The following conclusions can be drawn from the results discussed in Chapter 4:

- Tungsten ethoxide yields a gel $\text{WS}_{2.7}$ when it reacts with hydrogen sulfide in toluene at room temperature.
- Reaction of tungsten dichloride ethoxide and hydrogen sulfide in toluene yields a powder $\text{WS}_{1.7}$.
- Semi-transparent yellow colloidal ZnS gel is prepared from zinc tert-butoxide and H_2S

at room temperature if the concentration of the alkoxide is 0.024 M.

- Semi-transparent GeS_x gel is prepared from 0.029 M of germanium ethoxide and 0.019 M hydrogen sulfide in toluene at room temperature.
- The thin film prepared from GeS_2 and ZnS colloidal suspensions by dip process are uniform, transparent and well adhered to the substrate.
- The effective preparation of metal sulfide relies on preventing metal alkoxide hydrolysis by drying precursors and by maintaining a dry atmosphere during the reaction.
- It is possible to prepare pure monoclinic GeS_2 from a mixture of GeO_x - GeS_x gel by conversion of formed GeO_x with sulfur at 630°C .
- The chemical reaction of germanium ethoxide and hydrogen sulfide simplifies to thiolysis and the alcohol forming condensation when the ratio $[\text{H}_2\text{S}]/[\text{Ge}(\text{OEt})_4]$ is 9:1.
- The sol-gel reaction of germanium isopropoxide and hydrogen sulfide occurs by thiolysis and the hydrogen sulfide forming condensation if $[\text{H}_2\text{S}]/[\text{Ge}(\text{OPr}^i)_4]$ is 2.25:1.
- Regardless the reaction conditions, thiolysis is a slow step and condensations are fast in toluene.
- The negative activation entropy confirms that thiolysis and condensations occur by an $\text{S}_\text{N}2$ mechanism.
- All GeS_x dried gels are colloidal xerogels, made of primary and secondary particles.
- The concentration of precursors and reaction temperature influence the size of the GeS_2 primary particles.
- Primary and secondary particles of GeS_2 gel decrease the surface area by rapid aggregation in toluene.

- Gelation time of GeS_2 gel is affected by concentration of precursors and not by temperature in the range examined.
- Potentiometric titration is a suitable method for the quantitative determination of germanium sulfide and germanium mercaptide.
- Selectivity coefficient calculated from the solubility products determined from the plots $E = f[\log(C_p)]$ is in an excellent agreement with the coefficient determined by a method suggested in literature.
- A corrected equation $E = f[\log(C_s, C_{SH})]$ is in a good agreement with the experimentally obtained results.

5.3. FUTURE WORK

This work on sol-gel processing of metal sulfides can be continued on the following way:

- Synthesis of ZrS_2 and SrTiS_2 from $\text{Zr}[\text{O}(\text{CH}_2)\text{CH}_3]_4$ and $\text{SrTi}(\text{OC}_3\text{H}_7)_4$ at different reaction conditions (concentrations of alkoxides and reaction temperature).
- Processing of the thin films using metal alkoxides and hydrogen sulfide.
- The study of influence of the polar solvents on the thiolysis and condensation rate constants.
- The examination of the isothermal and non-isothermal heat treatment of metal sulfides prepared by this method.

- **Determination of physical, chemical, electrical and optical properties of metal sulfides prepared by sol-gel processing.**

REFERENCES

1. K.D. Moller, *Optics* (University Science Books, Mill Valley, 1988).
2. S. Musicant, *Optical Materials* (Marcel Dekker Inc, New York, 1985).
3. S.S. Savage, *J.Non-Cryst.Solids* **47** (1982) 101.
4. F.J. Clauss, *Solid Lubricants and Self-lubricating Solids* (Academic Press, New York, 1972).
5. A. Ennaoui, S. Fiechter, W. Jaegermann, H. Tributch, *J.Electrochem.Soc.* **133** (1986) 97.
6. J.J. Auburn, Y.L. Barberio, K.J. Hansen, D.M. Schleich, M.J. Martin, *J. Electrochem.Soc.* **134** (1987) 580.
7. S. Gobolos, Q. Wu, F. Delannay, P. Grange, B. Delmon, *Polyhedron* **5** (1986) 219.
8. C. Kaito, Y. Saito, K. Fujita, *J.Cryst.Growth* **94** (1989) 967.
9. A.C. Pierre, *Introduction to Sol-gel Processing* (Septima, Paris, 1992).
10. E. Matijević, D.M. Wilhelmy, *J.Colloid.Interface Sci.* **86** (1982) 4762.
11. P.J. Melling, *Amer.Ceram.Soc.Bull.* **63** (1984) 1427.
12. A.B. Seddon, S.N.B. Hodgson, *J.Amer.Ceram.Soc.* **26** (1991) 2599.
13. C.E. Johnson, D.K. Hickey, D.C. Harris, *Mat.Res.Soc.Sympo.Proc.* **73** (1986) 785.
14. P.N. Kumta, S.H. Risbud in *Ultrastructure Processing of Advanced Materials*, edited by D.R.Uhlmann and D.R.Ulrich, 1992, John Wiley & Sons, Inc., p.555.

15. M.A. Sriram, P.N. Kumta, *J.Amer.Ceram.Soc.* **77** (1994) 1381.
16. R. Williams, P.N. Yocom, F.S. Stofco, *J.Colloid.Interface Sci.* **106** (1985) 388.
17. B.M. Sinelnikov, A.R. Farakhmand, N.I. Karagin, *Neorg.Mater.* **29** (1993) 1367.
18. A. Celikkaya, M. Akinc, *J.Amer.Ceram.Soc.* **73** (1990) 245.
19. D.M. Wilhelmy, E. Matijević, *J.Chem.Soc., Faraday Trans.1* **80** (1984) 563.
20. A.E. Gorstein, N.Yu. Baron, N.Ya. Dubrovskaya, V.F. Chuprik, USSR SU 1,574,538 30 June 1990.
21. C.L. Czekaj, PhD thesis, Pennsylvania State University (1987).
22. C.L. Czekaj, M.S. Rau, G.L. Geoffroy, T.A. Guiton, C.G. Pantano, *Inorg. Chem.* **27** (1988) 3263.
23. T.A. Guiton, C.L. Czekaj, M.S. Rau, G.L. Geoffroy and C.G. Pantano in *Better Ceramics through Chemistry III*, Vol. 121 (Materials Research Society, Pittsburgh, PA, 1988) 503.
24. C.E. Johnson, D.C. Harris, C.B. Willingham, *Chem.Mater.* **2** (1990) 141.
25. C.E. Johnson, D.K. Hickey and D.C. Harris, in *Proceedings SPIE Infrared and Optical Transmitting Materials* **683** (1986) 112.
26. D.C. Bradley, R.C. Mehrotra, D.P. Gaur, *Metal Alkoxides* (Academic Press, New York, 1978).
27. V. Stanić, A.C. Pierre, T.H. Etsell, R.J. Mikula, *J.Mater.Res.* **11** (1996) 363.
28. V. Stanić, A.C. Pierre, T.H. Etsell, R.J. Mikula, *J.Non-Cryst.Solids*, accepted.

29. V. Stanić, A.C. Pierre, T.H. Etsell, R.J. Mikula, *Mater. Letters*, accepted.
30. V. Stanić, T.H. Etsell, A.C. Pierre, R.J. Mikula, *J.Mater.Chem.* **7** (1997) 105.
31. C.J. Brinker, G.W. Scherer, *Sol-gel Science* (Academic Press, San Diego, 1990).
32. W. Stöber, A. Fink, E. Bohn, *J.Colloid.Interface Sci.* **26** (1968) 62.
33. C.G. Tan, B.D. Bowen, N. Epstein, *J.Colloid.Interface Sci.* **118** (1987) 290.
34. B.Fegley Jr., E.A. Barringer in *Better Ceramics through Chemistry*, edited by C.J. Brinker, D.E. Clark and D.R. Ulrich (Elsevier Publishing Company, Inc., New York, 1984) 187.
35. B. Fegley Jr., D. White, H.K. Bowen, *Amer.Ceram.Soc.Bull.* **64** (1985) 1115.
36. T.Ogihara, T. Ikemoto, N. Mazutani, M. Kato, Y. Mitari, *J.Mater.Sci.* **21** (1986) 2771.
37. B.E. Yoldas, *Amer.Ceram.Soc.Bull.* **54** (1975) 286.
38. B.E. Yoldas, *J.Mater.Sci.* **10** (1975) 1856.
39. L-Y. Chane-Ching, L.C. Klein, *J.Amer.Ceram.Soc.* **71** (1988) 83.
40. L-Y. Chane-Ching, L.C. Klein, *J.Amer.Ceram.Soc.* **71** (1988) 86.
41. B.E. Yoldas, *J.Mater.Sci.* **21** (1986) 1080.
42. S. Komareni, R. Roy, E. Breval, *J.Amer.Ceram.Soc.* **68** (1985) 1041.
43. O. Yamaguchi, D. Tomihisa, H. Kawabata, K. Shimizu, *J.Amer.Ceram.Soc.* **70** (1987) 194.
44. M. Nogami, Y. Morija, *J.Non-Cryst.Solids* **48** (1982) 47.
45. C.J. Brinker, K.D. Keefer, D.W. Schaefer, C.S. Ashley, *J.Non-Cryst.Solids* **48**

- (1982) 47.
46. L.C. Klein, G.J. Garvey in *Better Ceramics through Chemistry*, edited by C.J. Brinker, D.E. Clark, D.R. Ulrich (Elsevier Science Publishing Company, Inc., New York, 1984) 33.
 47. W.G. Fahrenholtz, D.M. Smith, in *Better Ceramics through Chemistry*, edited by M.J. Hampden-Smith, W.G. Klemperer and C.J. Brinker (Materials Research Society, Pittsburgh, PA, 1992) 705.
 48. V. Stanić, A.C. Pierre, T.H. Etsell, R.J. Mikula, *J.Amer.Ceram.Soc.*, submitted.
 49. V. Stanić, A.C. Pierre, T.H. Etsell, R.J. Mikula, *J.Mater.Sci.*, submitted.
 50. V. Stanić, A.C. Pierre, T.H. Etsell, R.J. Mikula, *Chem.Mater.*, submitted.
 51. V. Strelko, *Kolloidn.Zh.* 32 (1970) 430.
 52. K.J. McNeil, J.A. DiCaprio, D.A. Walsh, R.F. Pratt, *J.Amer.Chem.Soc.* 102 (1980) 1859.
 53. R.A. Assink, B.D. Kay in *Better Ceramics through Chemistry*, edited by C.J. Brinker, D.E. Clark and D.R. Ulrich (Elsevier Science, Amsterdam, 1984) p.301.
 54. R.A. Assink, B.D. Kay, *J.Non-Cryst.Solids* 99 (1988) 359.
 55. R.A. Assink, B.D. Kay, *J.Non-Cryst.Solids* 104 (1988) 112.
 56. R.A. Assink, B.D. Kay, *J.Non-Cryst.Solids* 107 (1988) 35.
 57. D.H. Doughty, R.A. Assink, B.D. Kay in *Silicon-based Polymer Science*, edited by J.M. Zeigler and F.W. Fearon (American Chemical Society,

- Washington, DC, 1990) p.241.
58. J.C. Pouxviel, J.P. Boilot, J.C. Beloeil, J.Y. Lallemand, *J.Non-Cryst.Solids* 89 (1987) 345.
 59. J.C. Pouxviel, J.P. Boilot, *J.Non-Cryst.Solids* 94 (1987) 374.
 60. I. Artaki, S. Sinha, A.D. Irwin, J. Jonas, *J.Non-Cryst.Solids* 72 (1985) 391.
 61. J.C. Ro, I.J. Chung, *J.Non-Cryst.Solids* 110 (1989) 26.
 62. A.A. Kline, M.E. Mullins, B.C. Cornilsen, *J.Am.Ceram.Soc.* 74 (1991) 2559.
 63. A.A. Kline, T.N. Rogers, M.E. Mullins, B.C. Cornilsen, Lj.M. Sokolov, *J.Sol-Gel Sci. Technol.* 2 (1994) 269.
 64. J. Sanchez, R. Mary, A. McCormick in *Better Ceramics through Chemistry*, edited by B.J. Zelinski, J.C. Brinker, D.E. Clark and D.R. Ulrich (Mater.Res. Soc.Proc. 180, Pittsburgh, PA 1990) p.263.
 65. J. Liu, S.D. Kim, *J. Polym.Sci., Part B: Polym.Phys.* 34 (1996) 131.
 66. V. Satnić, A.C. Pierre, T.H. Etsell, R.J. Mikula, *J.Electroanal.Chem.*, submitted.
 67. J. Papp, *Cellul.Chem.Technol.* 5 (1971) 147.
 68. S.T. Chiu, L. Paszner, *Anal.Chem.* 47 (1975) 1910.
 69. H. Satake, T. Hisano, S. Ikeda, *Bull.Chem.Soc.Jpn.* 54 (1981) 1968.
 70. G.M. Dorris, V.C. Uloth, *J.Pulp Pap.Sci.* 20 (1994) 242.
 71. M.K. Papay, K. Toth, E. Pungor in *Ion-Selective Electrodes*, edited by E.Pungor (Akad.Kiado, Budapest, 1973) p.225.
 72. M.T. Neshkova, V.P. Izvekov, M.K. Papay, K. Toth, E. Pngor, *Anal.Chem.*

Acta **75** (1975) 439.

73. P. D'Orazio, G.A. Rechnitz, *Anal.Chem.* **49** (1977) 41.
74. S. Pinzauti, G. Papeschi, E. La Porta, *J.Pharm.Biomed.Anal.* **1** (1983) 47.
75. L.C. Gruen, B.S. Harrap, *Anal.Biochem.* **42** (1971) 377.
76. F. Peter, R. Rosset, *Anal.Chim.Acta.* **64** (1973) 397.
77. W. Selig, *Microchim.Acta* [Wien] (1973) 453.
78. P.K.C. Tseng, W.F. Gutknecht, *Anal.Chem.* **47** (1975) 2316.
79. S.W. Bateson, G.J. Moody, J.D.R. Thoomas, *Analyst* **111** (1986) 3.
80. D.L. Ehman, *Anal.Chem.* **48** (1976) 918.
81. H. Ledo di Medina, G. Gonzalez, J. Duran, *Anal.Lett.* **27** (1994) 625.
82. IP Method 272/71 (85), "Mercaptan sulphur and hydrogen sulphide content of liquified petroleum gases - electrometric titration method", in *Methods for Analysis and Testing* (Institute of Petroleum, London, 1985) p.272.1.
83. IP Method 342/79 (85), "Mercaptan sulphur in gasoline, kerosine, aviation turbine and distillate fuels - potentiometric method", in *Methods for Analysis and Testing* (Institute of Petroleum, London, 1985) p.342.1.
84. JCPDS Powder Diffraction File, Card 36-1463.
85. JCPDS Powder Diffraction File, Card 27-238.
86. S.P. Mukerjee, S.K. Sharme, *J.Amer.Ceram.Soc.* **69** (1986) 806.
87. Y. Kawamoto, C.Kawashima, *Mat.Res.Bull.* **17** (1982) 1511.
88. J.Poucher, *The Aldrich Library of IR Spectra* (Aldrich Chemical Co., 1981) 3rd ed.

89. J.H. de BOER, *The Structure and Properties of Porous Materials*, (Butterworths, London, 1958) pp.68.
90. JCPDS Powder Diffraction File, Card 8-247.
91. P.C. Heimenz, *Principles of Colloidal and Surface Chemistry* (Marcel Dekker, New York, 1986) 2nd ed.
92. S.J. Gregg, K.S.W. Sing, *Adsorption, Surface Area and Porosity* (Academic Press, New York, 1967).
93. S. Lowell, J.E. Shields, *Powder Surface Area and Porosity*, (Chapman & Hall, New York, 1991) 3rd ed.
94. JCPDS Powder Diffraction File, Card 05-0492(1986).
95. H.P. Klung and L.E. Alexander, *X-ray Diffraction Procedures for Polycrystalline and Amorphous Materials* (John Wiley & Sons, New York, 1974) pp. 687.
96. F.F. Bentley, L.D. Smithson, A.L. Rozek, *Infrared Spectra and Characteristic Frequencies 700-300 cm⁻¹* (John Wiley & Sons Inc., New York, 1968) p.367.
97. R.A. Nyquist, R.O. Kagel, *Infrared Spectra of Inorganic Compounds* (Academic Press Inc., New York, 1987) p.321.
98. K.S.W. Sing, *Pure Appl.Chem.* **54** (1982) 2201.
99. I.M. Kolthoff, E.B. Sandell, *Textbook of Quantitative Inorganic Analysis* (The Macmillan Comp., New York, 1952) 3rd ed.
100. W.E. Morf, G. Kahr, W. Simon, *Anal.Chem.* **46** (1974) 1538.
101. J. Veselý, D. Weiss, K. Stulík, *Analysis with Ion-selective Electrodes*, (Ellis

- Horwood Ltd. Publishers, Chichester, 1978).
102. J.H. Espenson, *Chemical Kinetics and Reaction Mechanisms*, (McGraw-Hill Book Company, USA, 1981).
 103. K.D. Keffer in *Better Ceramics through Chemistry*, edited by C.J. Brinker, D.E. Clark and D.R. Ulrich (Mater.Res.Soc., Pittsburg, 1986) p.295.
 104. R.K. Iler, *The Chemistry of Silica* (Wiley, New York, 1979).
 105. J. Zarzycki, *J.Non.Cryst.Solids* **48** (1982) 105.
 106. D.R. Uhlmann, *J.Non.Cryst.Solids* **7** (1972) 337.
 107. D.Hadzi, in *Manual Devices for Infrared Spectroscopy and Molecular Structure* (Elsevier Publishing Company, Amsterdam, 1963) pp.261.
 108. E. Matijević, *Chem.Mater.* **5** (1993) 412.
 109. I.M. Kolthoff, N.H. Furman, *Potentiometric Titration* (John Wiley & Sons, Inc., New York, 1926).
 110. P.W. Carr, *Anal.Chem.* **43** (1971) 425.
 111. A.K. Covington, T. Dickinson, *Physical Chemistry of Organic Solvent Systems* (Plenum Press, London, 1973).
 112. D.A. Skoog, D.M. West, *Fundamentals of Analytical Chemistry* (Holt, Rinehart and Winston, New York, 1976) 3rd. ed.
 113. M. Susić, *Electrochemistry* (Naucna knjiga, Beograd, 1970) pp.163.
 114. Orion Research Booklet for the Ag/Ag₂S ion selective electrode.
 115. R.M. Noyes in *Investigation of Rates and Mechanisms of Reactions*, edited by E.S. Lewis (John Wiley & Sons, New York, 1974) 3rd.ed., pp. 489.

116. J.F. Bunnett in *Investigation of Rates and Mechanisms of Reactions*, edited by E.S. Lewis (John Wiley & Sons, New York, 1974) 3rd. ed., pp. 129.
117. K.J. Laidler, *Chemical Kinetics* (McGraw-Hill Book Company, USA, 1965) 2nd ed.
118. S. Veljković, *Chemical Kinetics* (Gradjevinska knjiga, Beograd, 1969).
119. C.H. Langford, H.B. Gray, *Ligand Substitution Process* (W.A. Benjamin Inc., New York, 1966).
120. I. Filipović, S. Lipanović, *General and Inorganic Chemistry*, (Skolska knjiga, Zagreb, 1973).
121. W.D. Kingery, H.K. Bowen, D.R. Uhlmann, *Introduction to Ceramics* (John Wiley & Sons, New York, 1991) 2nd ed.

APPENDIX I

Table A1: Concentration of H₂S and Ge(OEt)₄, the concentration ratio R and reaction temperatures used for study of their influence on the microstructure of GeS₂ gels. Corresponding gelation times are also shown along with these data.

GEL	[H ₂ S] (M)	[Ge(OEt) ₄] (M)	R	t _{gelation}
IA	0.550	0.220	2.5	3 hours
III	0.110	0.044	"	12 hours
IV	0.073	0.029	"	2 days
V	0.055	0.022	"	5 days
VI	0.019	0.029	0.66	6 months
XI	0.027	"	0.93	--
VII	0.038	"	1.32	2 weeks
IV	0.073	"	2.50	2 days
VIII	0.146	"	5.00	3 days
IX	0.293	"	10.00	3 days
30°C	0.220	0.264	0.83	12 hours
40°C	"	"	"	11 hours
45°C	"	"	"	10 hours
50°C	"	"	"	11 hours

Table A2: The concentrations of sulfide (M) and mercaptide (C) evolved in the sol-gel reaction, when $[\text{H}_2\text{S}]/[\text{Ge}(\text{OEt})_4]$ is 9:1. The concentrations are in 10^{-3} M.

t(h)	30°C		40°C		45°C		50°C	
	[M]	[C]	[M]	[C]	[M]	[C]	[M]	[C]
1	0	0.20	0	3.0	0.04	0.49	0.10	0.74
2	0	0.40	0.05	0.50	0.08	0.60	0.28	1.05
3	0	0.70	0.08	0.15	0.81	0.15	0.60	1.21
4	0.07	0.71	0.12	0.98	0.20	1.11	0.96	1.24
5	0.11	0.75	0.18	1.15	0.30	1.21	1.52	1.29
6	0.15	0.83	0.26	1.25	0.66	1.31	2.32	1.41
7	0.30	0.88	0.51	1.43	0.83	1.62	3.33	2.73
8	0.45	0.96	0.84	1.81	1.49	2.22	5.20	4.04
9	0.51	1.31	1.23	2.10	2.85	4.55	8.10	6.08
10	0.73	1.82	1.80	2.42	4.55	5.55	11.10	8.08
11	0.89	2.02	2.50	3.10	6.56	7.07	17.20	12.14
12	1.07	2.32	3.70	4.80	11.62	8.58	29.30	14.14
13	1.32	3.04	4.85	6.90	19.19	13.13	---	---
13.5	1.77	3.54	--	--	--	--	--	--

Table A3: The concentrations of mercaptide (C) and sulfide (M) evolved in the sol-gel reaction, when $[H_2S]/[Ge(OEt)_4]$ is 1:1.2. The concentrations are in 10^{-3} M.

t(h)	30°C		40°C		45°C		50°C	
	[M]	[C]	[M]	[C]	[M]	[C]	[M]	[C]
0.5	0	0.45	0.13	0.52	0.20	1.34	0.22	2.63
1.0	0.09	1.00	0.20	1.40	0.45	2.00	0.78	3.63
1.5	0.20	1.15	0.53	1.37	0.71	3.10	0.98	5.15
2.0	0.30	1.40	0.67	1.62	0.90	4.90	1.30	6.36
2.5	0.51	1.60	1.10	2.02	1.20	4.90	1.49	8.69
3.0	0.53	1.90	1.20	2.22	1.40	5.90	1.80	10.30
3.5	0.71	2.20	1.30	2.63	1.60	8.10	2.50	12.12
4.0	1.30	2.80	1.32	3.03	1.80	13.30	3.10	14.70
4.5	1.60	3.20	1.82	3.43	2.01	16.20	4.00	16.30
5.0	2.00	4.50	2.53	5.45	2.80	18.10	5.30	19.30
5.5	2.70	5.50	2.83	6.87	--	--	7.80	24.70
6.0	3.60	6.00	4.55	7.47	5.00	22.20	12.00	34.70
6.5	4.80	7.00	5.45	9.29	7.00	27.80	18.40	64.50
7.0	5.80	8.00	9.10	11.10	10.00	32.00	28.90	90.80
7.5	6.50	8.90	11.10	14.95	15.50	40.40	42.00	135.80

Table A4: The concentrations of sulfide (M) and mercaptide (C) that appeared during sol-gel reaction of $\text{Ge}(\text{OPr})_4$ and H_2S . The concentrations are 10^{-3} M.

t(h)	25°C		30°C		35°C		40°C	
	[M]	[C]	[M]	[C]	[M]	[C]	[M]	[C]
0.5	0.02	0.05	0.04	0.47	0.02	0.07	0.16	0.94
1.0	0.03	0.45	0.08	0.91	0.07	0.45	0.40	1.50
1.5	0.04	0.63	0.14	1.69	0.11	1.15	0.68	2.10
2.0	0.07	0.63	0.25	1.94	0.26	1.65	0.90	2.60
2.5	0.12	0.68	0.45	2.00	0.50	1.95	1.10	3.00
3.0	0.18	0.73	0.70	1.90	0.80	2.00	1.25	3.40
3.5	0.23	0.79	0.95	2.10	1.10	2.40	1.35	3.70
4.0	0.25	0.86	1.00	1.90	1.30	2.60	2.00	3.90
4.5	0.28	0.95	1.25	2.00	1.60	2.80	2.60	3.90
5.0	0.35	1.21	1.45	1.80	1.90	3.10	3.60	4.00
5.5	0.38	1.47	1.75	1.70	2.20	3.20	4.80	3.90
6.0	0.42	1.78	1.90	1.45	3.00	3.20	6.80	4.00
6.5	0.50	2.20	2.30	1.20	3.50	3.20	-	-
7.0	0.56	2.60	-	-	4.50	3.20	-	-
7.5	0.60	3.00	-	-	5.50	3.25	-	-